DISSERTATION

SURFACE MODIFICATION OF POROUS POLYMERIC MATERIALS USING LOW-TEMPERATURE PLASMAS

Submitted by

Michelle L. Steen

Department of Chemistry

In partial fulfillment of the requirements

for the Degree of Doctor of Philosophy

Colorado State University

Fort Collins, Colorado

Fall 2001

ProQuest Information and Learning Company
300 North Zeeb Road
P.O. Box 1346
Ann Arbor, MI 48106-1346

COLORADO STATE UNIVERSITY

September 18, 2001

WE HEREBY RECOMMEND THAT THE DISSERTATION PREPARED UNDER OUR SUPERVISION BY **MICHELLE L. STEEN** ENTITLED **SURFACE MODIFICATION OF POROUS POLYMERIC MATERIALS BY LOW-TEMPERATURE PLASMAS** BE ACCEPTED AS FULFILLING IN PART THE REQUIREMENTS FOR THE DEGREE OF DOCTOR OF PHILOSOPHY.

Committee on Graduate Work

Advisor

Department Head

ABSTRACT OF DISSERTATION

SURFACE MODIFICATION OF POROUS POLYMERIC MATERIALS USING LOW-TEMPERATURE PLASMAS

This dissertation describes plasma surface modification of porous polymeric materials for permanent hydrophilicity. Our modification strategy entailed treating commercial polymeric membranes downstream from an inductively-coupled radio-frequency plasma source. The results presented in this dissertation demonstrate that H_2O plasma treatment achieves hydrophilic modification of polysulfone (PSf), polyethersulfone (PES), and polyethylene (PE) membranes. The observed increase in hydrophilicity observed for PSf, PES, and PE membranes is a direct result of covalently-bound O-H, C-O, and C-O_x (e.g. C=O, O=C-O) groups introduced by plasma treatment. Furthermore, our hydrophilic membrane modification is permanent as plasma-treated membranes remain wettable for more than one year after treatment. The depth of penetration of the hydrophilic membrane modification achieved was explicitly tested. Specifically, environmental SEM images of the membrane cross sections wetting *in situ* show whether hydrophilic surfaces were created throughout the porous structure. Overall, the extent and permanence of hydrophilic modification was correlated to the interactions between the

membrane and reactive plasma species and the degree of penetration of plasma species through the membrane.

This dissertation examined the underlying chemistry of the H_2O plasma surface modification system using three gas-phase analytical techniques. These analyses provided a comprehensive profile of plasma species and extensive data on the molecular-level chemistry from the gas phase, to the plasma-surface interface, to the actual surface modification. Characterization of gas-phase species, including those penetrating the membrane thickness, as well as molecules generated at the membrane surface *during* modification was performed using optical emission spectroscopy and mass spectrometry. Plasma-surface interactions of OH radicals were assessed with our direct, non-intrusive radical-imaging experiments based on laser-induced fluorescence (LIF). Collectively, these experiments provide information about the underlying chemistry occurring during surface modification and, ultimately, afford better process control for plasma treatments of polymeric materials.

Our LIF-based radical-imaging and mass spectral experiments were also brought to bear on a second plasma surface modification system to understand the mechanisms through which surfaces are made hydrophilic during NH_3 plasma treatment. Interactions of NH and NH_2 radicals with polymer and metal substrates during NH_3 plasma processing were investigated using our radical-imaging experiments. Gas-phase species, including

nascent plasma ions, were identified using mass spectrometry. To investigate the role of ions on the formation of NH_x radicals in the gas phase and at the surface, ions were removed (>98%) from the plasma molecular beam prior to interaction with the substrate. Surface interaction results for NH and NH_2 with and without ions provide the basis for a discussion of possible surface interactions for the polymer and metal substrates examined.

This dissertation also employed plasma deposition to produce tailored surface coatings for microporous polymeric materials. These coatings, designed for specific uses, were integrated throughout the porous structure. Considerable control of the film chemistry was achieved through downstream and pulsed plasmas. In addition, a combination of synthetic strategies were employed to synthesize concentric-tubular Au/polymer micro- and nanostructured composites. This involved the use of template synthesis to produce the inner gold tubules and plasma deposition to create the outer tubules. These systems demonstrate the range of materials chemistry and surface properties possible for integrated composites prepared using plasma deposition as one of the synthetic steps.

Michelle L. Steen
Department of Chemistry
Colorado State University
Fort Collins, Colorado, 80523-1872
Fall 2001

DEDICATION

For my grandmother, Iolanda (Violet) D'Amore

ACKNOWLEDGMENTS

I acknowledge the following people at Colorado State University who directly contributed to this dissertation: Professor Ellen Fisher, for direction of my research, financial support and several edits of this document; Professors Richard Finke and David Grainger, for their careful reading of this dissertation and helpful discussions; Dr. Carmen Butoi, for her patient training and previous work in the Fisher laboratories; Lynley Hymas and Alistair Jordan, for their contributions to the membrane work. I also thank the following people for providing additional analyses: Dr. David Castner at the University of Washington; Dr. Tony Allegrezza and Robin de la Parra at Millipore Corporation; and Dr. Jerry Ditter at US Filter.

I am grateful to: Professor Ellen Fisher, for fostering my career in science and allowing me to complete my degree in her group; Professor Larry Curtin, for introducing me to research and encouraging me to attend graduate school; my parents, Ronald and Donna Jacobson, for the desire to pursue my doctorate, and my husband, Jeff, for his unconditional love and never ending support. I also thank the rest of my friends and family, for their help and encouragement.

TABLE OF CONTENTS

CHAPTER 2. Experimental Methods

TABLE OF ABBREVIATIONS

Although not intended to be confusing to the reader, a number of abbreviations are used throughout the text of this dissertation for clarity and concision. A list of the more commonly-used abbreviations is provided below to assist the reader.

rf	radio-frequency	MS	mass spectrometry
CW	continuous-wave	LIF	laser-induced fluorescence
PGC	plasma-induced graft copolymerization	IRIS	imaging of radicals interacting with surfaces
sccm	standard cubic centimeters per minute	VASE	variable-angle spectroscopic ellipsometry
P	applied rf or plasma power	OES	optical emission spectroscopy
PSf	polysulfone	XPS	X-ray photoelectron spectroscopy
PES	polyethersulfone	CA	contact angle
PE	polyethylene	gm	grounded mesh
PTFE	polytetrafluoroethylene	ICCD	intensified-charge-coupled device
PI	polyimide	ASAA	Asfardjani, Segui, Aurelle and Abidine
PC	polycarbonate		
PET	polyester	UB	Ulbricht and Belfort
HMDSO	hexamethyldisiloxane		
HFPO	hexafluoropropyleneoxide		

CHAPTER 1

INTRODUCTION AND OVERVIEW

This dissertation chapter provides an introduction to plasma surface modification of polymeric materials. Modes of plasma generation and components of the plasma system configuration are briefly described. The types of plasma surface modifications and alternate surface modification methods are also discussed. This chapter also places the dissertation research in broader scientific context and addresses the major hypotheses driving this work. In addition, an overview of the research presented in Chapters 3-7 is provided in this chapter.

1.1 BACKGROUND

The following sections provide useful information to familiarize the reader with the fundamentals of plasma science, components of the plasma system configuration, and the types of plasma surface modification.

1.1.1 PLASMA FUNDAMENTALS. Plasmas are generated by supplying energy to a neutral gas causing the formation of charge carriers.[1] Although there are a number of ways to supply the necessary energy for plasma generation, applying an electric field to a neutral gas is the most commonly used method.[2] Energy is transferred by the electric field to free electrons in the neutral gas. These charge carriers acquire high energies as they are accelerated by the electric field. Typically, average electron energies range from 1 to 10 eV with some individual electrons possessing energies much higher than the average, which correspond to very high electron temperatures of $\sim 10^5$ K.[3] As a result, inelastic collisions between electrons and molecules generate more electrons as well as ions, free radicals, and molecules in excited states. The electrons do not, however, achieve thermodynamic equilibrium with gas molecules in such a "nonequilibrium" or low-temperature plasma. Thus, the enormous utility of low-temperature plasmas is directly related to their ability to induce chemical reactions at relatively low gas temperatures (<1000 K), without thermal degradation of the underlying substrate.

All of the species generated in the plasma can interact with polymer surfaces. These gas-phase species include electrons, reactive neutrals, positive ions, and photons, including highly energetic vacuum ultraviolet photons. In general, the nature of the interaction of the plasma species with solid surfaces is determined by plasma reactor

configuration and processing parameters. The major structural components of the plasma reactor configuration are: 1) a vacuum chamber to house the plasma and the substrates; 2) a pumping system to evacuate the chamber; 3) a gas inlet; and 4) an excitation source to impart energy to the gas. The excitation source is an electrical power supply (direct or alternating current), which can vary in frequency and power. The type of excitation source greatly affects the densities and energies of the electrons, and therefore, the degree of dissociation of the feed gas.[4] The studies presented in this work solely use inductively-coupled radio-frequency (rf) plasmas, generated by applying an alternating electric field. Additional factors that influence the densities and energies of plasma species include the plasma system configuration and processing conditions, as discussed in the following section.

1.1.2 PLASMA SYSTEM CONFIGURATIONS. In certain plasma system configurations, substrates reside directly in the chamber housing the plasma. Because the plasma exists at a greater electrical potential than any surface with which it is in contact, positive ions from the plasma are accelerated toward the substrate surface. Depending on processing conditions and system configuration, the average energy of ions striking the surface can be varied from several eV to 1000 eV.[4] These ions can have a major effect on chemical reactions occurring at the plasma-surface interface, and, in some cases, can impart enough energy to a solid surface to remove material (sputtering). Although this is desirable in some applications (i.e., plasma etching), ion bombardment can lead to considerable substrate damage.

In alternate reactor configurations, substrates reside in a location removed from

the plasma and, therefore, are not subjected to bombardment from ions accelerated toward the substrate surface.[4] Furthermore, charged species can be lost by electron-ion recombination reactions prior to interacting with the substrate. Such plasma system configurations, referred to as "downstream" or "remote", effectively eliminate the undesired effects of ion bombardment and can produce materials with unique properties. An alternative to downstream and remote continuous wave (CW) plasmas is the use of pulsed plasmas to decrease energetic species bombardment.[5] In this configuration, modulating the rf power allows charged species to decay or recombine during the time off period of the pulse sequence. Plasma radicals, on the other hand, typically possess much longer lifetimes than ionic species generated in the plasma. Because of this lifetime difference, the substrate is primarily exposed to radical species in pulsed plasma systems.[6]

1.1.3 PLASMA SURFACE MODIFICATION. Plasma processing can produce a wide range of surface chemistries depending on the selection of process gases, plasma system configuration, and processing parameters, all of which can be adjusted to chemically and/or physically modify polymer surfaces. As a result, any of the following plasma surface modifications, or combinations thereof, can result: 1) plasma deposition; 2) plasma etching; 3) chemical surface modification; and 4) plasma-induced graft copolymerization. For example, proper selection of gases from which the plasma is generated can result in deposition of organic or inorganic films.[7] Whereas plasma etching removes material, plasma deposition occurs when precursors to the deposited film, generated by fragmentation of the parent gas, react at the surface to form a stable solid film. Depending on the plasma system configuration and selection of process gases,

etching and deposition can simultaneously occur by chemical reactions, physical means (i.e. sputtering), or a combination of these two mechanisms.[4] Ultimately, the dominant process occurring during plasma processing is dictated by the interactions of plasma species with each other and the surface.

An alternate approach to plasma surface modification is implantation of new functional groups into the existing polymer backbone. Thus, the third category of plasma surface modification, chemical surface modification, results when gas-phase species react at the surface to form stable products with physical and or chemical properties that are different from the bulk.[7] Radicals, ions, electrons, metastables, and photons generated in the plasma can all interact simultaneously with the polymer surface. These species can impart enough energy to break polymer chains, creating free radical sites in the polymer. Reactive neutral species, primarily radicals, can combine at these sites, thereby altering the surface chemical composition.[5]

By far, oxygen is the most commonly used plasma for chemical surface modification, but other commonly used systems include NH_3, N_2, and H_2O plasmas. The processes by which plasmas modify surfaces include removal of a weakly bound surface layer by oxidation, cleaning by removal of adsorbed materials, crosslinking the polymer, and chemical reaction.[8] Although a number of chemical reactions are possible in these systems, plasma radicals are generally accepted to be the primary reactive species in initiating a modification reaction sequence.[9,10,11] Hansen and coworkers proposed that O atoms in O_2 plasmas induce chemical reactions at the surface to implant C=O, OH, and CO_2H groups at the polymer surface,[12] whereas H_2O plasmas produce similar polymer

surface compositions.[8] Low-temperature plasmas of ammonia and nitrogen-hydrogen mixtures result in creation of surface amine groups and improvements in wettability for a variety of polymers, including the relatively-inert polytetrafluoroethylene (PTFE).[13,14] The observed improvements in the wettability of polymer surfaces were attributed to these alterations in surface chemistry.

The fourth plasma surface modification is plasma-induced graft copolymerization (PGC), which entails grafting of a thin, highly adherent coating or film with the desired surface properties. In PGC, polymers are first exposed to a plasma (e.g., Ar) to create radicals at the surface. Modification occurs when the radicals created at the surface initiate polymerization of a gas- or liquid-phase monomer, yielding graft polymers on the surface. Vinyl monomers are frequently used as they polymerize rapidly at the plasma-treated polymer surface. PGC is a fast and highly effective means of hydrophilic surface modification. It is also suitable for hydrophobic modification with fluorinated monomers. Although not included in this dissertation, PGC methods are currently being developed in the Fisher laboratories.[15]

1.2 SCIENTIFIC CONTEXT

Because of their attractive thermal, mechanical, and electrical properties, polymers are important to a number of technological fields, including the biomedical, separation, microelectronics, food packaging, and printing industries.[16,17,18] Technological advances in these areas often require modification of the polymer surface or microstructuring for pattern definition, both of which are achievable with low-temperature plasmas.[3,19] Plasma

technology has been applied in the microelectronics industry since the late 1960s for stripping of polymer etching masks, deposition of dielectric thin films, and etching processes for microstructuring.[20,21,22,23,24,25] Although the use of plasmas has been spearheaded by the microelectronics industry, plasmas are used in other industries to tailor the surface properties of polymers for specific uses through deposition of thin films with the desired surface properties or through chemical surface modification.[5,6]

Under certain circumstances, low-temperature plasma treatment is an attractive alternative to other polymer surface modifications. Alternate methods include mechanical abrasion; treatment with solvents, caustic solutions, or acids;[26] graft polymerization of polar monomers from reactive sites generated at the surface (by wet or plasma techniques);[27,28] absorption of a polymer from solution;[29] and photochemical methods. For example, the surfaces of fluoropolymers, which are intrinsically difficult to modify, require treatment with reagents such as sodium napthalene, which defluorinate, unsaturate, and partially oxidize the bulk polymer to a depth of a few hundred nanometers.[30] In contrast, plasmas can alter the surface composition, wettability, and adhesion without changing the properties of the bulk material.[7] Plasmas are "dry" processes, eliminating the waste disposal issues associated with "wet" chemical processes. Modification is typically very fast, in many instances taking only seconds. Overall, plasma modification has distinct advantages over alternate surface modification methods in breadth of application, with a virtually unlimited number of available gas and surface chemistries.

The literature contains a numerous examples and several reviews of plasma treatment for polymer surface modification.[32] Plasmas have been used to provide

biocompatibility of materials such as poly(methylmethacrylate), poly(vinylchloride), and polyurethane.[33] As noted in Section 1.1.3, chemical surface modification via functional group implantation has been used since the 1960's to improve the wettability of polymers. Moreover, plasma deposition increases polymer versatility by generating non-fouling coatings on sensors and membranes; anti-scratch coatings on compact disks; biocompatible coatings on biomedical devices; and barrier films for food and pharmaceutical packaging.[34,35,36,37] Recently, downstream and pulsed plasma treatments have also been used in these applications to reduce surface damage of polymers and create films with unique chemical properties.[38]

Despite the apparent advantages of plasma surface modification and the enormous industrial utility of plasmas to improve the surface properties of polymers, there is currently little use of this surface modification strategy in large-scale polymeric membrane production. This is a considerable disadvantage to the membrane industry as surface modification of commercial polymeric membranes is a promising approach to circumventing the inordinate expense of developing new membrane materials and broadening the types of membrane surface chemistries available for a variety of applications.[39] For example, thermoplastics, such as polysulfone (PSf) and polyethersulfone (PES), are widely used because of their unique bulk properties. However, problems associated with the hydrophobicity of these materials severely limits their long-term use in many applications.[40] As a result, hydrophobic membranes must be made hydrophilic prior to use in most separation processes. Based on the technological and industrial utility of plasmas to improve the wetting properties of polymers, one

method toward achieving the desired change in hydrophilicity is to treat PSf and PES membranes with a low-temperature plasma.

H_2O-based plasmas have been used to modify PSf plane and hollow fiber membranes for hydrophilic modification. For example, Asfardjani, Segui, Aurelle, and Abidine (ASAA) observed that PSf membranes were significantly more hydrophilic after air and H_2O plasma treatment, as evidenced by a decrease in the water contact angle.[43] Ulbricht and Belfort also reported improvement in the hydrophilicity of PSf membranes treated with a 50:50 He:H_2O plasma.[47] In the latter study, the treated membranes were completely stable if stored in water; however, loss of the plasma-induced hydrophilicity occurred upon storage in ambient conditions. This is consistent with structural rearrangement of the polymer after plasma treatment to minimize surface energy.[47, 48] Such reports of low-temperature plasma treatment of polymeric membranes resulting in transient and or irreproducible hydrophilicity deter industrial use of plasma surface modification in large-scale membrane production.

We believe that the transient hydrophilicity reported by other researchers is attributed to poor understanding, and therefore, poor optimization of the plasma process. Many studies have concentrated on correlating polymer surface modifications to specific plasma conditions,[45,46] which provide simple relationships between the density of species originating in the glow discharge and surface modification induced in polymers. For example, ASAA optimized plasma processing conditions of PSf membranes by establishing relationships between: 1) plasma parameters; 2) the composition of the gas phase, particularly OH radicals believed to be responsible for surface modification; and 3)

the composition and wetting properties of the membrane surface after plasma treatment. Accordingly, optimal conditions giving the maximum contact angle change and surface oxidation corresponded to the plasma conditions that produced the greatest intensity of OH radicals in the plasma. Such studies correlating the identity and concentrations of species present in the plasma to specific polymer surface modifications provide useful, albeit somewhat indirect, information about the gas-surface interface in plasma surface modification systems.

ASAA proposed that OH radicals produced in air and H_2O plasmas modify PSf by producing covalently-bound C=O, C-O, O-H, and O-C=O groups at the surface.[7] ASAA suggested that plasma-generated OH radicals may combine with surface atoms to produce C-O bonds via process 1.1,

$$\begin{array}{ccc} CH_2 & & CH_2OH \\ -C- + OH^{\cdot} & \rightarrow & -C- \end{array} \qquad (1.1)$$

Although this process explains the empirical relationship between the gas-phase relationship of OH radicals and the incorporation of some functional groups, it is limited in that it does not account for the observed incorporation of C=O and O-C=O groups into PSf. Furthermore, given the susceptibility of alcohol groups to subsequent oxidation reactions, it is unlikely that these would be the only functional groups incorporated by plasma treatment.

1.3 STATEMENT OF DISSERTATION RESEARCH

The primary goal of this work was to make commercial PSf and PES membranes permanently hydrophilic using low-temperature plasmas. As a result, we worked closely with the membrane industry to develop a surface modification that would suit their application needs. According to industrial standards, a method for making hydrophobic membranes hydrophilic must satisfy the following criteria: 1) the surface must be modified with no alteration to the bulk properties of the membrane; 2) the modification must be permanent[a] and withstand prolonged use in a separation process as well as repeated sterilization; and 3) all membrane surfaces in the porous structure must be hydrophilic. Our strategy toward achieving these objectives was to use our understanding of plasma chemistry to optimize membrane processing.

Another important goal of this work was to understand the underlying chemistry in plasma surface modification systems. Formulating reliable chemical mechanisms for plasma modification of polymers is particularly difficult given the complexity of plasma chemistry: a wide variety of species are generated in the gas-phase, including ions, electrons, metastables, and radicals. In addition to gas-phase reactions between these species, surface interactions can also take place between gas-phase particles and solid

---

[a]We do not intend to confuse the reader with the use of the word, "permanent". This word is generally accepted in the membrane industry to denote "shelf life", which is defined as the period of time during which a material may be stored and remain suitable for use. Typically, a viable surface modification must have a minimum shelf life of one year. Furthermore, the modification must withstand prolonged use in a separation process and repeated sterilization by steam cleaning.

surfaces, both the reactor walls and the substrates being processed. Determining the nature of these gas-surface interactions is critical to identification of plasma reactions involved in surface modification, and controlling the overall plasma process. Understanding how each species influences the surface interactions of other plasma species is also essential for deciphering the underlying plasma chemistry and physics.

In general, knowledge about individual plasma species, their interactions with the surface, and the surface modification is necessary to understand these non-equilibrium, complex chemical systems. Therefore, a multi-faceted approach was adopted to elucidate the chemical reactions involved in surface modification. This entailed independent study of all aspects of the plasma system: the surface, the gas-phase, and the gas-surface interface. Our combined experimental approach, a significant departure from traditional plasma studies, is poised to provide relevant, and currently unavailable, chemical information about plasma systems. Hence, the unifying hypothesis of this work was that our combined approach affords process control by considering the molecular-level chemistry as well as achieving the desired membrane surface properties.

Our combined approach was brought to bear on two important plasma surface modification systems, H_2O and NH_3, to identify the reactive plasma species and the contribution of these species to the overall surface modification. In the H_2O system, our hypothesis was that OH radicals generated in the plasma are the primary reactive species involved in hydrophilic membrane modification. If this hypothesis is correct, then we would expect surface loss of OH radicals during plasma processing of polymeric membranes, which we can determine experimentally. Our second hypothesis was that OH

radicals produced in H_2O plasmas modify PSf membranes by producing covalently bound C=O, C-O, O-H, O-C=O and sulfate groups at the surface. Although it is infeasible to assign exact mechanisms without any kinetic information about these systems, the predictive value of organic structural theory should not be underestimated. In addition to oxidation of the methyl group as proposed by ASAA,[12] we believe that there are at least two other locations for oxidation on the polymer backbone as represented in Scheme 1.1.

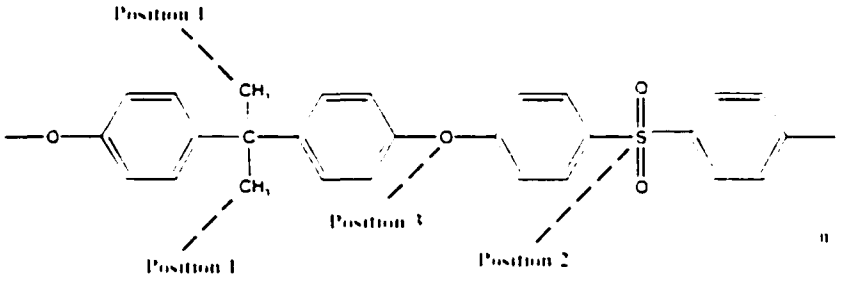

Scheme 1.1.

Oxidation at position 1 by a plasma species, presumably OH radicals, yields an aldehyde, which can be oxidized further to yield a carboxylic acid group, as shown in Process 1.2. A secondary oxidation pathway is at the sulfur (position 2, Scheme 1.1) resulting in sulfate-like groups, given in Process 1.3. Oxidation at the ether linkage is shown in Process 1.4. If surface modification does indeed occur via the oxidation pathways we proposed, then we would expect incorporation of a variety of chemical moieties into PSf by H_2O plasma treatment, including C-O, C=O, O-C=O, O-H, and sulfate groups.

The work involving the NH_3 plasma surface modification system was primarily motivated by previous studies in our group. First, we have used NH_3 plasmas to increase the hydrophilicity of metallic and polymeric substrates, including porous polymeric

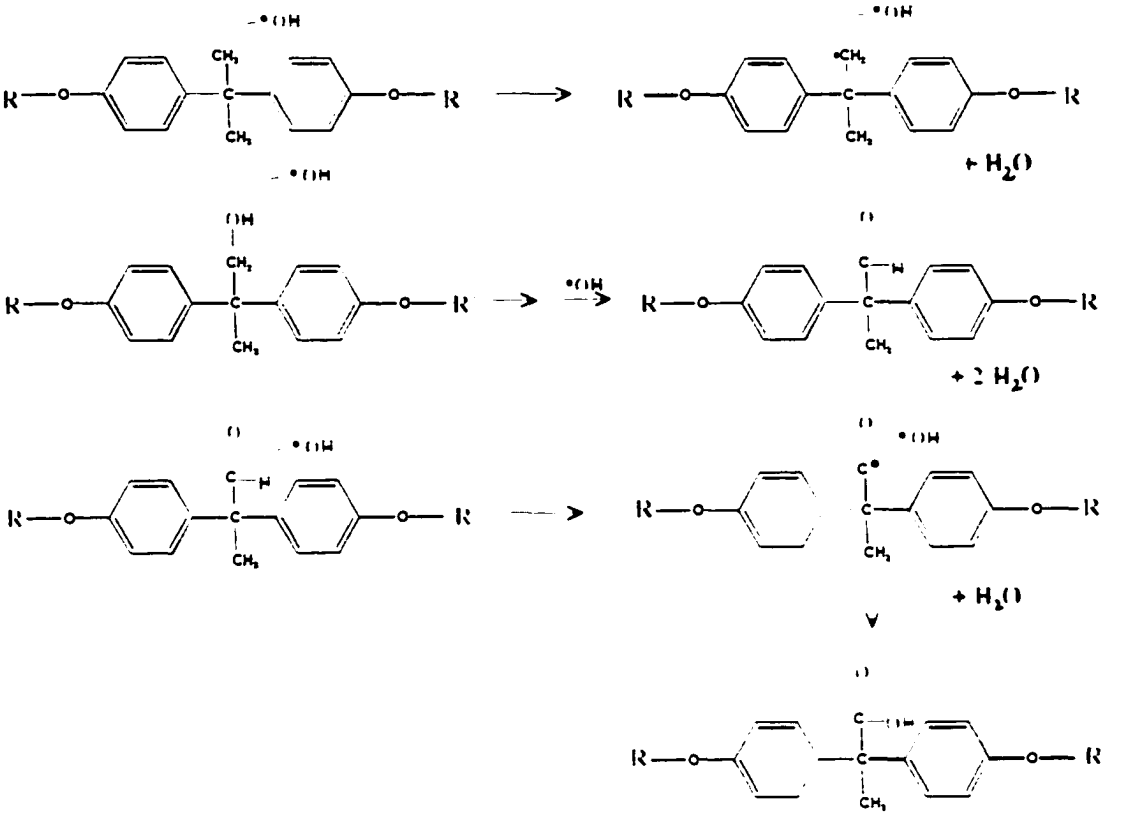

Process 1.2 Oxidation at position 1, Scheme 1.1.

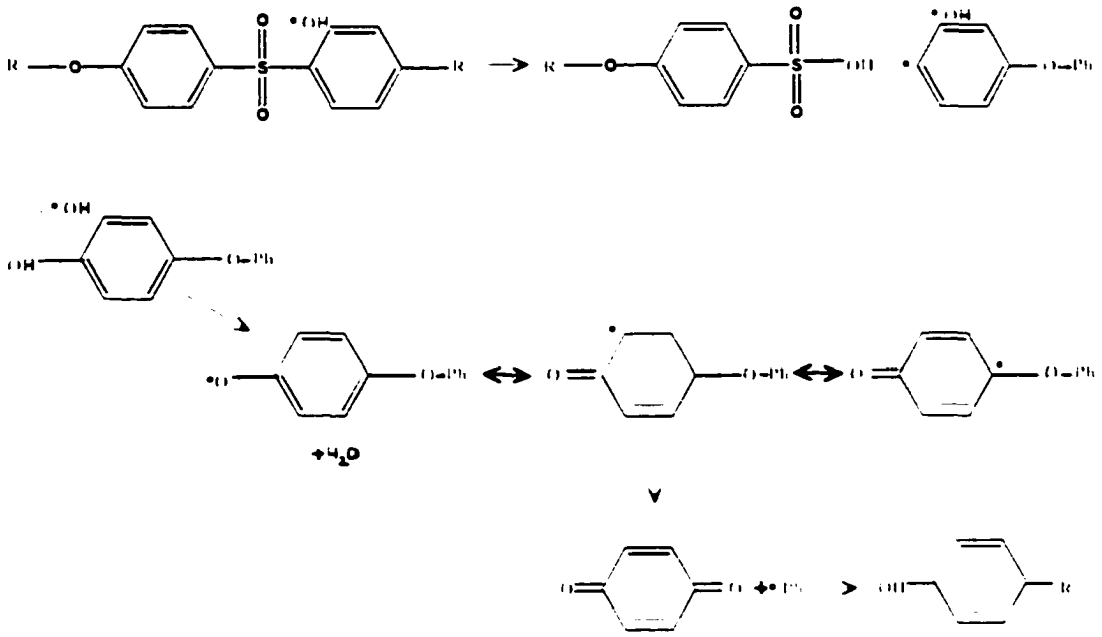

Process 1.3 Oxidation at position 2, Scheme 1.1.

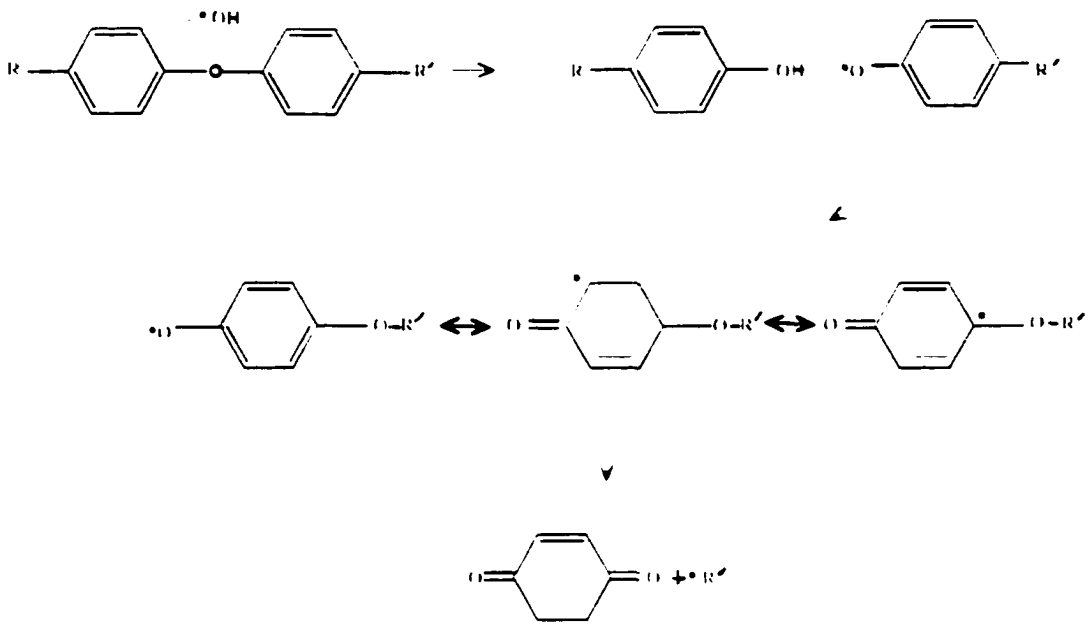

Process 1.4 Oxidation at position 3, Scheme 1.1.

membranes.[47,48] These results are consistent with previous work of NH_3 plasma treatment of polymers resulting in higher wettability relative to untreated surfaces.[44,45,46] Modification occurs via amine functional group implantation primarily by NH_2 radicals. Second, we have also previously reported extensive IRIS studies of NH_2 radicals in NH_3 plasmas, including translational temperatures for both beam and scattered species as well as surface reactivities for a number of substrates.[50,51] Our IRIS reactivity data show that NH_2 radical production occurs at the surface of nearly all substrates during NH_3 plasma processing under most experimental conditions, suggesting that other species in the molecular beam are contributing to the surface generation of NH_2.

A fundamental question originated by these data revolves around the mechanism for observed surface production of NH_2. One hypothesis, put forward in our previous NH_3 study, was that gas-phase NH radicals contributed to surface production of NH_2. This can be envisioned as occurring via one or both of the two processes given in Processes 1.5.

$$NH(g) + H(ads) \rightarrow NH_2(g) \qquad (1.5a)$$

$$NH(g) + H(ads) \rightarrow NH(ads) + H(ads) \rightarrow NH_2(g) \qquad (1.5b)$$

Process 1.5a represents an Eley-Rideal-type process,[53] wherein a reaction occurs between a gas-phase species and an adsorbed species, before the gas-phase reactant has equilibrated with the surface. Process 1.5b is a Langmuir-Hinschelwood-type process, wherein both reactants are equilibrated on the surface prior to reaction. While Eley-Rideal and Langmuir-Hinschelwood processes are used extensively to describe reactions that occur in solution catalysis[52] and in ultrahigh vacuum (UHV) systems,[53] they afford a

reasonable means with which to discuss possible surface interactions that result in generation of NH_2. If either of these processes transpires at the plasma-surface interface, we would expect that NH radicals would be lost at the surface.

1.4 OVERVIEW OF RESEARCH

The viability of plasma surface modification systems (e.g. O_2, H_2O, Ar, H_2) to produce the desired polymer surface properties was investigated using the inductively-coupled rf plasma reactor described in Chapter 2. These studies explored the variation of process parameters, such as reactor geometry, polymer material, plasma power, treatment time, and gas-phase composition. The resulting surface properties were analyzed by the characterization techniques described in Chapter 2 to determine the effects of these variables on the surface properties. Results from these analyses are reported in Chapters 3 and 4.[54,55]

Chapter 2 also describes three gas-phase analytical tools used to investigate the chemistry of H_2O and NH_2 plasma surface modification systems. Characterization of gas-phase species as well as molecules generated at the polymer surface during plasma modification was performed using optical emission spectroscopy (OES), mass spectrometry (MS), and laser-induced fluorescence (LIF). Of these, our LIF-based Imaging of Radicals Interacting with Surfaces (IRIS) technique is uniquely suited to provide relevant mechanistic information about plasma systems.[56] Experimentally-determined surface loss coefficients are obtained *in situ* and afford direct information on plasma-surface interactions. Chapters 5 and 6 describe reactivity

measurements for OH and NH radicals, respectively.[57,58] These measurements were made under different plasma processing conditions by varying parameters such as feed gas, plasma power, and substrate material. The role of ions on the radical-surface reactivity was explored by placing a grounded mesh in the path of the molecular beam to remove charged species prior to interacting with the substrate, Chapter 6.

Chapter 7 describes alternate surface modification strategies for porous polymeric materials. Here, plasma deposition was used to produce tailored surface coatings for microporous materials. Of the model systems described in Chapter 7, SiO_x and fluorocarbon polymers were applied to microporous supports to achieve conformal coverage of the underlying structure.[59] The resulting film chemistry was controlled via downstream and pulsed plasma treatments. In addition, Chapter 7 describes the combination of plasma deposition and template synthesis[60] to prepare concentric-tubular composite materials.[60]

1.5 REFERENCES

1. M. A. Lieberman and A. J. Lichtenberg. *Principles of Plasma Discharges and Material Processing:* (Wiley: New York. 1994).
2. H. Conrads and M. Schmidt. *Plasma Sources Sci. Technol.* **9,** 441. 2000.
3. N. Morosoff in *Plasma Deposition. Treatment. and Etching of Polymers:* R. d'Agostino. Ed. (Academic Press: San Diego. 1990. p. 2).
4. F. D. Egitto. V. Vukanovic. and G. N. Taylor. in *Plasma Deposition. Treatment. and Etching of Polymers:* R. d' Agostino. Ed. (Academic Press: Boston. M.A. 1990). p. 322.
5. N. Inagaki. *Plasma Surface Modification and Plasma Polymerization.* (Technomic Publishing: Lancaster. P.A. 1996).
6. H. Yasuda. *Plasma Polymerization:* (Academic Press: Orlando. FL. 1985).
7. F. D. Egitto and L. J. Matienzo. *IBM J. Res. Develop.* **38,** 423 (1994).
8. J. R. Hall. C. A. L. Westerdahl. A. T. Devine. and M. J. Bodnar. *J. Appl. Polym Sci.* **13,** 2085 (1969).
9. J. F. Battey. *IEEE Trans. Electron. Devices* **2,** 140 (1977).
10. J. M. Cook and B. W. Benson. *J. Electrochem. Soc.* **130,** 2459 (1983).
11. O. Joubert. J. Pelletier. and Y. Arnal. *J. Appl. Phys.* **65,** 5096 (1989).
12. R. H. Hansen. J. V. Pascale. T. De Benedictis. and P. M. Rentzepis. *J. Polym. Sci. A* **3,** 2205 (1965).
13. J. R. Hollahan. B. B. Stafford. R. D. Faub. and S. T. Payne. *J. Appl. Polym. Sci.* **13,** 807 (1969).
14. F. Poncin-Epaillard. B. Chevet. and J.-C. Brosse. *J. Adhesion Sci. Technol.* **8,** 455

(1994).

15. D. S. Wavhal and E. R. Fisher. *J. Memb. Sci.*, manuscript in preparation.

16. H. K. Yasuda. *J. Appl. Polym. Sci.: Appl. Polym. Symp.* **46,** 541 (1990).

17. *ibid.*, 439 (1990).

18. H. Von Boenig. *Fundamentals of Plasma Chemistry and Technology* (Technomic Publishing: Lancaster, PA, 1996).

19. R. J. Jensen and J. H. Lai, in *Polymers for Electronic Applications*, J. H. Lai, Ed. (CRC Press, Inc., Boca Raton, FL, 1989).

20. S. R. Ray, C. K. Maiti, S. K. Lahiri, and N. B. Chakrabarti. *Adv. Mater. Optics Electronics* **6,** 73 (1995).

21. K. Maeda and S. M. Fisher. *Solid State Technol.* June, 83 (1993).

22. G. W. Hills, A. S. Harrus, and M. J. Thoma. *Solid State Technol.* April 127 (1990).

23. R. D. Miller. *Science* **286,** 421 (1999).

24. L. Peters. *Semicond. Intern.* **22,** 56 (1999).

25. G. S. Mathad, D. W. Hess, and M. Meyyappan. *Electrochem. Soc. Interface* **8,** 34 (1999).

26. S. L. Kaplan and P. W. Rose. *Intl. J. Adhesion & Adhesives* **11,** 109 (1991).

27. D. E. Bergbreiter and K. Zhou. *J. Polym. Sci. Part A: Polym. Chem.* **30,** 2049 (1992).

28. E. T. Kang, K. G. Neoh, D. L. Tan, Y. Uyama, N. Morikawa, and Y. Ikada. *Macromolecules* **25,** 1959 (1992).

29. M. S. Shoichert and T. J. McCarthy. *Macromolecules* **24,** 1441 (1991).

30. See for example: a) M. Ulbricht and G. Belfort. *J. Appl. Polym. Sci.* **56,** 325 (1995); b) A. Nabe, E. Staude, G. Belfort. *J. Memb. Sci.* **133,** 57 (1992); c) H. Yamagishi, J. Crivello, and G. Belfort. *J. Memb. Sci.* **105,** 237 (1995); d) *ibid.*, p. 249.

31. E. M. Liston. *Proc. ACS. Div. Polym. Mater.: Sci. Eng.* (ACS Spring Meeting, Boston, MA) **62,** 442 (1990).

32. For example, see in their entirety : a) *Polymer Surfaces*, D. T. Clark and W. J. Feast, Eds. (John Wiley, New York, NY, 1978); b) *Plasma Deposition, Treatment, and Etching of Polymers*, R. d'Agostino, Ed. (Academic Press, Boston, MA, 1990).

33. S. Koontz and G. Spaulding, U. S. Patent Application filed 3/26/92; J. S. Brein, S. Greenhouse, and L. Pinatti. *Surf. Interface Anal.* **17,** 63 (1991); D. Li, J. Zhao, H. Gu, M. Lu, F. Ding, and J. Hu. *Chinese Phys. Lett.* **9,** 79 (1992).

34. R. Lamendola, P. Favia, F. Palumbo, and R. d'Agostino. *Eur. Phys. J.* **4,** 65 (1998).

35. R. Lamendola, R. d'Agostino, F. Fracassi. *Plasmas Polym.* **2,** 147 (1997).

36. P. Favia, R. d'Agostino, F. Palumbo. *J. Phys. IV France* **7,** C4-199 (1997).

37. D. C. Smith, R. M. Pillar, and R. Chernecky. *J. Biomed. Mater. Res.* **25,** 1045 (1991).

38. C. I. Butoi, N. M. Mackie, L. J. Gamble, D. G. Castner, J. Barnd, A. M. Miller, and E. R. Fisher. *Chem. Mater.* **12,** 2014 (2000); V. Panchalingam, X. Chen, C. R. Savage, R. B. Timmons, R. C. Eberhart. *J. Appl. Polym. Sci. Polym. Symp.* **54,**

123 (1994).

39. J. Pieracci, J. V. Crivello, and G. Belfort, *J. Memb. Sci.* **156,** 223 (1999).

40. M. Mulder, *Basic Principles of Membrane Technology*, 2nd Ed., (Kluwer Academic Press: New York, 1996).

41. K. Asfardjani, Y. Segui, Y. Aurelle, and N. Abidine, *J. Appl. Polym. Sci.* **43,** 271 (1991).

42. M. Ulbricht and G. Belfort, *J. Memb. Sci.* **111,** 193 (1996).

43. H. J. Griesser, J. H. Hodgkin, and R. Schmidt, *Prog. Biomedical Polym.* C. G. Gebelein and R. L. Dunn, Eds. (Plenum Press: New York, 1990).

44. T. R. Gengenbach, X. Xie, R. C. Chatelier, and H. J. Griesser, *J. Adhes. Sci Technol.* **8,** 305 (1994).

45. P. Favia, F. Palumbo, M. V. Stendardo, and R. d'Agostino in *Surface Modification of Polymeric Biomaterials*, B. D. Ratner and D. G. Castner, Eds. (Plenum Press: New York, 1996).

46. B. K. Bein, M. Wojczak, and J. Pelzl, *Mater. Sci. Eng.* **A122,** 93, (1989).

47. C. I. Butoi, Ph. D. thesis, Colorado State University, 2000.

48. K. R. Kull, M. L. Steen, and E. R. Fisher, *J. Memb. Sci.*, manuscript in preparation.

49. P. Favia, M. V. Stendardo, and R. d'Agostino, *Plasmas Polym.* **1,** 91 (1996).

50. P. R. McCurdy, C. I. Butoi, K. L. Williams, and E. R. Fisher, *J. Phys. Chem. B* **103,** 6919, (1999).

51. C. I. Butoi, M. L. Steen, J. R. D. Peers, and E. R. Fisher, *J. Phys. Chem.* **105,** 5957 (2001).

52. B. C. Gates. *Catalytic Chemistry*. (John Wiley, New York, NY, 1992). p. 223.

53. C. T. Rettner, D. J. Auerbach, J. C. Tully, and A. W. Kleyn. *J. Phys. Chem.* **100,** 13021 (1996).

54. M. L. Steen, L. Hymas, E. D. Havey, N. E. Capps, and E. R. Fisher. *J. Memb. Sci.* **188,** 97 (2001).

55. M. L. Steen, A. C. Jordan, and E. R. Fisher. *J. Memb. Sci.*, submitted for publication.

56. P. R. McCurdy, K. H. A. Bogart, N. F. Dalleska, and E. R. Fisher. *Rev. Sci. Instrum.* **68,** 1684 (1997).

57. M. L. Steen, C. I. Butoi, and E. R. Fisher. *Langmuir*, submitted for publication.

58. M. L. Steen, K. R. Kull, and E. R. Fisher. *J. Appl. Phys.* submitted for publication.

59. M. L. Steen, W. C. Flory, N. E. Capps, and E. R. Fisher. *Chem. Mater.* **13,** 2749 (2001).

60. V. M. Cepak, J. C. Hulteen, G. Che, K. B. Jirage, B. B. Lakshmi, E. R. Fisher, and C. R. Martin. *J. Mater. Res.* **13,** 3070 (1998).

CHAPTER 2

EXPERIMENTAL METHODS

This dissertation chapter has three sections. The first section of this chapter contains a description of our plasma reactor used to process polymeric materials. The types of membrane materials employed in this study and the experimental conditions for materials processing are described. The second section of this chapter provides a detailed list and description of surface analyses. The third section of this chapter describes the gas-phase analytical methods used to study the molecular-level chemistry in plasma surface modification systems. The components of the imaging of radicals interacting with surfaces (IRIS) apparatus are also described in this section.

2.1 MEMBRANE TREATMENTS

2.1.1 GENERAL. Unless otherwise noted, plasma treatments were performed in the tubular, glass inductively-coupled, low density rf (13.56 MHz) reactor shown in Fig. 2.1a.[12] Some design changes were made to better suit porous materials.[7] Specifically, a glass cylindrical membrane holder (30 mm diam.) orients the membrane perpendicular to the gas flow. This allows maximal exposure and penetration of the plasma through the thickness (~125 μm) of the membrane. This specially designed membrane holder differentiates our work from prior studies by facilitating modification of the entire membrane cross section. The membrane holder was situated in the glass reactor ~9 cm downstream from the most intense region of the plasma glow to minimize plasma-induced damage to these relatively fragile materials. In addition, Chapter 5 describes the use of two alternate reactor geometries, shown in Figs. 2.1b and 2.1c.

2.1.2 HYDROPHILIC MEMBRANE MODIFICATION. Chapters 3, 4, and 5 entail H_2O plasma treatment of a variety of polymeric membranes for permanent hydrophilicity. A number of plasma systems were explored, including 100% Ar, 100% He, 100% O_2, 100% H_2O, 15% H_2O_2/H_2O, and 50% Ar H_2O. In addition, plasma treatments with H_2 (25 W, 1 standard cubic centimeters per minute, sccm flow rate, 100 mTorr pressure, 2 min) are described in Chapter 5. The flow of feed gases ranged from 1 to 20 sccm and was controlled by an MKS mass flow controller. Prior to use, liquid samples underwent several freeze-pump-thaw cycles to remove trapped atomospheric gases and were then introduced into the reactor from a 100 mL Pyrex glass sidearm vacuum flask with Teflon stopcocks. The vapor pressure was controlled (within ±2%)

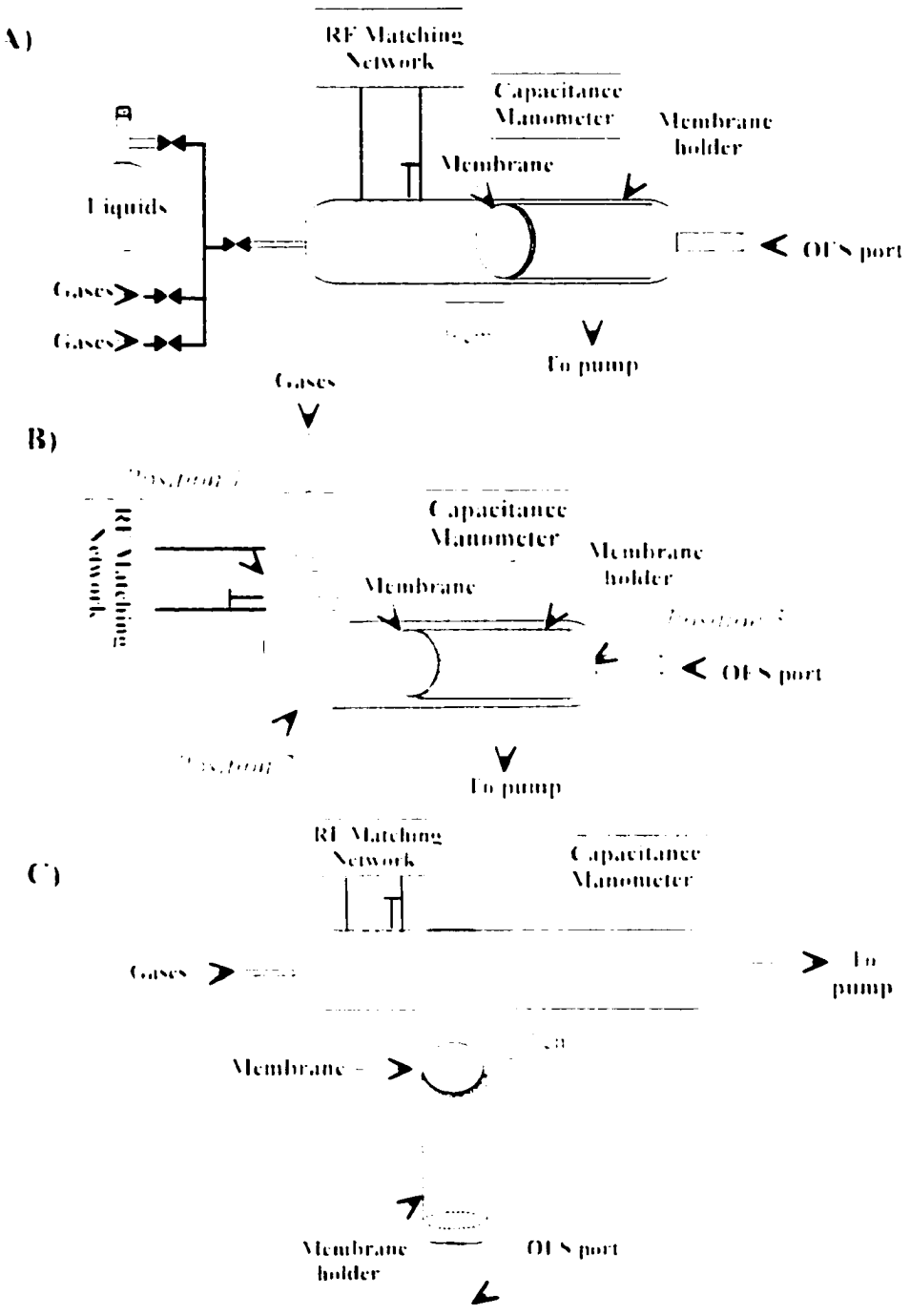

Figure 2.1 Schematics of different plasma reactor configurations used to treat polymeric membranes: (A) our standard reactor used to process membranes; (B) L-shaped reactor; and (C) T-shaped reactor.

using a Nupro bellows-sealed metering valve. For the 50:50 Ar:H_2O system, the H_2O pressure was allowed to stabilize prior to the addition of Ar (4.8 grade). Thus, the amount of H_2O admitted to the reactor is constant (± 2%). The pressure in the chamber was monitored with an MKS Baratron capacitance manometer which is insensitive to differing gas compositions.

The extensive parameter study performed included 5-100 W applied rf power (P), 50-100 mTorr chamber pressure, and treatment times from 0.25 to 10 min. From this study, the optimal conditions for hydrophilic modification were determined to be H_2O (no additives), 25 W applied rf power, 50 mTorr pressure for 2 minutes. These conditions were used in all experiments unless otherwise noted.

Chapter 3 describes plasma treatment of polysulfone (PSf) membranes. Figure 2.2a shows a cross-sectional scanning electron micrograph (SEM) of an asymmetric PSf membrane. The term "asymmetric" refers to a distinct pore gradient with gradual transition from much smaller (< 0.1 μm) to much larger pores (>10 μm) across the thickness (~125 μm) of the membrane.[4] The large and small pore sides of the membrane are referred to as the "open" and "tight" sides, respectively. Asymmetric PSf membranes are commercially available (US Filter) with average pore sizes ranging from 1.2 μm (BTS 5) to ~0.01 μm (ultrafiltration, UF). BTS55, BTS80 and UF membranes were primarily used in these experiments. For consistency, the open side of the membrane was oriented closest to the inductor coil; however, identical results were achieved with the tight side upstream. A non-porous PSf resin (Westlake Plastics) and commercial polyethersulfone (PES), polyethylene (PE), and polytetrafluoroethylene (PTFE) membranes were also used.

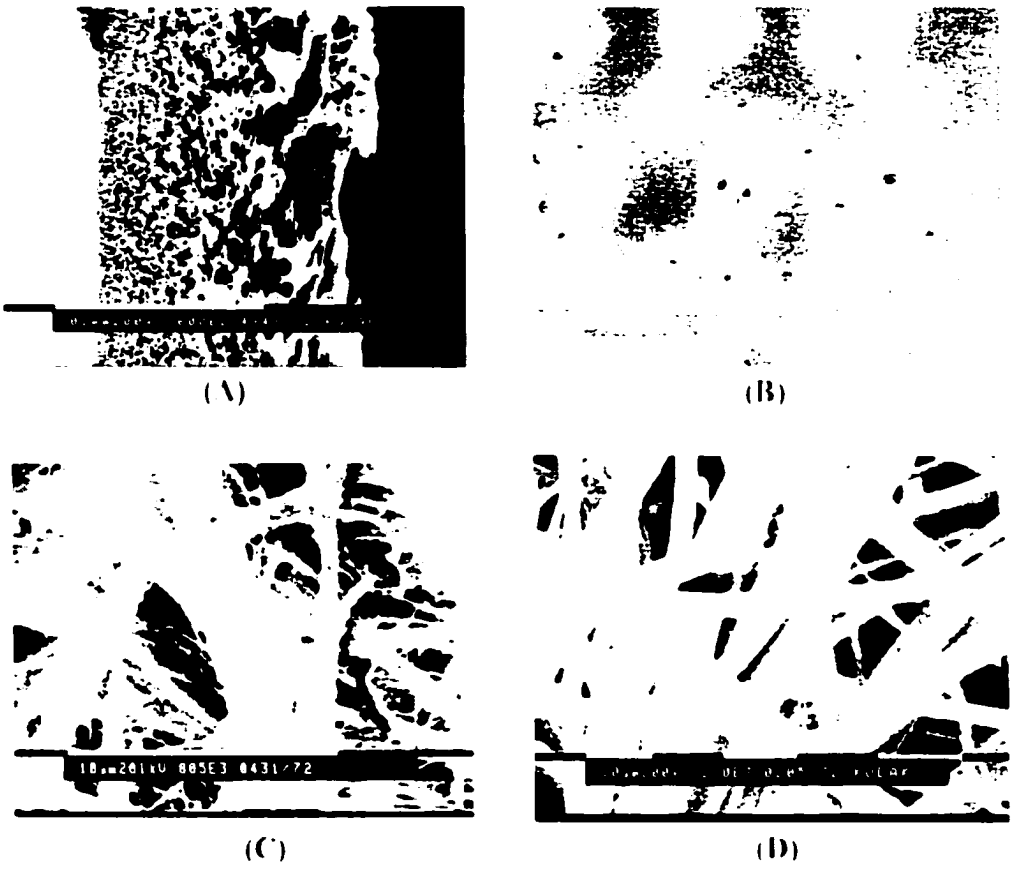

Figure 2.2 SEM images of the various porous polymeric host materials employed in this study: (A) cross section of an asymmetric PSf membrane; (B) track-etched PET membrane; (C) microporous PE membrane; and (D) non-woven PET fibers.

2.1.3 ALTERNATE MODIFICATION STRATEGIES. Chapter 6 reports synthesis of three different porous composite materials employing plasma deposition as one of the synthetic steps. These model systems demonstrate the range of materials chemistry and surface properties possible for composites prepared by plasma deposition. All three systems used the plasma reactor shown in Fig. 2.1a. The first system used gold tubes (200 nm-2 μm) prepared by template synthesis. This method entails deposition of the desired material in the pores of template track-etched polyester (PET) membranes, Fig. 2.2b.[5] An electroless deposition method previously described in detail was used to deposit Au to produce a Au tube or fiber in each pore.[7] The membrane was then removed with hexafluoro-2-propanol to reveal free-standing Au structures. To form a Au polymer composite, an outer tubule of the electronically conductive polymer polypyrrole was deposited on the Au tubules via a pulsed pyrrole plasma (5% duty cycle,[b] 200 W peak applied rf power, pressure = 150 mTorr).[7]

The second system used ~100 μm thick microporous symmetric PE membranes, Fig. 2.2c, and non-woven PET fibers as host materials, Fig. 2.2d. In this system, an SiO_x thin film coating was deposited from a hexamethyldisiloxane (HMDSO)/O_2 (1:9) plasma (P = 25 W; pressure = 100 mTorr).[8] The third system involved hydrophobic membrane modification of BTS55 membranes, Fig. 2.2a. This system used pulsed hexafluoropropylene oxide (HFPO) plasmas to deposit a thin fluoropolymer membrane coating. The optimal conditions for achieving the desired surface properties were 16%

---

[b]Duty cycle is defined as the ratio of on time to total cycle time multiplied by 100.

duty cycle, 300 W peak applied rf power, pressure of 230 mTorr.[3] These latter two systems used the membrane holder to facilitate modification of the porous structure.

The optimal conditions reported above were determined by exploring the parameter space of each plasma system. Optimization of these systems involved establishing relationships between: 1) the plasma parameters (e.g. plasma power, pressure, treatment time); 2) the membrane composition (X-ray photoelectron spectroscopy, XPS); and the wetting properties (contact angle measurements) of the surface after plasma treatment. As thin film characterization was difficult to perform on these nonplanar substrates, Si wafers and KBr pellets housed in the plasma reactor during deposition were analyzed by FTIR, variable-angle spectroscopic ellipsometry (VASE), and profilometry as described in the following section.

2.2 CHARACTERIZATION METHODS

2.2.1 BUBBLE POINT ANALYSIS. The bubble point of the membrane is the pressure of air needed to expel liquid (e.g. water) from the pores of the membrane.[4] The relationship of the bubble point (P) to the average pore diameter (d) of the membrane, the surface energy of the wetting liquid (γ) and the contact angle (θ) between the wetting liquid and the membrane surface is given by equation 2.1.

$$BP = (4\gamma\cos\theta)/d \qquad (2.1).$$

Thus, the bubble point provides information about the wetting properties with a particular liquid for a membrane with a known average pore diameter. Likewise, the average pore diameter can be determined by porometry using a completely wetting liquid ($\theta = 0$).[4]

Bubble point measurements were obtained with a home-built apparatus consisting of a sample holder (49 cm^2), a pressure gauge and a compressed air cylinder (4.8 grade). Prior to obtaining a bubble point measurement, the membrane was immersed in 100 mL of the wetting liquid. Due to the hydrophobicity of PSf, the membrane was first wet with a 50:50 isopropyl alcohol (IPA)/H_2O solution. The aqueous IPA solution was gradually replaced with deionized water to effectively wet the pores with water. The wet membrane sample was placed in the sample holder between two protective metal screens with the tight side of the membrane upstream of air flow. The delivery pressure was then slowly increased until a breakthrough pressure (i.e. the bubble point) was observed on the pressure gauge located downstream from the sample holder. Unless otherwise noted, bubble points for treated membranes were measured within 24 hours of plasma treatment. The average pore diameter was determined independently using porometry and porisimetry within a few days of plasma treatment at U.S. Filter and Millipore Corporation, respectively

2.2.2 CONTACT ANGLE MEASUREMENTS. Independent of bubble point and porometry analyses, changes in the hydrophilicity induced by plasma treatment were assessed from static contact angles measured by the sessile drop method. In Chapters 3 and 6, these measurements were performed with a contact angle goniometer (Ramé Hart Model 100).[3] All contact angle measurements were made on both sides of water drops at ambient temperature, immediately after 1 μL drops were applied to the surface and the needle tip was removed from the surface. The hysteresis of the water drop was evaluated by measuring the contact angle on both sides of the drop. In addition, measurements were

made on both sides of the untreated and treated membranes. For each sample, three drops were placed at different locations and the average of these measurements is reported for at least three samples. Unless otherwise noted, contact angles were measured immediately after plasma treatment.

In Chapters 4, static contact angles were measured by the sessile drop method with our new contact angle goniometer (Krüss DSA 10) equipped with video capture.[7] The automatic dosing feature of the DSA 10 dispenses a water drop with a known volume (1 μL) on the membrane surface and subsequently withdraws the needle. The video capture system images the water drop on the membrane surface. The advancing CA the drop makes with the surface is analyzed by one of six contact angle profiles available with the DSA 10 imaging software. To ensure no errors were introduced by selection of a fitting routine, our CA values were verified with two contact angle profiles (circle fitting and height/width for contact angles of 15-75°). Measurements were made on both sides of the membranes, using three drops placed at different locations on the membrane. Here, reported CA measurements are the average of the measurements made by the circle fitting method for at least three membranes. Unless otherwise noted, contact angles were measured immediately after plasma treatment.

For most of the plasma-treated membranes, static CA measurements were impossible to perform as the water drop disappeared into the membrane (i.e., contact angle of 0°). To quantify the time it takes for the water drop to completely disappear, a series of images were acquired in the movie mode of the DSA 10. In a typical acquisition, an image was recorded every 50 milliseconds and a water CA was determined for each

image by the circle fitting method. Contact angle as a function of the age of the drop was then plotted to determine the time it took for the membrane to absorb the drop. Unless otherwise noted, these data were obtained immediately after plasma treatment.

2.2.3 ACCELERATED AGING STUDIES. We also analyzed contact angles and bubble points of H_2O plasma-treated membranes exposed to extremes in heat and humidity, Chapter 3.[3] To simulate hot, humid conditions, plasma-treated membranes were placed in a glass, cylindrical membrane holder modified to fit inside a conventional pressure cooker. The pressure cooker was then heated until the pressure inside reached ~15 psi above atmospheric pressure or ~121 °C. Once these conditions were reached, the membrane was steam-treated for 15 minutes. Plasma-treated membranes were also exposed to high, dry temperatures by heating the membranes at 130 °C and 170 °C in a conventional oven for times ranging from minutes to hours.

2.2.4 MEMBRANE STACKED ASSEMBLIES. In Chapters 3 and 4, penetration of our H_2O plasma treatment was demonstrated by treating multiple membranes simultaneously.[3,12] For example, two PSf membranes were stacked in the membrane holder such that both open sides of the membrane faced the inductor coil. As a result of stacking the membranes, the sides of the membranes on the interior of the stacked assembly were not directly exposed to the plasma. We then measured contact angles on all four sides of the membranes *immediately* after plasma treatment.

2.2.5 SCANNING ELECTRON MICROSCOPY. SEM images were obtained using a Phillips 505 microscope with an accelerating voltage of 20-30 keV and a spot size of 50 nm. Prior to SEM analysis, the membrane was affixed to a standard SEM sample

stub by double-sided Cu tape (3M) with the open or tight side face up, depending on which side was imaged. Cross-sectional SEM images were obtained by freeze-fracture of the membrane in liquid nitrogen. To prevent surface charging during SEM analysis, a thin film (20 nm thick) of Au was sputtered onto the surface of all samples prior to imaging.

In Chapter 4, H_2O plasma-treated PES and PE membranes were also evaluated as they wet by an Electroscan Environmental SEM 3 (Phillips Electron Optics) located at Millipore Corporation, Bedford, MA. A portion of each treated membrane sample was freeze-fractured to expose the membrane cross section and mounted on a Peltier stage cooled to 5 °C. The samples were oriented tight side to the top of the frame. The ESEM chamber was evacuated to 5 Torr and then flushed with H_2O vapor to 10 Torr using the flood control. When the chamber pressure reached 5 Torr a second time, the chamber was again flushed with H_2O vapor to 10 Torr. This procedure was repeated a third time to ensure saturation of the chamber environment with H_2O vapor. The chamber pressure was then maintained at 7 Torr. Fine adjustments to both chamber pressure and stage temperature were made to maintain liquid H_2O on the sample stub. A series of images of the membrane wetting *in situ* were acquired with the Orion Image Acquisition System, using a beam accelerating voltage of 10 kV.

2.2.6 X-RAY PHOTOELECTRON SPECTROSCOPY. XPS analyses were performed on a Surface Science Instruments S-probe spectrometer located at the University of Washington, NESAC-BIO center and on a PHI5800 spectrometer located at CSU. The Washington system has a monochromatic Al K_α X-ray source ($h\nu$ = 1486.6 eV), hemispherical analyzer, and resistive strip multichannel detector. A low energy (< 5

eV) electron gun was used for charge neutralization on the nonconducting samples. For all samples, multiple spots were analyzed. Similar conditions were used to collect spectra on the CSU instrument. The compositions were determined from 0-1000 eV survey scans acquired with an analyzer pass energy of 150 eV. The high-resolution C_{1s}, O_{1s}, and S_{2p} spectra were acquired at an analyzer pass energy of 25 eV and collected at a 55° takeoff angle, which is the angle between the surface normal and the axis of the analyzer lens. Spectra and compositional analyses obtained on the two instruments were nearly identical.

2.2.7 FTIR. Transmission FTIR spectra on Si wafers and KBR pellets housed in the plasma reactor during deposition were obtained *ex situ* with a Nicolet Magna 760 FTIR spectrometer using a resolution of 8 cm^{-1} and averaging over 128 scans.[7] The FTIR spectrometer was purged with N_2 during spectra acquisition. Spectra were corrected only for a sloping baseline.

2.2.8 VARIABLE-ANGLE SPECTROSCOPIC ELLIPSOMETRY. Si wafers housed in the plasma reactor during deposition were analyzed by a Woolam VASE32 ellipsometer. Spectra from 65° and 75° were acquired from 240 to 1700 nm for three locations on each sample. All experimental data were simulated using a Cauchy model with film thickness being the only adjustable parameter. Films deposited with 90% O_2, 10% HMDSO plasmas were also reproduced with the SiO_2 model available in the VASE32 software.[9] Film thicknesses were independently confirmed by profilometry. In these measurements, a portion of the Si substrates was masked during deposition and then the resulting step height was measured with a Sloan-Dektak IIA profilometer. Deposition rates were calculated by dividing the average film thickness determined by profilometry

and VASE by the deposition time.

2.3 GAS-PHASE ANALYTICAL METHODS

2.3.1 OPTICAL EMISSION SPECTROSCOPY. All three reactors shown in Fig. 2.1 were fitted with a replaceable fused silica window located at one end of the reactor. The placement of this window in the Figs. 2.1a and 2.1b designs allows coaxial observation of plasma emission. The OES port is oriented perpendicular to the plasma emission in the configuration shown in Fig. 2.1c. Plasma emission was imaged onto the 10 mm entrance slit of an Ocean Optics S2000 triple spectrometer using three optical fibers. The spectrometer is equipped with three 1800 grooves mm holographic gratings and three 2048 element linear charge coupled device-array detectors, allowing detection of wavelengths from 425 to 713 nm. Emission signals were integrated for times between 0.5 and 2 s.

2.3.2 DOSIMETER FOILS. The amount of ionizing and UV radiation generated in our glow discharge was quantified with RISO B3 film dosimeters with a dose range of 5-100 kGy, Chapter 5. The dosimeter films (~ 20 μm thick), used as received, were placed either in the coil region or 9 cm downstream (Fig. 2.1a) and treated with a 25 W H_2O plasma. Upon exposure to ionizing radiation, the films change from clear to pink, allowing for analysis with UV-Visible spectroscopy (Perkin Elmer). From spectra taken between 750 and 250 nm, an absorbance maximum was observed at 554 nm. The intensity of this maximum has been correlated to the amount of ionizing and UV radiation exposure to the dosimeter film by RISO National Laboratory, Roskilde, Denmark.

2.3.3 RADICAL-IMAGING EXPERIMENTS. The IRIS method, Fig. 2.3, has been described in detail previously.[12] In a typical IRIS experiment, feed gases enter a cylindrical, glass tubular reactor similar to that shown in Fig. 2.1a, rf power is applied and a plasma is produced. Expansion of the plasma into a differentially-pumped vacuum system generates an effusive molecular beam consisting of virtually all species present in the plasma, including the species of interest. Based on mean-free path calculations, once the species exit the plasma chamber, a collision-free molecular beam is formed, such that minimal loss of species occurs prior to the interaction region.

An excimer-pumped (XeCl, 100 mJ, 100 Hz) tunable dye laser beam intersects the molecular beam downstream from the plasma source and induces fluorescence of a particular species in the plasma molecular beam. Spatially-resolved LIF signals are collected by an electronically-gated, intensified charge-coupled device (ICCD) located perpendicular to both the molecular beam and the laser beam, directly above the interaction region. A substrate is rotated into the path of the molecular beam and LIF signals are again collected. Differences between the spatial distributions with the surface in and out of the path of the molecular beam are used to measure the ratio of incident radicals in the molecular beam to those scattering off the surface.

A complete description of the model used to quantify IRIS surface reactivity data is given elsewhere.[13] Briefly, our model calculates the spatial distribution of the radical number density along the laser path for molecules in the molecular beam and scattering from the surface and is based on the geometry of the IRIS apparatus. For the scattered molecules, the model assumes a cosine distribution about the surface normal along the

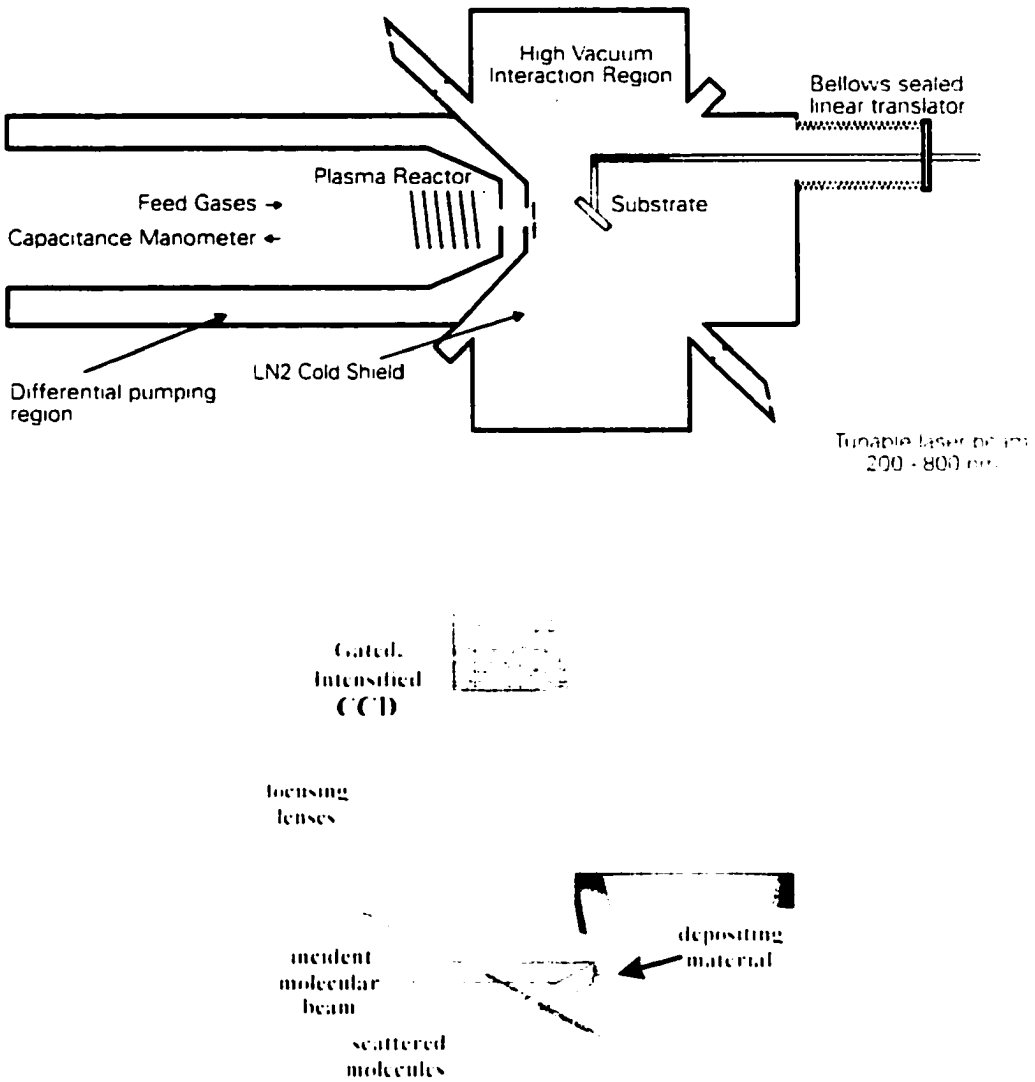

Figure 2.3 Schematic of the IRIS instrument.

laser path. The calculation also assumes all of the incident molecules scatter from the surface. To determine the scattering coefficient, *S*, of the radicals, the generated curve for the scatter is multiplied by a scaling factor to best fit the experimental data. We define surface reactivity, *R*, as 1- *S*. Thus, *R* can be considered as an effective surface loss coefficient for a given species.

In the present work, the IRIS method was used to examine the surface interactions of reactive species in two polymer modification systems: 1) OH radicals produced in H_2O plasmas; and 2) NH radicals produced in NH_3 plasmas. In both IRIS studies, a 340 nm cutoff filter was used between the chamber and the ICCD to minimize collection of light from plasma emission. The ICCD camera had a 1.0 μs gate width, while the gate delay varied between 1.65 and 1.95 μs. Individual images were obtained with 4 x 4 binning, integrating for 60-300 sec. One-dimensional cross sections of the data were produced by averaging 20 columns of pixels (~7 mm) along the laser path. Because we were operating in the power-saturated regime of the laser for both molecules, no corrections for laser power were made.

In Chapter 4, IRIS data were generated by collecting OH LIF signal produced by 307.05 nm excitation (Rhodamine B) of the $A^2\Sigma$ -$X^2\Pi$ (0,0) transition. To eliminate background effects, signal acquired using an off-resonance frequency at 307.15 nm was subtracted from the 307.05 nm data (i.e., on resonance). Data were obtained with a 100% H_2O plasma as the source of the molecular beam, collimated by two slits with widths of 1.2-1.3 mm and 1.5-1.6 mm. The sidearm vacuum flask (250 mL) was heated to maintain a constant H_2O vapor pressure of 50 mTorr (± 2%), measured inside the plasma reactor

with an MKS Baratron capacitance manometer. Data were collected at 25, 75, and 125 W applied rf power using the substrates listed in Table 5.1.

In Chapter 7, IRIS data were generated by collecting NH LIF signal produced by the 336.030 nm excitation of the $A^3\Pi$ - $X^3\Sigma^-$ (0,0) transition. The 336.030 nm data were corrected for background signal from the laser and the plasma. Data were obtained with a 100% NH_3 plasma as the molecular beam source. The first collimating slit was 1.2-1.4 mm wide and was mounted on a liquid nitrogen cold shield cooled to -200 °C. The second slit was 1.4-1.7 mm wide. The total source pressure was maintained in the 40-60 mTorr range, and the flow rate was 20 sccm. NH scatter coefficients were obtained as a function of plasma power (P = 75-225 W) for polyimide, PTFE and platinum substrates. The effects of ion bombardment on the surface reactivity of NH were investigated by placing a grounded mesh (gm) screen on the last defining slit to remove charged species.

2.3.4 MASS SPECTRAL EXPERIMENTS. The addition of a mass spectrometer (Dycor 100) to the IRIS apparatus allows identification of both neutral and ionic species in the molecular beam, Fig. 2.4.[14] Data for the H_2O and NH_3 plasma molecular beams were acquired with the ionizer of the mass spectrometer set to 30 eV. Disabling the ionizer of the mass spectrometer allows identification and detection of the nascent ions generated in the plasma. All of the reported spectra were background subtracted, correcting for the spectrum obtained with just the molecular beam (i.e., no plasma). Additionally, data were collected for the NH_3 plasma molecular beam with and without the gm, Chapter 7. With a membrane on the beam collimating slits, inset of Fig. 2.3, only those species permeating the membrane are detected by the mass spectrometer, Chapter 5.

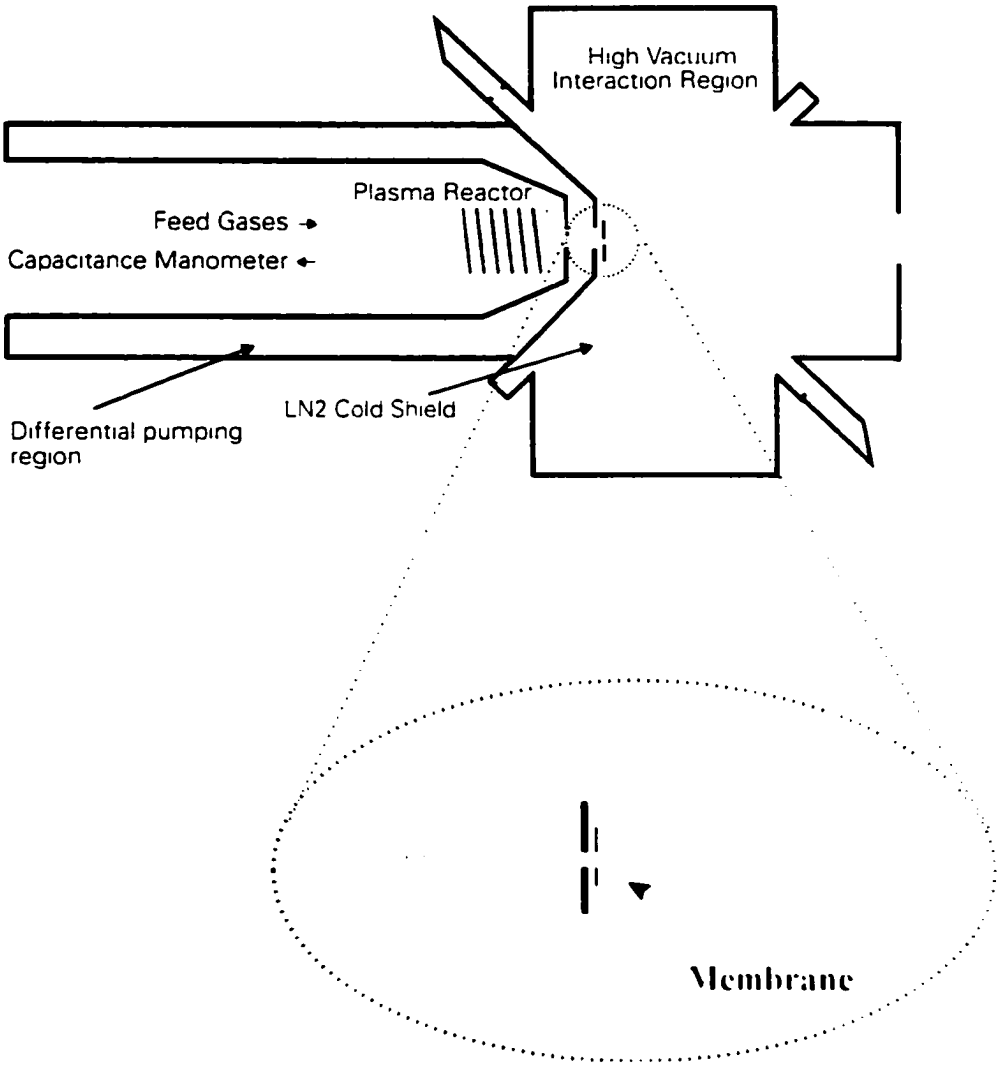

Figure 2.4 Schematic of the modified molecular beam apparatus used to perform mass spectral experiments. Inset shows detail of the mass spectral experiment when a membrane is placed on the beam collimating slits. In this configuration, plasma species permeating the membrane are detected downstream by the mass spectrometer.

2.4 REFERENCES

1. N. M. Mackie, N. F. Dalleska, D. G. Castner, and E. R. Fisher. *Chem. Mater.* **9,** 349 (1997).
2. C. I. Butoi, N. M. Mackie, L. J. Gamble, D. G. Castner, J. E. Barnd, A. M. Miller, and E. R. Fisher. *Chem. Mater.* **12,** 2014 (2000).
3. M. L. Steen, L. Hymas, E. D. Havey, N. E. Capps, D. G. Castner, and E. R. Fisher. *J. Memb. Sci.* **188,** 97 (2001).
4. M. Mulder. *Basic Principles of Membrane Technology*, 2nd Ed., (Kluwer Academic Press: New York, 1996), p. 13.
5. V. M. Cepak, J. C. Hulteen, G. C. Che, K. B. Jirage, B. B. Lakshmi, E. R. Fisher, and C. R. Martin. *J. Mater. Res.* **13,** 3070 (1998).
6. V. P. Menon and C. R. Martin *Anal. Chem.* **67,** 1920 (1995); M. Nishisawa, V. P. Menon, and C. R. Martin. *Science* **268,** 700 (1995).
7. Duty cycle is defined as the ratio of on time to total cycle time multiplied by 100.
8. M. L. Steen and E. R. Fisher. *J. Electrochem. Soc.*, manuscript in preparation.
9. See reference 4, p. 165.
10. See reference 4, p. 167.
11. M. L. Steen, A. C. Jordan, and E. R. Fisher. *J. Memb. Sci.*, submitted for publication.
12. P. R. McCurdy, K. H. A. Bogart, N. F. Dalleska, and E. R. Fisher. *Rev. Sci. Instrum.* **68,** 1684 (1997).
13. K. H. A. Bogart, J. P. Cushing, and E. R. Fisher. *Chem. Phys. Lett.* **267,** 377 (1997); K. H. A. Bogart, J. P. Cushing, and E. R. Fisher. *J. Phys. Chem. B* **101,**

9425 (1997).

14. C. I. Butoi, M. L. Steen, J. R. D. Peers, and E. R. Fisher, *J. Phys. Chem. B*. **105**, 5957 (2001).

CHAPTER 3

LOW-TEMPERATURE PLASMA TREATMENT OF ASYMMETRIC POLYSULFONE MEMBRANES FOR PERMANENT HYDROPHILIC SURFACE MODIFICATION

Reprinted with permission from: M. L. Steen, L. Hymas, E. D. Havey, N. L. Capps, and E. R. Fisher, *Journal of Membrane Science*, Vol. 188, 97-114 (2001).

This dissertation chapter contains results from a full paper published in *Journal of Membrane Science*. The manuscript was written by M. L. Steen and edited by Professor E. R. Fisher. This chapter describes permanent hydrophilic modification of microporous and ultrafiltration polysulfone membranes. Membrane processing conditions and the plasma reactor configuration are discussed. The results of extensive materials characterization for plasma-treated membranes are presented. In addition, this chapter explores the extent and permanence of the hydrophilic modification.

3.1 INTRODUCTION

Asymmetric membranes are ubiquitous in numerous ultrafiltration processes (e.g., food and dairy industries, pharmaceuticals, water treatment).[1] Furthermore, asymmetric polysulfone (PSf) membranes are the mostly widely used as PSf, a thermoplastic, is heat and somewhat chemically resistive. One issue with using these membranes in protein-based separations is membrane fouling, which is partially the result of the hydrophobicity of PSf. This problem severely limits the long-term use of these membranes in many filtration systems. Thus, it is desirable to use a polymeric membrane with a hydrophilic surface, requiring the use of a wetting agent. Extractables from the wetting agent may leach out of the membrane, causing contamination of the permeate and loss of hydrophilicity. Thus, developing a robust treatment to make PSf membranes hydrophilic, has been an important but elusive goal.[2]

Other issues associated with making PSf membranes hydrophilic include penetration of the treatment and alteration to the bulk properties of the material. Conceivably, a particular method may modify the outer surfaces of the membrane without achieving the desired modification inside the pore cavities. Furthermore, the treatment should not overly reduce the permeability (i.e., water flux) of the membrane. Other adverse physical changes to be avoided include embrittlement, shrinkage, and pinhole defects. Therefore, the optimal method for making polymeric membranes more wettable would achieve the desired modification to *all* surfaces of the membrane without altering its bulk physical properties.

One option is to treat PSf membranes with a low-temperature plasma to achieve

the desired change in hydrophilicity.[3,4] Plasma modification of polymeric membranes is a logical extension of the technological and industrial utility of plasmas to improve wetting properties of polymers.[5,6] As noted in Chapter 1, surface oxidation by plasma treatment (e.g. O_2 and H_2O) improves the wettability of polymers such as polyethylene (PE) and poly(methyl methacrylate);[7] however, there is also a lack of permanency resulting from surface rearrangement for these treatments.[5] Indeed, previous attempts to make PSf membranes hydrophilic by plasma treatment, primarily with O_2 plasma, resulted in only transient hydrophilicity with contact angle changes within 24 hours of plasma treatment.[3] Furthermore, only the outer membrane surface was modified.

As noted in Chapter 1, there are two main works in the literature that focus on using H_2O-based plasmas to modify PSf membranes. The first entails H_2O and air plasma treatment of polyetherimide and PSf plane and hollow fiber membranes for hydrophilic modification.[8] The second describes H_2O/He plasma treatment of polyacrylonitrile and PSf ultrafiltration (UF) membranes to promote anti-fouling properties.[9] Neither of these studies investigated the extent of plasma modification through the cross section of the materials. Limited chemical analysis is provided in both studies, making it difficult to determine the actual chemical and physical changes resulting from plasma treatment. Moreover, the first work did not report the permanence of the hydrophilic modification and the second work found that the membrane modification was not permanent upon storage in air, with significant contact angle increases over time.

Here, we report results for a H_2O plasma treatment developed in our laboratory that renders PSf membranes completely hydrophilic. Treated membranes remain wettable

for a minimum of eighteen months after plasma treatment. The dramatic change in wettability we observe is a result of chemical changes in the membrane induced by plasma treatment. Furthermore, we have substantial evidence that our H_2O plasma treatment penetrates the thickness of the membrane, equally modifying both sides of the membrane.

3.2 RESULTS

3.2.1 HYDROPHILIC SURFACE MODIFICATION. The nomenclature used to categorize PSf membranes (Table 3.1) corresponds to the nominal bubble point of the membrane. For example, BTS55 and BTS80 membranes have nominal bubble points of 55 psi and 80 psi, respectively. Table 3.1 shows bubble points measured in our laboratory for untreated PSf membranes. The bubble points measured were typically 10 psi higher than the nominal bubble point for the material. BTS55 membranes gave the best agreement between our measurements (57.0 ± 3.3 psi) and the nominal bubble point. As a result, BTS55 membranes were used in our initial parameter space study of applied plasma power, H_2O vapor flow rate (pressure), and treatment time. BTS55 membranes were treated with a 25 W H_2O vapor plasma (50 mTorr total pressure) for times ranging from 15 seconds to 10 minutes. Figure 3.1 shows there is a 20-25 psi increase in the bubble point for all treatment times examined (0.25-10 min). An increase in the bubble point could be a result of a decrease in the contact angle *or* a decrease in the overall pore diameter. Hence, the observed change in bubble point for treated membranes may correspond to an increase in hydrophilicity or to adverse physical alteration in membrane structure as a result of plasma treatment.

Table 3.1. Bubble points measured for untreated PSf membranes.

Membrane[a]	Average Pore Size (μm)	Bubble Point (psi)[b]
BTS5	1.2	14.6 ± 1.7
BTS25	0.45	40.4 ± 2.9
BTS55	0.2	57.0 ± 3.3
BTS80	0.1	92.6 ± 3.2
UF	~0.01[c]	N.A[d]

[a]The numbers 5, 25, 55 and 80 refer to the nominal bubble point of the membrane with water.

[b]Bubble point determined in our laboratory.

[c]Molecular weight cutoff ~100 kD.

[d]Could not be tested as pressures higher than those used for a standard test are required.

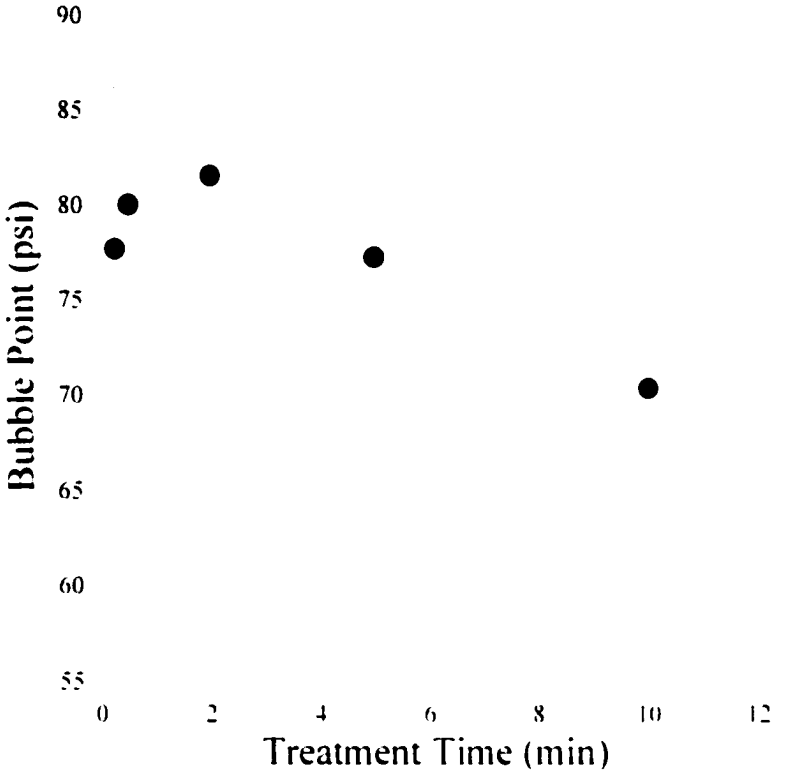

Figure 3.1 Bubble point as a function of treatment time for BTS55 membranes treated with H_2O plasma (25 W, 50 mTorr). Dashed line indicates bubble point for untreated BTS55. Error bars represent deviations in the bubble point measured for a minimum of three treated membranes.

To ascertain whether the plasma adversely altered the physical properties (i.e. pore size) of the membrane, SEM images were obtained for treated BTS55 membranes, Fig. 3.2. The open sides of the membranes were imaged as these sides were oriented closest to the plasma glow during treatment and were, therefore, more likely to be physically damaged by the plasma than the downstream sides. These images are compared to that of an untreated membrane (Fig. 3.2a). It is evident that prolonged exposure to H_2O plasma ($\geq$10 minutes) introduces visible pitting of the membrane surface, thereby increasing the porosity of the membrane (Fig. 3.2c). Membranes treated for 2 minutes, however, do not exhibit any structural damage (Fig. 3.2b). Applied plasma powers >25 W also adversely affect the structural integrity of the membrane, as demonstrated by the image in Fig. 3.2d for a 100 W H_2O plasma treatment. Thus, high applied rf powers and prolonged plasma exposure were avoided and typical treatments employed relatively low plasma powers (25 W) and pressures (50 mTorr) for short times ($\sim$2 min).

In addition to SEM analysis, changes in pore diameter of PSf membranes were quantified by porometry. Porometry results for treated BTS55 membranes are summarized in Table 3.2. These results indicate that the average pore size or mean flow pore (MFP) is negatively affected by plasma treatment. Overall, pore sizes are ~35% larger than pore sizes for the untreated; however, the pore sizes of the treated membranes are nearly identical to the values obtained for BTS55 membranes treated with a wetting agent.[2] Therefore, our plasma treatment produces comparable results to those obtained by the convention of applying a wetting agent to make hydrophobic membranes hydrophilic.

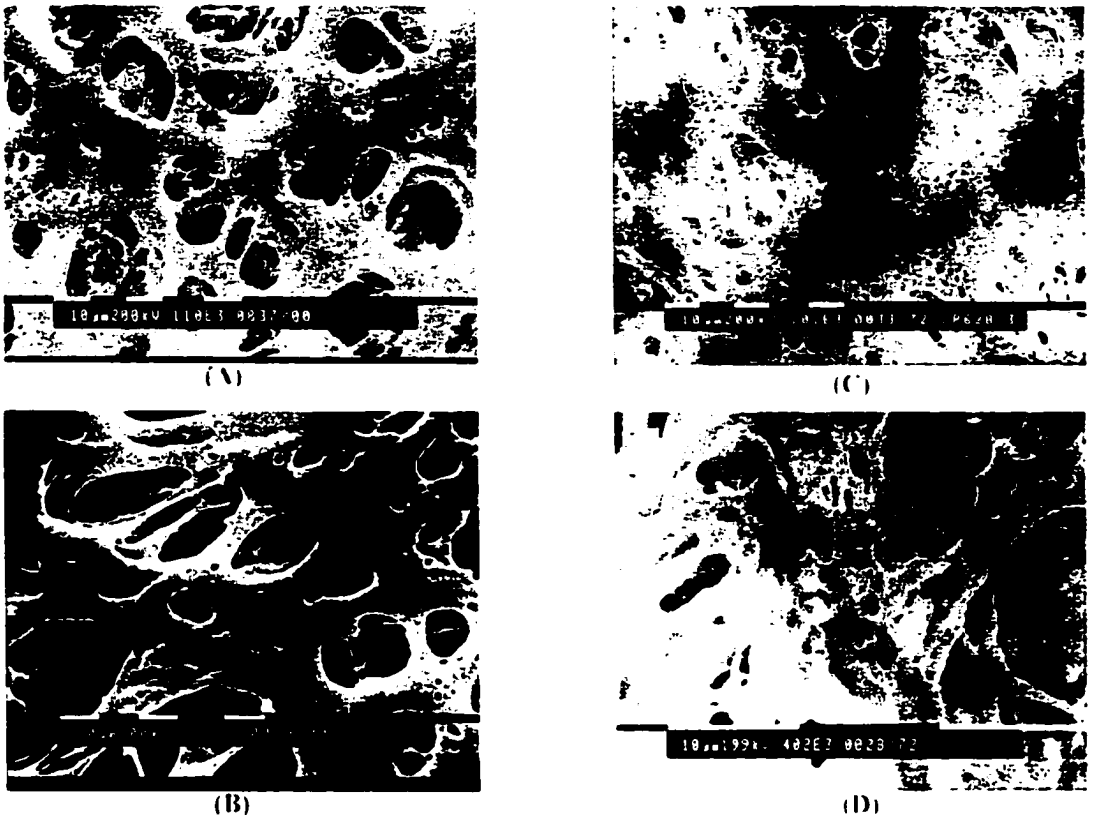

Figure 3.2 SEM images of BTS55 membranes: A) untreated; B) treated with a 25 W H_2O plasma for two minutes; C) treated with a 25 W H_2O plasma for ten minutes; and D) treated with a 100 W H_2O plasma for two minutes. All images are taken of the open side of the membranes, upstream during plasma treatment. No physical changes were observed on the tight side of the membranes, regardless of plasma conditions.

Table 3.2 Porometry data for untreated and treated PSf membranes.

Membrane[a]	Mean Flow Pore (μm)	Max. Pore (μm)	Min. Pore (μm)
untreated BTS55	0.165	0.212	0.133
treated BTS55	0.221	0.327	0.178
untreated BTS80	0.084	0.100	0.080
treated BTS80	0.095	0.164	0.082

[a] UF membranes could not be tested as the tight pores associated with these membranes require pressures higher than those used for a standard test.

To determine whether H_2O plasma treatment improves the hydrophilicity of PSf membranes, water contact angles were measured on both membrane surfaces *immediately* after plasma treatment. Table 3.3 summarizes the results of these measurements. For both sides of the untreated membranes, the average contact angle is ~90°. Contact angle measurements on treated BTS55 membranes were impossible to perform as the water drop immediately disappeared into the membrane (i.e., contact angle of 0). This effectively demonstrates that these membranes are rendered completely water-wettable as a result of H_2O plasma treatment. Furthermore, the upstream and downstream sides of the treated membranes are both completely wettable. This is an important result as it suggests that the plasma penetrates the thickness of the membrane (~125 μm), thereby equally modifying both sides of the membrane.

For comparison, we also placed a non-porous PSf resin in the membrane holder and treated it with identical plasma conditions. Table 3.3 includes the results of contact angle (CA) measurements before and immediately after plasma treatment. The side of the resin closest to the inductor coil (Side A) was more wettable after treatment than before treatment. However, the downstream side (Side B) was not as wettable as the upstream side, suggesting that the complete modification of PSf membranes is related to their high porosity. One possible explanation for the observed decrease in the CA on the downstream side of the resin is the low (but non-zero) gas permeability of the polymer.

We tested the effectiveness of the H_2O plasma treatment by extending the study to other PSf membranes. BTS80 (0.1 μm diam.) and UF (~0.01 μm diam.) membranes (Table 3.1) were treated with a H_2O plasma for 2 minutes. Table 3.3 lists the contact

Table 3.3. Contact angles[a] for untreated, treated and aged PSf materials.

	BTS55		BTS80		UF	
	open	**tight**	**open**	**tight**	**open**	**tight**
untreated	90.0 ± 9.0°	86.2 ± 9.3°	79.7 ± 4.7°	79.0 ± 2.0°	64.3± 4.7°	66.3 ± 4.7°
treated	wettable	wettable	wettable	wettable	wettable	wettable

	PSf resin	
	Side A[b]	**Side B[c]**
untreated	73.0 ± 2.0°	71.0 ± 2.0°
treated	14.9 ± 5.5°	44.4 ± 13.1°

[a]Values reported are the average of a minimum of three drops on each side of the material.

[b]Side A faces the inductor coil during plasma treatment.

[c]Side B is downstream from the inductor coil during plasma treatment.

angles measured on both sides of these materials before and after plasma treatment. These results are analogous to those obtained for BTS55 membranes. Both sides of BTS80 and UF membranes were rendered completely wettable as a result of plasma treatment. Porometry results obtained for BTS80 membranes before and after plasma treatment are similar to those obtained for BTS55 membranes (Table 3.2). Overall, an increase in the pore sizes associated with BTS80 and BTS55 membranes is observed after plasma treatment. As noted above, this phenomenon is also observed for membranes treated with a chemical wetting agent.

3.2.2 PERMANENCE OF HYDROPHILIC MODIFICATION. We have examined the permanence of our plasma treatment by measuring contact angles and bubble points for samples aged days, weeks, and months after plasma treatment. Figure 3.4 shows the effect of aging on the average bubble point of treated BTS55 membranes. The average bubble point, analyzed *immediately* after plasma treatment, is 75 ± 2 psi. This is ~20 psi higher than the average bubble point for untreated BTS55 membranes (57 ± 3 psi). Figure 3.4 illustrates that the average bubble points measured for samples aged for up to one month decrease slightly from the average bubble point of samples analyzed immediately after plasma treatment, but remain ~20 psi higher than the average bubble point of untreated BTS55 membranes. These results indicate that the change in the bubble point observed for plasma-treated membranes is not affected by aging.

The most compelling evidence for the permanence of our hydrophilic modification is contact angle measurements made on plasma-treated samples stored under ambient laboratory conditions. BTS55, BTS80, and UF membranes remain completely wettable

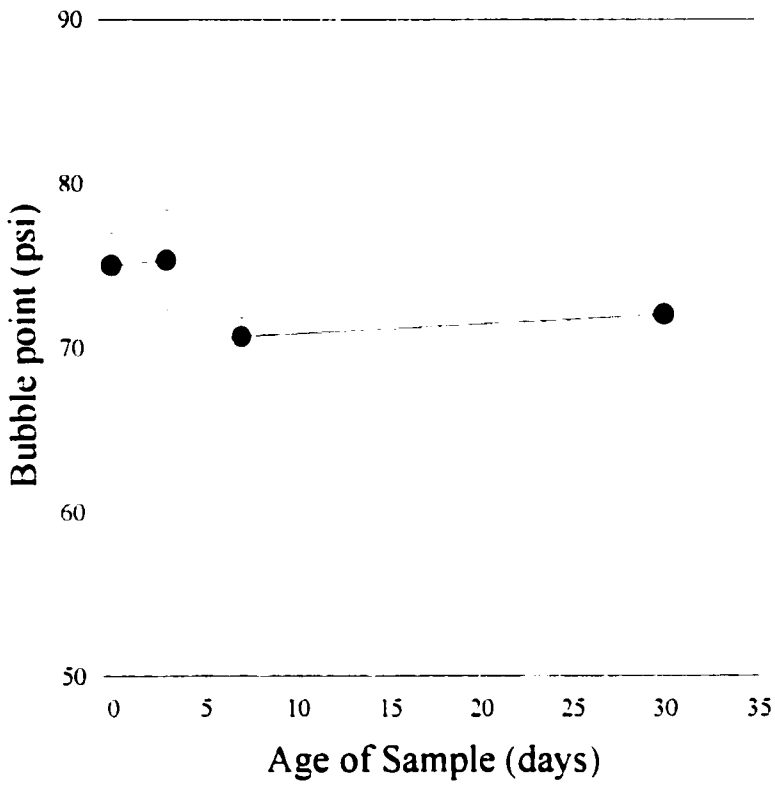

Figure 3.4 Bubble point as a function of time after plasma treatment for BTS55. Dashed line indicates bubble point for untreated BTS55. Treated samples stored in ambient conditions. Error bars represent deviations in the bubble point measured for a minimum of three treated membranes.

for at least eighteen months after plasma treatment. In contrast, previous attempts to make PSf membranes hydrophilic by plasma treatment resulted in significant contact angle changes within 24 hours of treatment.[29] Our results clearly indicate that our plasma treatment of both microporous and UF PSf membranes is permanent, as it withstands long-term aging under ambient conditions.

3.2.3 ACCELERATED AGING STUDIES. The permanence of the hydrophilic membrane modification was further tested by subjecting plasma-treated BTS55 membranes to accelerated aging. These experiments exposed membranes to extremes in humidity and temperature (e.g., steam, boiling H_2O and "dry" heat). The permanence of the modification was then determined by measuring contact angles and bubble points after the wet or dry treatment. CA measurements for the steam-treated membranes indicated they were less wettable than plasma-treated membranes without steam treatment; however, a visible contact angle could not be measured on either side of the steam-treated membranes. Specifically, steam-treated membranes did not immediately absorb the water drop, but absorbed the drop in ~ 60 seconds. Although steam-treated BTS55 membranes do not lose hydrophilicity, steam treatment affects the instantaneous wettability of the membranes. However, the average bubble point of plasma-treated membranes analyzed after steam treatment (72 ± 1 psi) is essentially unchanged from the average bubble point measured immediately after plasma treatment (75 ± 2 psi).

Plasma-treated membranes were steam-treated under the same conditions three times in succession, drying between steam cycles. Contact angles were measured on each side of the membrane following the last steam treatment. The results obtained for multiple

steam treatments were similar to those obtained for membranes steamed only once. Overall, the steam-treated membranes did not immediately absorb the water drop but instead absorbed the drop in ≤90 seconds. Likewise, the average bubble points obtained for membranes steamed multiple times are identical to the average bubble point obtained for membranes steamed only once. Therefore, repeated steam treatments do not cause further losses in hydrophilicity.

As another test of extreme conditions, plasma-treated BTS55 membranes were placed in a clean beaker of boiling H_2O (MΩ) for one hour. The membranes were then allowed to completely dry in air. CA measurements performed after treatment showed an increase to ~65° for both sides of the membranes. While this is a significant increase, it is still not comparable to contact angles for untreated BTS55 membranes (~90°).

We also examined the effect of hot, dry conditions on the hydrophilicity induced by H_2O plasma treatment by heating plasma-treated BTS55 membranes in an oven. Contact angles were measured on both sides of the membrane after heat treatment. Contact angles measured for membranes heated at 130 °C as a function of heat treatment time are shown in Figs. 3.5 and 3.6. Overall, heat treatment has a deleterious effect on the plasma-induced hydrophilicity as CA changes are measured after heat treatment; however, the plasma-treated membranes never reverted to the degree of hydrophobicity associated with the untreated material. For example, Fig. 3.5 illustrates that the average CA for both the open and tight sides of the membrane does not exceed 60° even after heating for four hours at 130 °C. This is similar to what was observed for the boiling H_2O experiment.

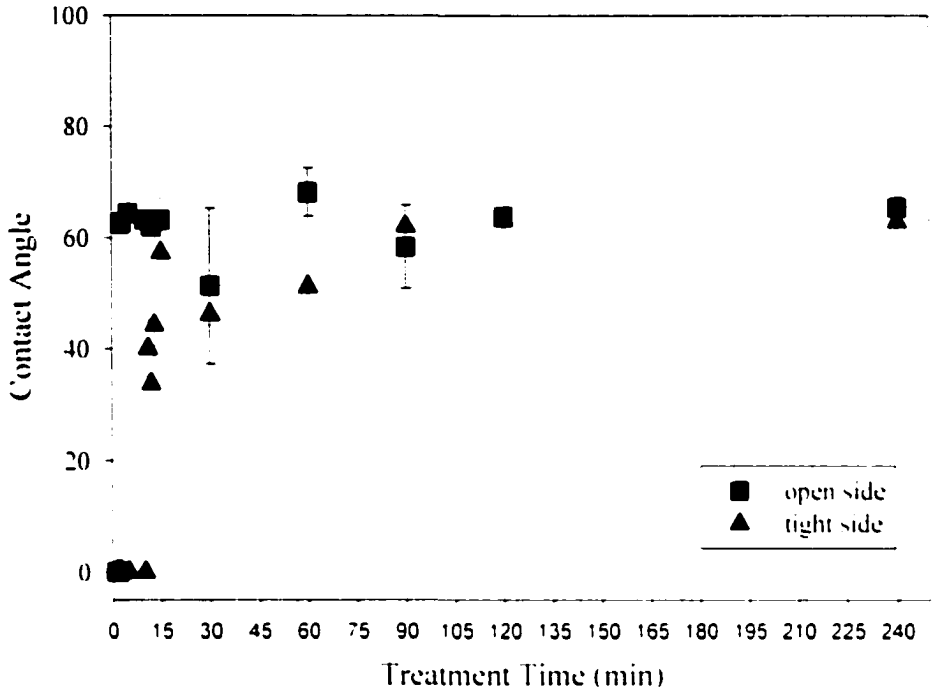

Figure 3.5 Contact angle for treated BTS55 as a function of heat treatment. Treated membranes were heated in a conventional oven at 130 °C for a maximum of four hours. Contact angles were measured on both the open (■) and tight (▲) sides of the membrane after heat treatment. Data for membranes heated at 170 °C for 4 hours was not shown for clarity.

There is a significant difference in the time required for the open and tight sides to lose plasma-induced hydrophilicity, Fig. 3.6. Specifically, the contact angle on the open side increases to > 60° if heated for 2.5 minutes or longer at 130 °C. Conversely, the tight side of the membrane remains wettable until heated for ~10 minutes at 130 °C. This effect is not dependent on the orientation of the membrane in the oven during heat treatment, as the tight side remains wettable for much longer (~8-10 min) than the open side (~2 min) under *all* heating conditions.

Results for plasma-treated membranes heated at 170 °C are also shown in Fig. 3.6. At this higher temperature, the contact angles on *both* the open and tight sides increase to >60° after being heated for 2.5 minutes. Therefore, heat-treating at higher temperatures causes an immediate decay of the plasma-induced hydrophilicity, in contrast to the gradual decay observed for membranes heated at 130 °C. Notwithstanding, the plasma-treated membranes never revert to the degree of hydrophobicity of the untreated material even after 4 hours at 170 °C.

3.2.4 PENETRATION OF PLASMA TREATMENT. We devised an experiment to further investigate the penetration of the plasma treatment by treating multiple membranes simultaneously. Two membranes were stacked in the membrane holder such that both open sides of the membrane faced the inductor coil. As a result of stacking the membranes, the sides of the membranes on the interior of the stacked assembly were not directly exposed to the plasma. We then measured water contact angles on all four sides of the membranes *immediately* after plasma treatment.

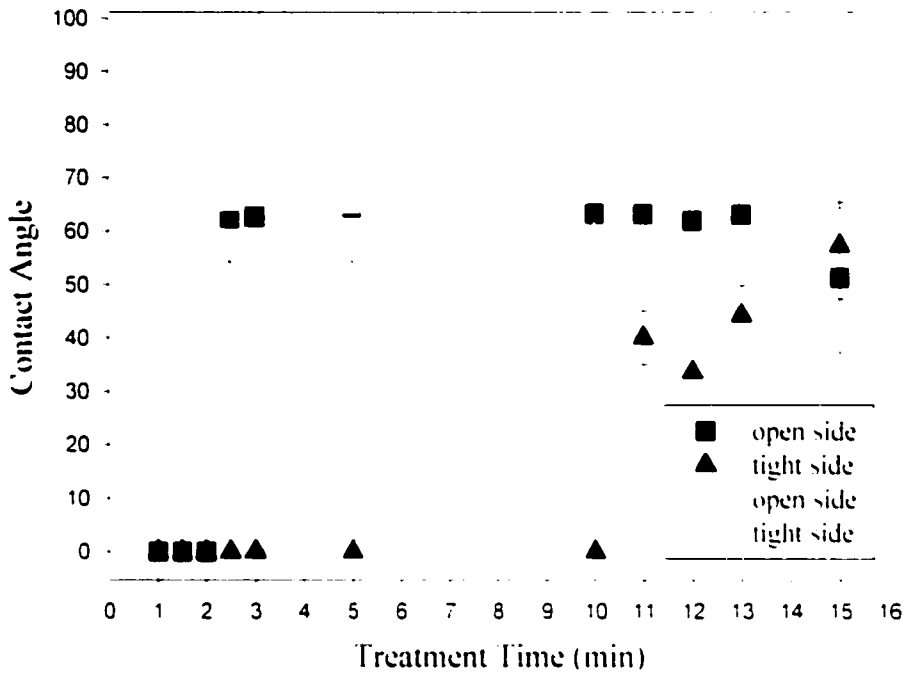

Figure 3.6 Contact angles for plasma-treated BTS55 as a function of heat treatment. Treated membranes were heated in a conventional oven at 130° C (closed symbols) and 170° C (open symbols). Data shown are for membranes heated for a maximum of 15 min. Contact angles were measured on both the open (squares) and tight (triangles) sides of the membrane after heat treatment.

Table 3.4 includes the results for experiments in which two BTS55 membranes were simultaneously treated for either 2 or 3 minutes. In both cases, the surfaces of the membrane closest to the inductor coil (surfaces 1 and 2) were completely wettable after plasma treatment. Likewise, the open side of the second membrane (surface 3) was also completely wettable after plasma treatment. The only way the surfaces on the interior of the stacked assembly (surfaces 2 and 3) could be treated by the plasma is if the plasma penetrated the thickness of the membrane closest to the inductor coil.

For the 2 minute plasma treatment, the surface farthest downstream from the inductor coil (surface 4) was less wettable than the other three surfaces of the membranes in the stacked assembly. Although surface 4 was not completely wettable, a decrease in the contact angle relative to the untreated membrane was observed. Increasing the treatment time to 3 minutes resulted in all four surfaces of the membranes being rendered completely wettable. These results estimate the depth of penetration of our plasma treatment to be at least 250 μm or the thickness of two membranes.

We also investigated whether the porosity of the PSf membranes affects the depth of penetration of plasma treatment. Table 3.4 summarizes the results of multiple membrane experiments performed for BTS80 and UF membranes at different treatment times. For both sets of experiments, the surfaces of the membrane closest to the inductor coil (surfaces 1 and 2) are completely wettable after a 2 minute plasma treatment. In contrast to the results obtained for BTS55 membranes, surfaces 3 and 4 of treated BTS80 and surfaces 2, 3, and 4 in the UF experiment were not immediately completely wettable after a 2 minute plasma treatment. These results indicate that the low porosity associated

Table 3.4 Results for multiple membranes experiments.

Treatment	Time (min)	H_2O Contact Angle[a]			
		Side 1 (open)[b]	Side 2 (tight)[c]	Side 3 (open)[c]	Side 4 (tight)[d]
BTS55	2	wettable	wettable	wettable	55.3 ± 3.1°
BTS55	3	wettable	wettable	wettable	wettable
BTS80	2	wettable	wettable	62.7 ± 2.7°	wetted <60 s[e]
BTS80	5	wettable	wettable	wettable	wettable
UF	2	wettable	wetted <90 s[e]	wetted <90 s[e]	55.3 ± 3.1°
UF	6	wettable	wettable	wettable	wettable

[a]Values reported are the average of a minimum of three drops on each side of the material.

[b]Side of membrane closest to coil.

[c]Sides of membrane on interior of stacked assembly.

[d]Side of membrane farthest downstream from coil.

[e]Water drop did not immediately absorb, but was completely absorbed in the time indicated.

with these membranes affects the throughput of the plasma necessary to treat those sides not directly exposed to the plasma glow. All four surfaces of the BTS80 and UF membranes can be rendered completely wettable by increasing the treatment time, with UF membranes requiring the longest treatment time (~ 6 min) to obtain wettability for all four sides. This suggests that the relatively low porosity of the UF materials slows, but does not prevent simultaneous plasma modification of multiple membranes.

3.2.5 SURFACE COMPOSITION. We ascertained the chemical changes that occur in PSf membranes as a result of H_2O plasma treatment by XPS analysis. Tables 3.5 and 3.6 summarize the results from XPS analysis for treated and untreated BTS55 membranes. The elemental composition for the untreated membrane is in excellent agreement with the structure of PSf, Table 3.5. In addition, no significant difference in composition was detected between the open and tight sides of the untreated BTS55 membrane.

The results in Table 3.5 indicate that H_2O plasma treatment increases the oxygen concentration of PSf membrane surfaces. Data for membranes aged ~1-4 days show the oxygen content for both sides of membranes (~22%) is significantly higher than that for the untreated membrane (~12%). Specifically, the increase in the high binding region of the C_{1s} spectrum upon treatment is consistent with the presence of ketone/aldehyde and carboxylic acid/ester groups. Table 3.6 provides the detailed results of the C_{1s} spectrum for untreated and treated BTS55 membranes (aged ~1-4 days). As a result of plasma treatment, the CH_x percentage decreases relative to the untreated material. This decrease is counterbalanced by an increase in the percentages of C-O and C-O_x groups. As there

Table 3.5. XPS results for controls, untreated and plasma-treated BTS55.[a]

Material	XPS Atomic Percent				
	C	O	S	F	N
PTFE	33.8 ± 0.2			66.2 ± 0.2	
TFAA-PS[b]	99.9 ± 0.1				
TFAA-PVA[c]	44.9 ± 0.2	20.4 ± 0.2		34.6 ± 0.1	
Stoichiometric Psf	84.4	12.5	3.1		
untreated PSf (open)	84.3 ± 0.8	12.0 ± 0.5	3.7 ± 0.3		
untreated PSf (tight)	84.5 ± 0.2	11.8 ± 0.1	3.7 ± 0.3		
treated PSf (open)[d]	74.4 ± 0.2	22.1 ± 0.5	2.6 ± 0.1		0.7 ± 0.2
treated PSf (tight)	73.7 ± 0.6	21.5 ± 0.1	2.6 ± 0.1		0.6 ± 0.1
aged PSf (open)[d,e]	67.7	26.5	2.0		1.0
aged PSf (tight)[e]	74.7	21.8	2.4		0.6
untreated open-TFAA[f]	82.2 ± 0.2	13.0 ± 0.2	3.5 ± 0.1	1.2 ± 0.2	
untreated tight-TFAA	80.6 ± 0.4	13.7 ± 0.2	3.8 ± 0.2	1.5 ± 0.2	
treated open-TFAA	73.1 ± 0.8	18.9 ± 0.3	2.8 ± 0.1	4.2 ± 0.2	0.6 ± 0.3
treated tight-TFAA	72.1 ± 0.8	18.8 ± 0.1	2.4 ± 0.1	5.7 ± 0.3	

[a]Unless otherwise noted, all data were acquired ~1-4 days after plasma treatment.

[b]Negative derivatization control.

[c]Positive derivatization control.

[d]Trace impurities (<1%) of atomic silicon also detected.

[e]Data acquired on samples aged ~1 year. Errors on these values are estimated to be ±1%.

[f]Trace impurities (<1%) of atomic sodium also detected.

Table 3.6 XPS C_{1s} Percent for controls, untreated and plasma-treated BTS55.[a]

Sample	XPS C_{1s} Percent				
	CH_x	C-O	C-Ox[b]	CF_2	CF_3
PTFE				100	
TFAA-polystyrene[c]	100				
TFAA-polyvinylalcohol[d]	28	25	23		24
PSf	85	15			
untreated PSf (open)	84	16			
untreated PSf (tight)	83	17			
treated PSf (open)	75	19	9		
treated PSf (tight)	74	18	8		
treated PSf (open)- TFAA	76	17	6		1

[a]Data listed were acquired ~1-4 days after plasma treatment.

[b]C-O_x is the total amount of C=O, O=C-O, etc.

[c]Negative derivatization control.

[d]Positive derivatization control.

are no C-O_x groups present in the untreated material, these functional groups must be introduced by the plasma treatment. From the high-resolution S_{2p} spectra, a small amount of sulfate-like groups were also introduced by the plasma treatment. These results suggest that the increase in hydrophilicity observed for H_2O plasma-treated membranes is indeed a result of the formation of covalently bound hydrophilic functional groups.

The membranes were further derivatized with trifluoroacetic anhydride (TFAA) to detect the presence of OH groups introduced by plasma treatment. Quantification of the surface alcohol content was obtained using the trifluoroacetic anhydride (TFAA) derivatization technique. This allows differentiation between C-O-H and C-O-C. In this procedure, hydroxyl groups are converted to $OC(O)CF_3$ groups via an esterification process.[10,11] As shown in Table 3.6, a small number of OH groups (~1%, as 3 F atoms are substituted for each OH group) are incorporated; however, it is essential to consider possible cross-reactions and derivatization efficiencies when analyzing the results of the TFAA derivatization experiments.[11] Thus, this should be considered as an upper limit to the amount of OH present on the surface of the membrane.

XPS analysis was also performed on treated samples aged ~1 year. Overall, the membranes retained their increased oxygen content and the same functional groups were detected in the C_{1s} spectrum. There was, however, an additional increase in the oxygen content (~26%) for the open side of the membrane, relative to the tight side (~22%). This difference is likely the result of a higher concentration of trapped radicals on the open side of the membrane as it was the side directly exposed to the plasma.

3.2.6 ALTERNATE PLASMA TREATMENTS. To determine the effects of various possible reactive species in our plasmas and for comparison to previous literature results,[5,7,12] the alternate plasma systems of 100% O_2, 100% Ar, and 100% He were examined. With O_2 plasma treatment, both surfaces of BTS55 were rendered completely wettable after plasma treatment. Similar to prior attempts to make PSf membranes permanently hydrophilic by O_2 plasma treatment, the improvement in hydrophilicity was not permanent and significant contact angle increases were observed within 3 days of treatment. With both the Ar and He plasmas, only the upstream side became hydrophillic. The downstream side displayed reduced contact angles of ~75 . Upon standing, contact angle increases were observed within days after treatment. Thus, all three plasma treatments do afford temporary changes in wettability, but none are permanent modifications. Moreover, the rare gas plasmas do not equally modify both surfaces, suggesting complete penetration by reactive species is not achieved in these systems.

3.2.7 CHEMICAL COMPOSITION OF H_2O PLASMA. One important factor contributing to the observed differences in membrane treatments between the H_2O system and the alternate plasmas discussed in Section 3.2.6 is the chemical nature of the plasma species. Figure 3.7a shows an optical emission spectrum of a 25 W H_2O vapor plasma (50 mTorr), providing data on the excited-state gas-phase composition of the plasma. This spectrum identifies the presence of OH radicals (at 306.95 and 309.14 nm), as well as H atoms (at 486.18 and 656.45 nm) in the H_2O plasma. No emission from other species is observed.

Figure 3.7b shows the OES spectrum of a 25 W H_2O vapor plasma (50 mTorr)

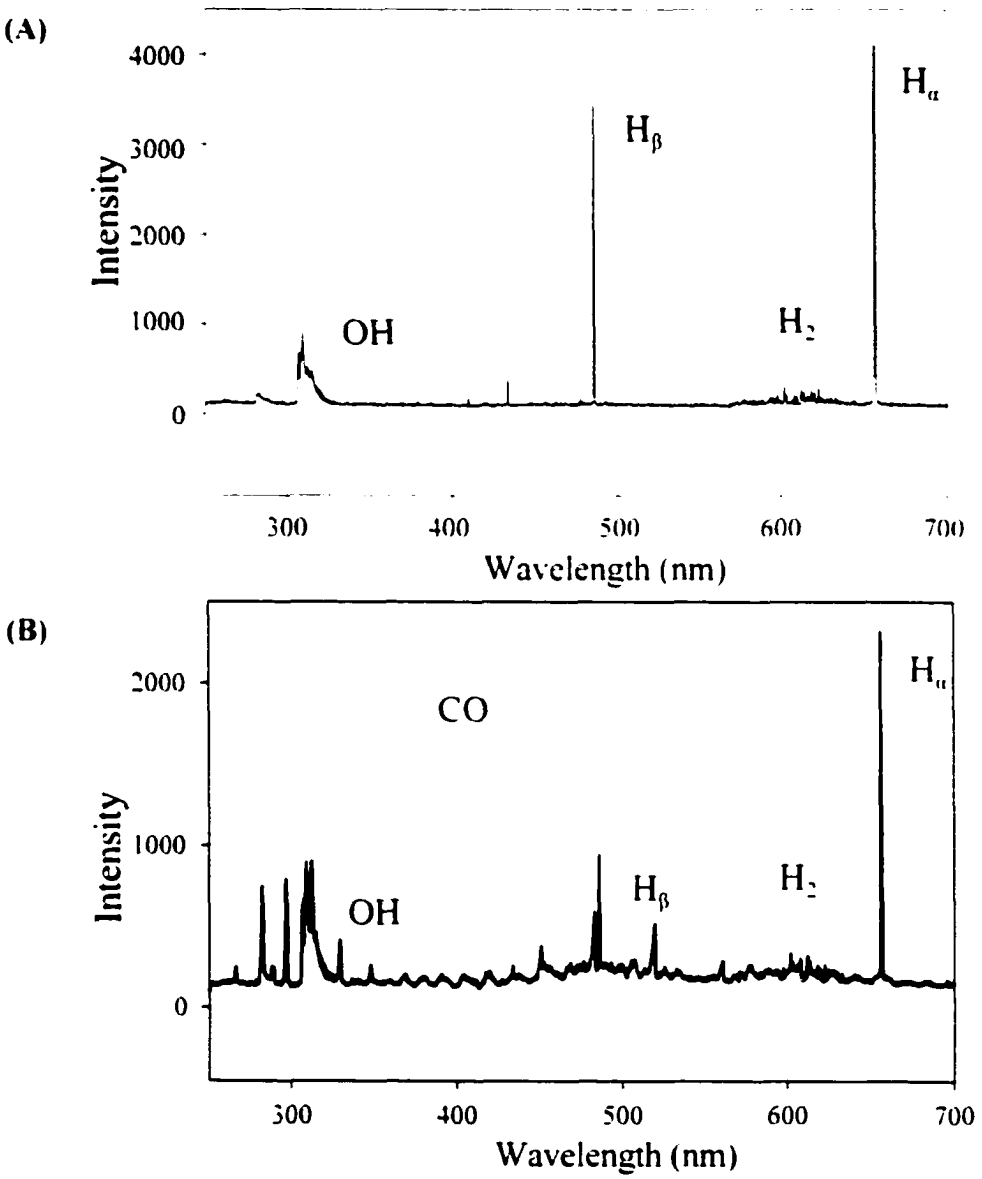

Figure 3.7 Optical emission spectra of a 25 W H_2O plasma (50 mTorr) (A) without and (B) with a BTS55 membrane in the reactor.

when a PSf membrane is placed horizontally directly in the coil region of the plasma reactor. While emission from OH and H atoms is still evident in this spectrum, there are clearly strong emission lines at 282.68, 297.02, 312.71, 329.75, 483.17, and 519.48 nm. Less intense emission lines are also observed at 348.50, 450.75 and 560.67 nm. All of these new lines can be attributed to emission from CO in the plasma.[13] This observation confirms we are oxidizing the PSf, as CO is a known product of most polymer oxidation.[3]

3.3 DISCUSSION

As mentioned in Section 3.1, several groups have previously noted improved wettability for PSf membranes as a result of plasma treatment; however, there are several compelling differences between the results described here and previous studies. These include: 1) demonstration of complete penetration of the modification; 2) degree and permanency of plasma-induced hydrophilicity; 3) degree of chemical modification; 4) consideration of structural damage by plasma treatment; and 5) understanding of the underlying chemical processes. The following sections discuss these points in detail.

3.3.1 PENETRATION OF MEMBRANE MODIFICATION. A major difference between our work and prior studies is that we have demonstrated explicitly that penetration of both microporous and UF membrane modification is complete such that *all* surfaces of the membranes are treated. To understand why we have achieved such complete modification, it is instructive to point out the experimental differences between our work and three relevant investigations of plasma penetration of porous materials. First, a recent study by Johansson and Masuoka (JM) examined the penetration of pores in

polycarbonate (PC), poly(vinylidene fluoride) (PVDF), and nylon membranes by plasma forming species using a butane plasma.[15] A significant change in the surface contact angle was observed with the track-etched PC membranes; however, no contact angle changes were found with the nylon and PVDF after plasma treatment. This was largely attributed to the membrane thickness and the tortuosity of the PVDF and nylon membranes in comparison to the track-etched pores of the PC membranes. Second, Yasuda and coworkers have explored the penetration of nonwoven fabrics using fluorocarbon plasmas.[16] They found that some penetration was obtained, but it was dependent on the porosity of the materials (~90%) and the nature of the fluorocarbon gas. In both studies, polymer-forming plasmas were employed, leading to deposition of a chemically different material on the membrane surfaces.

In the third work, Onishi and coworkers used plasma graft copolymerization (PGC) to hydrophilize polypropylene membranes for blood plasma separation.[17] PGC involves exposure of a polymer surface to an Ar plasma for surface activation. The activated polymer is then exposed to a polymerizable monomer, which is then grafted onto the polymer surface. This system deposits an appreciable amount of material on the membrane surfaces, which was observable in Onishi's SEM images.[17] Based solely on this result, they claim complete modification of the entire cross section. Note that, similar to the techniques employed by JM and Yasuda, the PGC method deposits a chemically different material onto the membrane surface.

In contrast to these three works, we observe complete penetration of our highly asymmetric membranes for a variety of pore sizes. We attribute this extensive membrane

modification to the unique design of our membrane holder, which allows maximum penetration of the plasma through the membrane. We believe that JM did not achieve complete penetration of their membranes, primarily because of their experimental design.[15] Yasuda et al. did observe some penetration, but did not optimize their experimental design to achieve modification of all membrane surfaces.[16] Although Onishi and coworkers may have achieved some penetration, it seems unlikely given their high deposition rate and an experimental design not optimized for complete penetration as the membranes were not oriented perpendicular to gas flow.[17]

Choice of plasma system also appears to be a controlling factor in membrane penetration. For example, Yasuda et al. did not achieve complete penetration of their nonwoven fabrics when polymer-forming plasmas (e.g. C_2F_4) were used.[16] Complete penetration was observed, however, using a non-polymer forming plasma (i.e. CF_4), similar to the results obtained here for H_2O plasmas. Our results from inert gas systems demonstrate, however, that complete penetration is not achieved by all non-polymer forming plasmas. We believe these differences are due primarily to the chemical nature of the reactive species present in the plasma.

We have also shown the effectiveness of the H_2O plasma treatment is not limited to microporous PSf membranes, but is also effective for membranes with smaller pore sizes. The results obtained for BTS80 and UF membranes show that the penetration of the membrane modification is extensive regardless of the average pore size (i.e. porosity) of the membrane. Thus, it is not clear that the pore size or the tortuosity of the membranes is controlling the ability of reactive species to modify our membranes.

Demonstrating that complete penetration has been achieved is challenging as the interior of a porous material is difficult to probe. Our multiple membranes experiments explicitly show that penetration of our membranes by the H_2O plasma is occurring. In these definitive experiments, even the interior surfaces of stacked membranes become hydrophilic. Other studies in our laboratories confirm, through environmental SEM (ESEM) data, *in situ* wetting of the entire membrane structure, Chapter 4.[18] Moreover, penetration is not dependent on the membrane material as we have also achieved complete modification of both polyethersulfone and polyethylene membranes. Clearly, the extent of our membrane modification technically differentiates our work from other studies involving hydrophilic modification of membranes.

3.3.2 DEGREE AND PERMANENCY OF MODIFICATION. Although other studies have reported hydrophilic changes as a result of plasma treatment, the changes have not been permanent. For example, Ulbricht and Belfort (UB) reported that PSf UF membranes were significantly more hydrophilic after 50:50 He:H_2O (25 W, 200 mTorr, 30 sec) and 100% He (25 W, 100 mTorr, 30 sec) plasma treatment as evidenced by a decrease in the contact angle.[c,9] These measurements were performed on membranes immersed in water for 1-3 days after plasma treatment. UB found that the treated membranes were completely stable if stored in water; however, surface rearrangement

---

[c]Note that the authors measured octane/water contact angles because the air/water contact angles were < 20°. For octane/water contact angle measurements, the membrane is in the "wet" state and, therefore, is less susceptible to wicking effects.

occurred during storage in ambient conditions resulting in contact angle changes.[4] Asfardjani, Segui, Aurelle and Abidine (ASAA) also observed contact angle changes for PSf membranes treated with air and H_2O plasmas.[8] However, the authors did not include data on the stability of their plasma-treated membranes. Comparatively, our hydrophilic membrane modification is permanent as treated membranes remain wettable for over a year upon storage in air.

One of the key factors affecting the permanence of the treatment is the chemical nature of the plasma. For example, the wetting properties of poly(hydroxybutyrate-co-9%hydroxyvalerate) films have been studied as a function of the type of plasma treatment (e. g. Ar, O_2, H_2O and H_2O_2 plasmas).[10] Of these, H_2O and H_2O_2 were considered milder treatments, as they resulted in less surface etching and cross-linking of the polymer. The degree of crosslinking was found to influence the permanence of the plasma treatment as H_2O and H_2O_2 plasma-treated films lost hydrophilicity upon standing sooner than films treated with Ar and O_2 plasmas. Loss of plasma-induced hydrophilicity is generally attributed to chain migration from the surface to the bulk to minimize surface energy; hence, the degree of cross-linking affects the facility with which the chains can migrate from the surface into the bulk.[9]

Exposure to environmental extremes such as heating in an oven or exposure to boiling H_2O increases the hydrophobicity of our plasma-treated membranes. In both

---

[4]These data are for membranes treated with a 25 W He plasma (100 mTorr) for 30 seconds. Permanency data were not provided in Reference 4 for UF membranes treated with a 50:50 He:H_2O plasma.

cases, chain motion is likely the cause of loss in hydrophilicity for treated membranes exposed to high temperatures as heating has been shown to increase chain motion in polymers.[6] This type of change in plasma-modified polymers with high temperatures has been observed for hydrophobic treatments of polystyrene.[20] Similarly, a degradation in adhesion properties of polyimide/polyimide plasma treated interfaces has been observed upon exposure to humid environments.[21] Notwithstanding, our membranes are stable when stored in ambient conditions. Although extremes in heat and humidity have a deleterious effect on the degree of wettability, the membrane never reverts to its untreated, hydrophobic state. We attribute the permanency of our modification to the milder, optimized plasma conditions employed in our study. It is also likely related to the extent of modification as the treated membrane surface area is significantly higher than that for a one-sided treatment. Some surface rearrangement occurs after plasma treatment as the XPS analysis shows the oxygen content increases over time (~1 year after treatment) for the open side of the membranes; however, no measurable decrease in the hydrophilicity is observed on either side, even 18 months after treatment.

3.3.3 DEGREE OF CHEMICAL MODIFICATION. The permanency of the hydrophilic membrane modification developed in our laboratory is also likely related to the chemical changes in PSf as a result of plasma treatment. Incorporation of new, more hydrophilic functional groups that are covalently bound to the polymeric backbone results in permanent modification. Indeed, the oxygen concentration increases to more than 20% after plasma treatment (Table 3.5) as new C-O_x and a small number of OH groups are introduced by plasma treatment. This increase is the same for both surfaces of the treated

membranes, further demonstrating equal modification is occurring.

These results are consistent with previous studies of surface oxidation of many types of polymers by plasma treatment (e. g. O_2, air, H_2O, H_2O_2).[7,22] ASAA also reported an overall increase in the surface oxygen concentration and wettability of PSf as a result of air and H_2O plasma treatment.[8] UB also noted a slight increase in the oxygen content due to He:H_2O plasma treatment.[9] These studies, however, did not report the amount of surface oxygen detected.

3.3.4 CONSIDERATION OF STRUCTURAL DAMAGE. We also treated PSf membranes with inert gas:H_2O plasmas, but did not determine any added benefit with this gas mixture. Although diluents can increase the fragmentation of H_2O in the plasma (i.e. increase the concentration of OH radicals), the addition of a diluent may also have a deleterious effect as it could lead to etching of the polymeric material. These thin, porous materials are highly susceptible to plasma-induced damage and, therefore, require special considerations in experimental design.

All of the conditions employed here are relatively mild (low applied rf power and pressures as well as brief treatment times). Furthermore, the membrane is placed 9 cm downstream from the inductor coil, limiting exposure to energetic species. ASAA also performed treatments as much as 45 cm downstream from the inductor coil;[8] however, relatively extreme plasma conditions were still employed with applied rf powers as high as 200 W (at 150 mTorr). Although UB operated under milder plasma conditions (25 W, 100-200 mTorr), the effect of He on the physical properties of their PSf UF membranes was not explored.[9]

Although our membranes did not appear damaged by H_2O plasma treatment on the scale of the SEM experiment, treated BTS55, BTS80, and UF membranes all exhibited an increase in average pore size, as determined by porometry. The increase in pore diameter resulting from plasma treatment is, however, comparable to the increase in pore diameter observed for membranes treated with a wetting agent. UB also observed a significant increase in the water flux after $He:H_2O$ plasma treatment, suggesting adverse pore size changes.[4]

3.3.5 UNDERSTANDING OF THE UNDERLYING CHEMISTRY. Many studies have concentrated on correlating polymer surface modifications to specific plasma conditions, which provides simple relationships between the density of species originating in the glow discharge and surface modification induced in polymers. For example, ASAA optimized plasma processing conditions of PSf UF membranes by establishing relationships between 1) plasma parameters (power, pressure and distance from the inductor coil); 2) composition of the gas phase (OES), particularly OH radicals believed to be responsible for surface modification; and 3) membrane composition (XPS) and wetting properties (contact angle measurements) of the surface after plasma treatment.[8] Accordingly, optimal conditions giving the maximum contact angle change and concentration of oxygen at the surface corresponded to the plasma conditions that produced the greatest intensity of OH radicals in the plasma.

There are several caveats to this type of empirical approach. ASAA observed excited-state OH radicals generated under the same conditions employed to treat PSf UF membranes. The mechanism by which excited-state OH radicals are likely produced in

H_2O plasmas is given in eq. (3.1).

$$e^- + H_2O \rightarrow OH^* + H^* + e^- \quad (3.1).$$

Although this reaction accounts for OH radicals in the plasma, the authors did not identify the species present in the plasma *during* plasma processing of a membrane. We have also identified the presence of excited-state OH radicals in a H_2O plasma under the same operating conditions we use to process PSf membranes (Fig. 3.7a). Moreover, we also identified the presence of additional species generated *only* during plasma modification of PSf membranes. The OES data in Fig. 3.7b show the presence of excited-state CO, which are not observed in a H_2O plasma without a PSf membrane. Thus, we were able to detect reactive excited-state plasma species as well as excited-state products of the reaction with PSf.

More importantly, an empirical approach does not provide information about the actual interactions of OH radicals with the surface of the membranes, data critical to elucidation of the mechanisms responsible for modification of the surface properties of PSf. Interestingly, independent data in our laboratories using laser-induced fluorescence (LIF) to measure gas-phase densities of ground-state OH radicals also indicate that higher applied rf powers lead to higher OH concentrations in H_2O plasma, Chapter 5.[23] Data in Fig. 3.2, however, show that higher powers result in plasma-induced damage to the PSf membranes. Clearly, more detailed information is needed for a complete understanding of the mechanisms involved in PSf membrane modification.

ASAA proposed that OH radicals produced in air and H_2O plasmas modify PSf by producing covalently bound C=O, C-O, O-H, and O-C=O groups at the surface, as

evidenced by XPS data. By comparing the results obtained for polyacrylonitrile and PSf UF membranes treated with H_2O:He and He plasmas, UB also concluded that PSf is more susceptible to modification by oxygen-containing plasmas.[49] ASAA proposed that plasma-generated OH radicals may combine with surface atoms to produce C-O bonds via eq. (3.2).

$$\begin{array}{l} CH_2 \\ | \\ -C- + OH^{\bullet} \end{array} \rightarrow \begin{array}{l} CH_2OH \\ | \\ -C- + H^{\bullet} \end{array} \qquad (3.2).$$

Interestingly, we have observed essentially no change in the C-O groups of the polymer after plasma treatment (Table 3.5). Furthermore, results obtained from TFAA derivatization indicate only a small number (~1%) of alcohol groups introduced by the plasma. There is, however, a significant increase in the number of CO_2 groups, such as aldehyde/ketone and carboxylic acid/ester groups. Although these groups could be introduced by oxidation of alcohol groups plasma-generated by reaction 3.2, oxidation may occur at other sites in the polymer backbone.

In addition to oxidation of the methyl group as proposed by ASAA, we believe there are two other locations for oxidation on the polymer backbone as represented in Scheme 1.1.

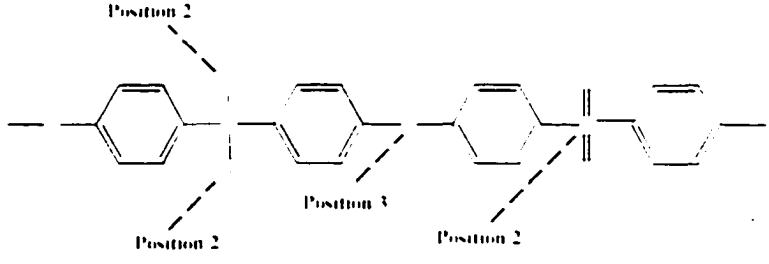

Scheme 1.1

As detailed in Chapter 1, oxidation at position 2 yields an aldehyde, which can be further oxidized to yield a carboxylic acid group. A secondary oxidation pathway is at the sulfur (position 2) resulting in sulfate-like groups as seen in the high resolution S_{2p} spectra. Additionally, oxidation can occur at the ether linkage (position 3). Finally, our XPS results indicated the presence of nitrogen on the treated samples suggesting the presence of amide-like groups, possibly at position 2. These groups are likely the result of radical quenching by air after plasma treatment. Therefore, the detailed chemical information we obtained from XPS clearly confirms our hypothesis of concurrent reaction pathways, in contrast to the unidirectional mechanism suggested by ASAA.

It is also possible that additional oxygen may be incorporated at the surface by post-plasma treatment radical quenching with atomospheric oxygen.[3] Indeed, this has been observed previously for plasma treatment of various polymers. For example, Griesser and coworkers found a continuous increase in the oxygen content over time for fluorinated ethylene propylene (FEP) and polytetrafluoroethylene treated with ammonia plasma.[5] The O/C ratio, measured as 0.05 immediately after plasma treatment, increased four-fold within 10 days of plasma treatment. This increase was attributed to oxidation of trapped radicals and subsequent secondary reactions. XPS analysis of our samples aged ~1 year did show an increase in oxygen incorporation on the open side of the membrane. For our samples, however, the O/C ratio only changes from 0.30 on the ~1 day-old samples to 0.39 on the ~1 year-old samples. Furthermore, essentially no change in the O/C ratio is observed on the tight side of the treated membrane. Although post-treatment oxidation may be contributing to the increase in surface oxygen observed here for aged

membranes, we believe oxygen-containing radical species in the H_2O plasma are primarily responsible for the chemical modification of PSf. Indeed, direct evidence of the nature of the plasma-surface interactions is needed to ultimately define the contribution of plasma treatment to the observed changes in the composition and wettability of PSf.

3.4 SUMMARY

The results described here demonstrate that the H_2O plasma treatment developed in our laboratory achieves permanent and complete hydrophilic modification of PSf membranes. Furthermore, this study encompasses microporous as well as UF membranes, illustrating the universality of this method. As discussed in Chapter 4, we have also treated different polymeric membrane materials to achieve permanent and complete hydrophilic modification. Our H_2O plasma similarly modifies these membranes regardless of material. Hence, we have developed a general method for rendering asymmetric polymeric membranes permanently and completely hydrophilic.

To further explore the molecular-level chemistry in this system, we have studied the surface reactivity of OH radicals during H_2O plasma processing of PSf and other polymeric membranes, Chapter 5. Results from our direct, non-intrusive radical imaging experiments provide chemical information about the plasma-surface interactions occurring during processing. Thus, our combined experimental approach affords better process control by considering the molecular-level chemistry as well as achieving the desired membrane surface properties.

3.5 REFERENCES

1. M. Mulder. *Basic Principles of Membrane Technology*. 2nd Ed., (Kluwer Academic Press: New York, 1996.)
2. J. Ditter. U.S. Filter Inc., personal communication.
3. P. W. Kramer, Y.-S. Yeh, and H. Yasuda. *J. Membr. Sci.* **46,** 1 (1989).
4. M. Ulbricht and G. Belfort. *J. Appl. Polym. Sci.* **56,** 325 (1995).
5. H. J. Griesser, J. H. Hodgkin, and R. Schmidt. *Prog. Biomedical Polym.*, C. G. Gebelein and R. L. Dunn, Eds., (Plenum Press: New York, 1990).
6. T. R. Gengenbach, X. Xie, R. C. Chatelier, and H. J. Griesser. *J. Adhes. Sci. Technol.* **8,** 305 (1994).
7. F. D. Egitto and L. J. Matienzo. *IBM J. Res. Develop.* **38,** 423 (1994).
8. K. Asfardjani, Y. Segui, Y. Aurelle, and N. Abidine. *J. Appl. Polym. Sci.* **43,** 271 (1991).
9. M. Ulbricht and G. Belfort. *J. Membrane Sci.* **111,** 193 (1996).
10. M. A. Leich, N. M. Mackie, K. L. Williams, and E. R. Fisher. *Macromolecules* **31,** 7618 (1998).
11. A. Chilkoti and B. D. Ratner. *Surf. Interface. Anal.* **17,** 567 (1991).
12. J. Hopkins and J. P. S. Badyal. *J. Polym. Sci. A: Polym. Chem.* **34,** 1385 (1996).
13. W. R. Harshbarger, R. A. Porter, T. A. Miller, and P. Norton. *Appl. Spectrosc.* **31,** 201 (1977).
14. E. O. Degenkolb, C. J. Mogab, M. R. Goldrich, and J. E. Griffiths. *Appl. Spectrosc.* **30,** 520 (1976).
15. J. Johansson and T. Masuoka. *Macromol. Rapid Commun.*, 20 (1999) 12.

16. T. Yasuda, T. Okuono, M. Miyama, and H. Yasuda, *J. Polym. Sci. A: Polym. Chem.* **32,** 1829 (1994).

17. T. Masuoka, O. Hirasa, Y. Suda, and M. Onishi, *Radiat. Phys. Chem.* **33,** 421 (1989); M. Onishi, K. Shimura, Y. Seita, S. Yamashita, A. Takahashi, and T. Masuoka, *Radiat. Phys. Chem.* **39,** 569 (1992).

18. M. L. Steen, A. C. Jordan, and E. R. Fisher, *J. Membrane Sci.*, submitted for publication.

19. A. Mas, H. Jaaba, and F. Schue, *Pure Appl. Chem.* **A34,** 67 (1997).

20. E. Occhiello, M. Morra, P. Cinquina, and F. Garbassi, *Polym. Prepr.* **31,** 308 (1990).

21. Y. Satsu, O. Miura, R. Watanabe, and K. Miyazaki, *Electron. Commun. Japan. Part 2* **74,** 489 (1991).

22. S. Kanazawa, M. Kogoma, S. Okazaki, and T. Moriwaki, *Nucl. Instrum. Methods in Phys. Res.* **B37/38,** 842 (1989).

23. M. L. Steen, C. I. Butoi, and E. R. Fisher, *Langmuir*, submitted for publication.

24. R. d'Agostino, F. Cramarossa, F. Fracassi, F. Illuzzi, in *Plasma Deposition, Treatment and Etching of Polymers*, R. D'Agostino, Ed. (Academic Press: San Diego, 1990), pp. 95-162.

CHAPTER 4

HYDROPHILIC MODIFICATION OF POLYMERIC MEMBRANES BY LOW-TEMPERATURE H$_2$O PLASMA TREATMENT

This dissertation chapter contains results from a full paper submitted for publication to *Journal of Membrane Science*. The manuscript was written by M. L. Steen and edited by Professor E. R. Fisher. The coauthor was A. C. Jordan. This work continues our studies on plasma modification of hydrophobic materials for permanent hydrophilicity. The role of membrane material (composition) and structure (degree of asymmetry) in the modification were investigated. This work demonstrates that the extent and permanence of hydrophilic modification can be correlated to: 1) the mechanisms of interaction between the polymer and reactive plasma species; and 2) the degree of penetration of these species through the porous structure.

4.1 INTRODUCTION

Microporous polymeric membranes are commercially available in a variety of pore sizes and composition to address the needs of nearly any separation process, including filtration of particulates and macromolecules from aqueous streams.[1] The membranes used in these applications are generally constructed from durable thermoplastics (e.g., polysulfone), the majority of which are hydrophobic.[2] As a consequence, the surface of these membranes must be rendered hydrophilic through the addition of a wetting agent and/or by chemical modification of the membrane structure prior to use in aqueous separations. Issues frequently encountered with these methods include a lack of permanency of the modification and unmodified areas in the pore structure.[3,4] Hence, an optimal method for making hydrophobic membranes wettable would achieve permanent hydrophilicity and uniform modification of all membrane surfaces.

Chapter 3 reported a H_2O plasma treatment developed in our laboratory for asymmetric polysulfone (PSf) membranes that achieves permanent hydrophilicity of these hydrophobic membranes.[5] The permanence of the hydrophilic modification is a direct result of covalently-bound sulfate, O-H, C-O and C-O_x (e.g., C=O, O-C=O) groups introduced by plasma treatment. Furthermore, H_2O plasma treatment modifies the entire membrane cross section of these highly asymmetric membranes. We attribute this extensive membrane modification to the unique design of our membrane holder, which orients the porous materials perpendicular to the plasma, allowing maximum penetration of the plasma through the membrane.

We have also examined the underlying chemistry of the H_2O plasma surface

modification system using three gas-phase analytical tools. Chapter 5.[7] These analyses provided a comprehensive profile of plasma species and a fairly extensive set of data from which mechanistic information was gleaned. Characterization of gas-phase species, including those penetrating the membrane thickness, as well as molecules generated at the membrane surface *during* modification was performed using mass spectrometry (MS) and optical emission spectroscopy (OES). Plasma-surface interactions of OH radicals generated in the plasma were assessed with our direct, radical-imaging experiments based on laser-induced fluorescence (LIF). Results show OH has a moderate reactivity of ~50% at the surface of the polymeric membranes employed in this study. These data indicate OH radicals are involved in our hydrophilic membrane modification. Furthermore, the same moderate OH reactivity was measured for PSf, polyethersulfone (PES) and polyethylene (PE) membranes, suggesting that H_2O plasma treatment is general to a variety of membrane materials.

In this chapter, we have extended our H_2O plasma treatment to PES and PE membranes to investigate the role of membrane material (chemical composition) and structure (i.e., degree of asymmetry) in our hydrophilic modification. The wetting properties of PES and PE membranes were evaluated by contact angle (CA) measurements and environmental SEM (ESEM). CA measurements as a function of the age of the sessile drop on the surface quantified the amount of time it took for the plasma-treated membranes to wet. ESEM images show the extent of hydrophilic modification through the PES and PE cross sections. Overall, we demonstrate that the wetting properties and surface composition can be correlated to the degree of penetration of

molecular species generated in the H_2O glow discharge.

4.2 RESULTS AND DISCUSSION

4.2.1 MODIFICATION AND PERMANENCE. The images acquired with our DSA 10 goniometer (Figure 4.1) demonstrate hydrophilic modification of hydrophobic PES membranes by H_2O plasma treatment. For clarity, the two sides of the membrane, the open, upstream side (closest to the plasma) and the tight, downstream side of the membrane will be referred to as Surfaces 1 and 2, respectively (Fig. 4.2a). CA data as a function of the age of the drop for untreated and plasma-treated PES membranes are shown in Fig. 4.2b. Note that the contact angles on the open (69.5 ± 0.1°) and tight (63.0 ± 0.1°) sides of the untreated membrane do not significantly change with drop age. For the plasma-treated membranes, the CA decreases rapidly with drop age until the drop completely disappears, within 2 seconds for both sides of the PES membrane, Fig. 4.2b. This suggests that the plasma penetrates the thickness of the membrane, thereby equally modifying both sides of the membrane. As noted in Section 4.1, these results are consistent with H_2O plasma treatment of microporous and ultrafiltration (UF) PSf membranes. Figure 4.2b also shows CA data as a function of drop age for treated PES membranes aged for ~9 months, demonstrating that both sides of the membrane still wet in < 2 seconds. Hence, no significant change in the wettability occurs as a result of aging. This is also consistent with our results for H_2O plasma-treated PSf membranes, which withstand long-term aging (>18 months) under ambient conditions.[5]

In contrast to PES membranes, PE membranes treated under identical conditions

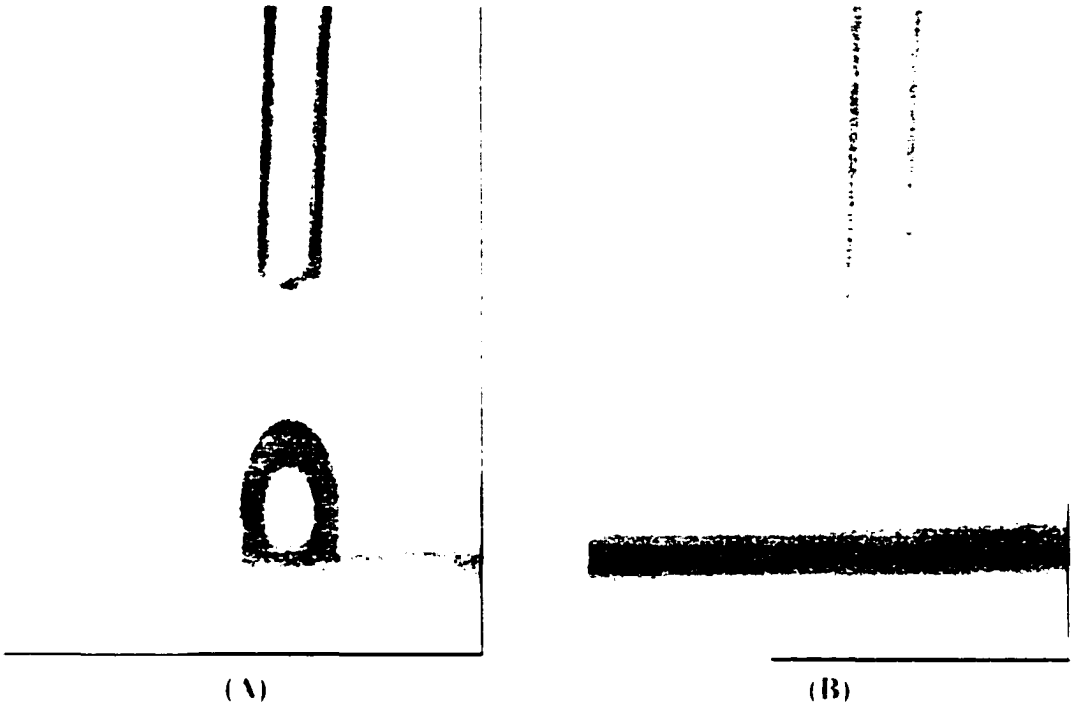

Figure 4.1 Images acquired with digital image capture of the DSA 10 before (A) and after (B) plasma treatment.

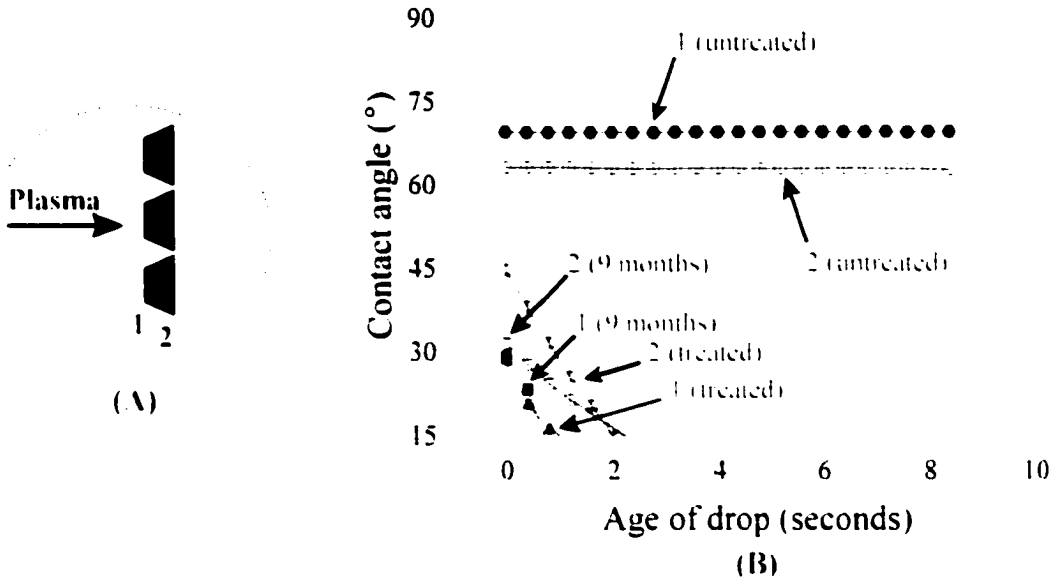

Figure 4.2 A) Schematic illustrating that the membrane is oriented in the membrane holder with the open side (Surface 1) closest to the plasma and the tight side (Surface 2) downstream from the plasma. B) Contact angle data as a function of drop age for untreated PES membranes (circles). PES membranes treated with a 25 W H_2O (50 mTorr) plasma for 2 minutes (triangles), and PES membranes ~9 months (squares) after plasma treatment. Measurements in (B) were made on Surface 1 (closed symbols) and Surface 2 (open symbols) and are the average of measurements made over a 10 second time period after applying the drop to the surface. Note CA measurements are reliable above 15°.

show a difference in the degree of wetting between the opposing sides of the membrane (Fig. 4.3a). Specifically, for Surface 1, the water drop disappears within 25 seconds of being applied to the membrane. In contrast, the water drop never completely disappears from the downstream side of the treated membrane. Note, however, Surface 2 does show significantly improved wettability in comparison to untreated PE, with an overall decrease of ~90° in the contact angle. PE membranes were treated for longer than 2 minutes to improve the wettability of Surface 2. Figure 4.3b shows CA data as a function of drop age for PE membranes treated with a 25 W H_2O plasma for 4 minutes and 9 minutes. For PE membranes treated longer than 2 minutes, it takes ~15 seconds for the drop to disappear from Surface 1, whereas the average CA on Surface 2 remained ~40°. Hence, increasing the treatment time affords some improvement in the wettability of both surfaces. The downstream side, however, does not become completely wettable even with the 9 minute treatment. Additional parameter optimization included increasing the applied rf power (P) and chamber pressure. Membranes treated with P = 25 W at 100 mTorr for 2 minutes showed no further improvement in the wettability on the downstream side with an average contact angle of ~41°. Similar results were obtained for PE membranes treated with P = 35 W at 50 mTorr for 2 minutes. PE membranes treated at P > 35 W were, however, visibly charred, consistent with plasma-induced damage observed for PSf membranes treated with high P.[5]

Most significant is that modification of PE membranes is not permanent, with changes in the CA measurements observed within 48 hours after plasma treatment, Fig. 4.3c. Specifically, the upstream side of the membrane took longer to completely wet

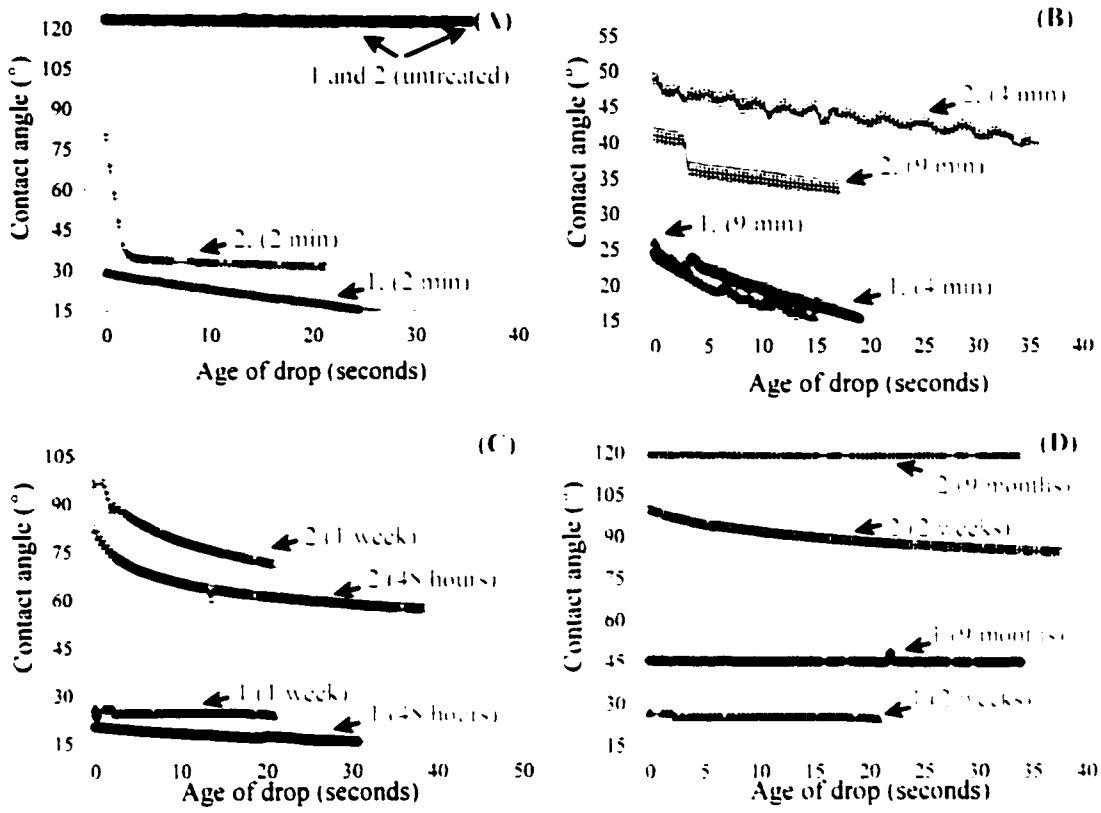

Figure 4.3 Contact angle data as a function of drop age for (A) untreated PE membranes (circles) as well as surfaces 1 and 2 of PE membranes treated with a 25 W H_2O (50 mTorr) plasma for 2 minutes (triangles); (B) PE membranes treated for 4 minutes (circles) and 9 minutes (triangles); (C) PE membranes ~48 hours (circles), and ~1 week (triangles); and (D) PE membranes aged ~2 weeks (triangles) and ~9 months (diamonds) after plasma treatment. All measurements were made on Surface 1 (closed symbols) and Surface 2 (open symbols).

(~30 seconds) and CA increases of ~20° were observed on Surface 2. Further loss of hydrophilicity was observed for plasma-treated membranes aged for longer times in ambient conditions. After 1 week, Surface 1 was no longer completely wettable, with an average CA = 25.1 ± 0.4° and the average CA on Surface 2 had risen to 73.1 ± 8.4°. Surface 2 becomes even more hydrophobic (CA ~ 90°) 2 weeks after plasma treatment. Fig. 4.3d. CA data as a function of drop age for plasma-treated PE membranes aged ~9 months indicate an average CA on Surface 1 of 45.1 ± 0.4°. Fig. 4.3d. Although this is a significant increase from the 2 week data, the upstream side of the membrane does not revert to the same degree of hydrophobicity as the untreated material (122.5 ± 0.6°), even after 9 months. In contrast, the average CA measured on Surface 2 after 9 months, was ~118.8 ± 0.2°, nearly the same as the untreated PE membrane.

Similar losses in hydrophilicity upon storage are typically observed for many plasma-treated polymers. For example, polymers modified to create a hydrophilic surface and stored in contact with air often revert to a state of lower surface energy within hours or days of treatment.[7,8] Aging of surface-modified polymers is attributed to migration of polar surface groups into the polymer and untreated polymer chains to the surface, structural rearrangement to bury chemical groups introduced at the surface, and/or chemical reactions with atmospheric oxygen and moisture. Loss of the surface properties induced by surface treatment is observable in changes in the air/water contact angles, as demonstrated here, and by surface spectroscopic methods (e.g. XPS). Hence, the aging effects we observe for our plasma-treated PE membranes are consistent with the post-treatment surface restructuring typically observed for modified polymeric surfaces. In

contrast, no measurable decrease in hydrophilicity is observed for our plasma-treated PES and PSf membranes, even after long-term aging.

4.2.2 SURFACE OXIDATION. XPS analysis (Tables 4.1 and 4.2) indicates the chemical changes that occur in PES and PE membranes as a result of H_2O plasma treatment. Results for PSf membranes are also included for comparison.[5] As shown in Table 4.1, the elemental composition for the untreated membranes is in excellent agreement with the known structures of PSf, PES, and PE. In addition, no significant differences in composition were detected between the opposing sides of the untreated membranes.

The results in Table 4.1 for plasma-treated membranes indicate that H_2O plasma treatment increases the oxygen concentration for all three membrane materials. An increase of ~8-10% is observed on both sides of PES and PSf membranes with a concomitant decrease of ~8-10% in the carbon concentration. Furthermore, both sides of PES and PSf are equally modified by plasma treatment, suggesting penetration of the plasma through the membrane. Likewise, there is a substantial incorporation of oxygen in the treated PE membranes, which originally contained no detectable oxygen, Table 4.1. For PE membranes, however, the oxygen content on the upstream side is considerably higher (~24%) than that detected on the downstream side (~15%). A decrease in the carbon content is also observed for plasma-treated PE membranes. Again, a larger decrease is observed on the side facing the plasma (~28%) than on the downstream side (~16%). These data suggest incomplete penetration of PE membranes by the plasma under the same conditions which showed complete penetration of PSf and PES.

Table 4.1 XPS results of untreated, treated, and aged PSf, PES and PE membranes.

Material	XPS Atomic Percent				
	C	O	S	F	N
Stoichiometric PSf	84.3	12.0	3.7		
Stoichiometric PES	75	18.8	6.3		
Stoichiometric PE	100				
untreated PSf	84.5 ± 0.5	11.8 ± 0.5	3.7 ± 0.1		
treated PSf (open)[b]	74.4 ± 0.2	22.1 ± 0.5	2.6 ± 0.1		0.7 ± 0.2
treated PSf (tight)[a,b]		73.7 ± 0.6	21.5 ± 0.1	2.6 ± 0.1	0.6 ± 0.1
untreated PSf- TFAA	82.2 ± 0.2	13.0 ± 0.2	3.5 ± 0.1	1.2 ± 0.2	
treated PSf (open)- TFAA[b]	69.4 ± 1.4	18.9 ± 0.8	2.6 ± 0.4	5.0 ± 0.1	1.9 ± 0.4
treated PSf (tight)- TFAA	73.1 ± 0.8	18.9 ± 0.3	2.8 ± 0.1	4.2 ± 0.2	0.6 ± 0.3
aged PSf (open)	67.7 ± 1.0	26.5 ± 1.0			
aged PSf (tight)	74.7 ± 1.0	21.8 ± 2.4			
untreated PES (both sides)[c]	75.5 ± 0.9	17.1 ± 0.6	6.8 ± 0.4		
treated PES (both sides)[b]	67.9 ± 1.1	25.2 ± 0.5	4.7 ± 0.2		1.4 ± 0.9
untreated PES- TFAA[c]	75.4 ± 0.4	17.8 ± 0.4	6.6 ± 0.2		
treated PES- TFAA[b]	70.1 ± 0.7	20.3 ± 0.6	5.0 ± 0.1	3.4 ± 0.5	0.9 ± 0.2
untreated PE (both sides)	100				
treated PE (A)[b,d]	72.3 ± 3.5	23.5 ± 1.7			0.8 ± 0.2
treated PE (B)[b,d]	84.4 ± 2.3	15.4 ± 2.1			
untreated- TFAA	100				
treated PE- TFAA	82.0 ± 0.6	12.2 ± 0.5		5.1 ± 0.3	0.7 ± 0.4
aged PE (A)[b,d]	81.6 ± 1.0	16.7 ± 1.0			
aged PE (B)[d]	95.0 ± 1.0	5.0 ± 1.0			

[a] trace impurities (<1%) of atomic sodium also detected
[b] trace impurities (<2%) of atomic silicon also detected
[c] trace impurities (<1%) of atomic chlorine also detected
[d] side A is facing the coil and side B is the downstream side during plasma treatment

Table 4.2 XPS C_{1s} Percent for untreated and treated PSf, PES and PE membranes.

Sample	XPS C_{1s} Percent		
	CH_x	C-O	C-Ox[a]
Stoichiometric PSf	85	25	
Stoichiometric PES	83	17	
Stoichiometric PE	100		
untreated PSf (both sides)	84	16	
treated PSf (open)	75	19	9
treated PSf (tight)	74	18	8
untreated PES (both sides)	83	17	
treated PES (both sides)	76	19	5
untreated polyethylene (both sides)	100		
treated PE (A)	74	18	8
treated PE (B)	86	7	7

[a] C-O_x is the total amount of C=O, O=C-O, etc.

Table 4.2 provides detailed results for the C_{1s} spectra for untreated and plasma-treated PSf, PES, and PE membranes. The increase in the high binding region of the C_{1s} spectrum upon plasma treatment is consistent with the presence of ketone/aldehyde and carboxylic acid/ester groups. As there are no C-O_x groups present in the untreated PSf and PES materials and no C-O_x or C-O groups in the untreated PE membranes, these functional groups must be introduced by plasma treatment. Furthermore, both surfaces of PSf and PES membranes are equally modified by the plasma. In contrast, the number of C-O groups introduced on Surface 1 (~18%) of PE membranes is more than double the number introduced on Surface 2 (~7%). This increase in C-O and C-O_x groups is accompanied by a decrease in the CH_x content. Plasma-treated membranes were further derivatized with TFAA to detect the presence of OH groups.[7] As shown in Table 4.1, TFAA derivatization of PSf, PES, and PE membranes confirmed a small number of OH groups (~1-3% as 3 F atoms are substituted for each OH group) are introduced by plasma treatment. Overall, the formation of C-O, OH, and CO_x groups at the polymer surface by plasma treatment is likely responsible for the significant improvement in wettability we observe for our materials.[10] These results are consistent with previous studies of surface oxidation of different types of polymers by different plasma treatments (O_2, air, H_2O, H_2O_2).[11]

OES provides further evidence that PSf, PES, and PE membranes are oxidized by H_2O plasma treatment. We employed OES to determine the excited state gas-phase composition of our H_2O plasma, Fig. 3.7a. These data identified the presence of OH* radicals (at 306.95 and 309.14 nm), as well as H* atoms (at 486.18 and 656.45 nm) in the

H_2O plasma. Figure 4.4 shows the OES spectra obtained during H_2O plasma processing of PES and PE membranes. These spectra are nearly identical to that obtained with a PSf membrane in the reactor, Fig. 3.7b. While emission from OH and H atoms is still evident in these spectra, there are clearly strong emission lines at 282.68, 297.02, 312.71, 329.75, 348.50, 450.75, 483.17, 519.48 and 560.67 nm. All of these lines can be attributed to CO in the plasma.[12] The formation of gas-phase CO during plasma processing of all three membrane materials confirms we are oxidizing these polymers, as CO is a product of polymer oxidation.[13] The production of CO during plasma treatment of PE is significant because PE does not contain oxygen, suggesting that gas-phase CO and the oxygenated carbon centers on the polymer backbone are indeed the product of plasma-surface reactions.

Mechanistically, surface oxidation of PE proceeds primarily through abstraction of H atoms from the surface,[14,15] and reaction of a plasma species, presumably OH, at these activated sites.[18] Formulating reliable chemical mechanisms for PSf and PES is more difficult because both polymers contain a variety of functional groups, increasing the number and complexity of possible plasma-surface interactions. Although oxygenated carbon centers in PSf may be formed by hydrogen abstraction from the methyl substituent,[16] this is not the only oxidation pathway for PSf membranes. As discussed in Chapter 3, additional locations for oxidation on the PSf backbone include a secondary oxidation pathway at the sulfone group which results in sulfate formation, confirmed by our XPS data.

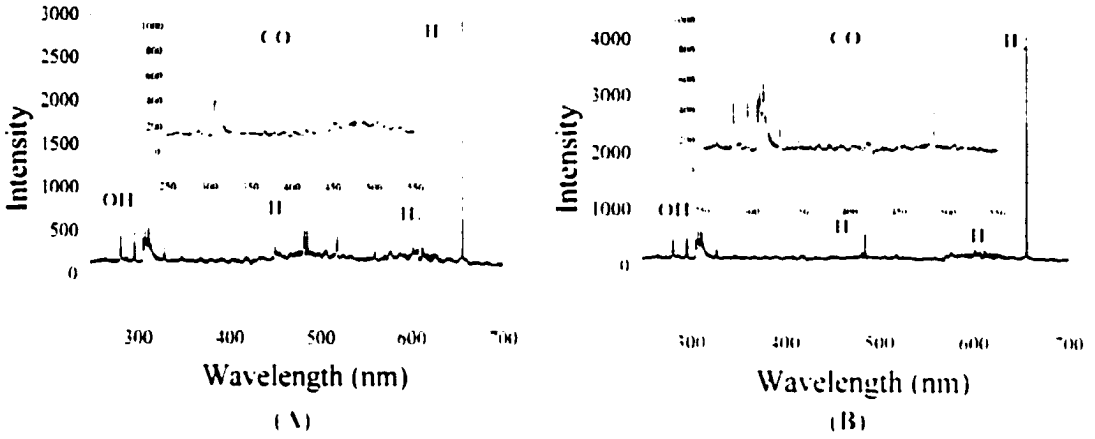

Figure 4.4 Optical emission spectra of a 25 W H_2O plasma (50 m Torr) with (A) a PES membrane and (B) a PE membrane in the reactor.

Results for PES membranes also support additional reaction pathways as the same degree of modification is achieved even though PES does not contain the methyl group present in PSf. Conceivably, surface modification of PSf and PES may result from hydrogen abstraction from the phenyl group, present in both materials. However, abstraction of this hydrogen as well as the α-hydrogen atom in aromatic polymers is difficult, leading to scission of more labile bonds along the polymer chain.[18]

The differences in the reaction mechanisms of aliphatic and aromatic polymers is related to the ease of surface modification, primarily as a result of energy requirements for bond scission. In Chapter 3, we proposed that modification of PSf proceeds through cleavage of C-S, C-C, C-O, or C-H bonds. Similarly, with PES, the C-O (~2.3 eV) and C-S (~1.1 eV) are broken during plasma treatment.[7] In contrast, the C-H (~4.3 eV) and possibly the C-C (~3.8 eV) bonds are broken during PE modification. Note that the energy requirements for bond cleavage increase in the following way: C-S < C-O < C-C < C-H. Consequently, the ease of polymer modification follows a similar trend as PSf and PES are easier to modify (i.e. milder conditions produce desired surface properties) than PE. This is clearly consistent with our CA and XPS data for all three membrane materials.

Interestingly, we identified the same plasma-polymer interfacial reaction products and intermediates during plasma processing of all three membrane materials. As discussed in Chapter 5, our LIF-based radical-imaging experiments confirm that OH reacts with the same moderate reactivity (~50%) at the surface of PSf, PES, and PE membranes.[7] Furthermore, CO is produced in the gas-phase during plasma modification of PSf, PES, and PE. Although OH and CO are present in the gas-phase during processing of all three

membrane materials, the reaction mechanism by which OH reacts at the surface and CO is generated at the surface differs for PE membranes. Hence, the mechanisms of interaction between the polymer and plasma depend not only on the nature of the reactive species generated in the plasma, ultimately defined by the plasma conditions, but also on the chemical composition of the polymer.[18]

In addition to the degree of modification, the permanence of the plasma treatment can also be attributed to the composition of the polymer. Specifically, the rigidity of the aromatic backbone of PSf and PES may reduce polymer chain migration from the surface to the bulk, thereby retaining the modified polymer chains at the surface.[19] This is consistent with our CA and XPS data, analyses typically used to monitor aging of modified surfaces. As previously noted, no significant changes in wettability occur as a result of aging PSf and PES membranes for prolonged periods (~1 year). In addition, Table 4.1 shows that treated PSf membranes aged for ~1 year retained their increased oxygen content and the same functional groups were detected in the XPS C_{1s} spectrum. There was, however, a slight increase in the amount of oxygen (~4%) on the open side of the membrane, presumably from reaction with atmospheric oxygen.[11] The downstream side of the membrane, however, did not show any additional oxygen incorporation, with an O/C ratio of 0.29 immediately after treatment and after storage in air for ~1 year. Thus, no significant changes in surface composition were observed for aged PSf membranes.

In contrast, both sides of the PE membranes showed considerable compositional changes within 6 weeks of plasma treatment (Table 4.1). Specifically, the O/C ratio

decreased from 0.33 to 0.20 on the upstream side of the membrane. Moreover, the downstream side showed an even larger decrease in the O C ratio from 0.18 to 0.05. With a 95% carbon content and an average CA of 118 ± 0.2 , the aged membranes closely resemble untreated PE. These data are indicative of extensive surface rearrangement, resulting in a nearly complete loss of hydrophilicity for our plasma-treated PE membranes.

4.2.3 MEMBRANE STRUCTURE. In addition to chemical composition, we must also consider the physical structure of the membranes to accurately describe plasma modification of porous polymeric materials. Figure 4.5 shows SEM images of the PES membrane surfaces. These images illustrate the high degree of asymmetry associated with these membranes as the open side, Fig. 4.5a, comprises much larger pores (0.8-9.0 μm) than those on the tight side of the untreated membrane (0.3-1.2 μm), Fig. 4.5b. Conversely, PE membranes have a more gradual pore gradient than that of asymmetric PES. Figure 4.6a shows the open side of the untreated PE membrane has pore diameters ranging from 0.3 to 1 μm, and ~0.3 μm pores on the opposing side. Therefore, the porous structure of PE membranes is less open than that of asymmetric PES.

Water flux experiments and bubble point measurements for untreated PES and PE membranes provide further evidence of the differences in membrane structure. The open structure of the untreated PES membranes affords an order of magnitude increase in the water flux relative to untreated PE, Table 4.3. Moreover, the isopropanol (IPA) bubble point (inversely proportional to pore size, equation 2.1) for untreated PE membranes is significantly higher than that for untreated PES membranes, Table 4.3. These data are consistent with our SEM images, again illustrating that the porous structure of PES is

(A)

(B)

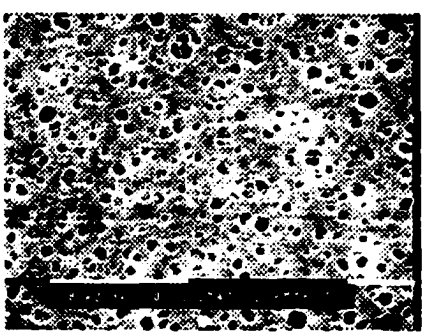

(C)

Figure 4.5 SEM images (5000X) of the (A) open and (B) tight sides of an untreated as well as (C) open side of a plasma-treated PES membrane (25 W, 2 min)

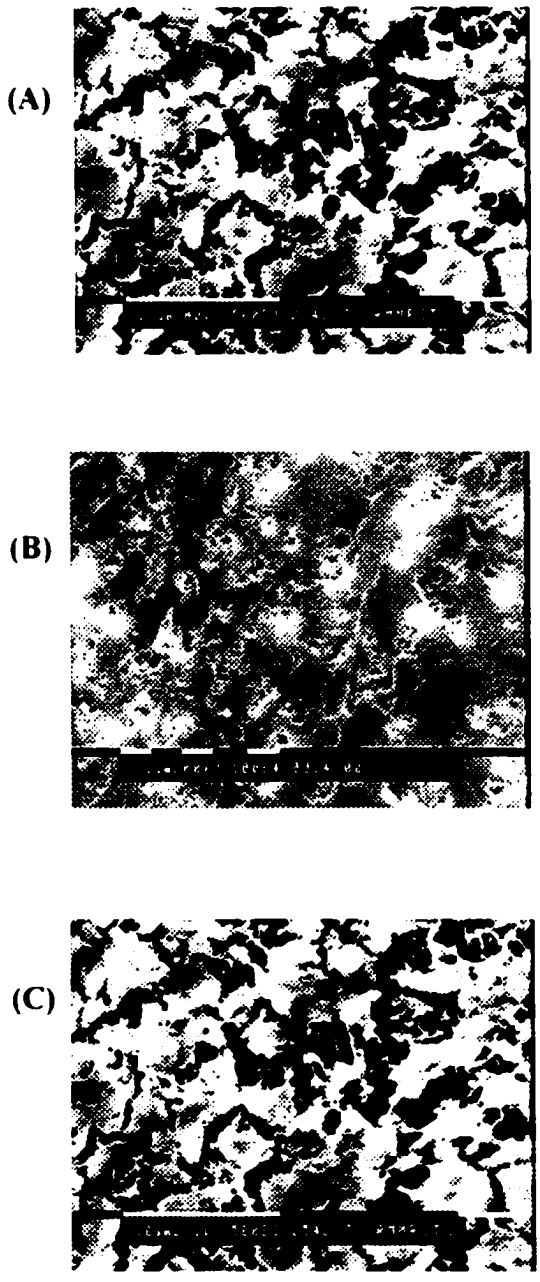

Figure 4.6 SEM images (10,000X) of A) the open side of an untreated PE membrane. B) the tight side of an untreated PE membrane; C) the upstream side of a membrane treated at 25 W for 2 minutes; and D) the upstream side of a PE membrane treated at 25 W for 9 minutes.

Table 4.3 Water flux and bubble point measurements for PES and PE membranes.

Membrane	**Flux (gfsd/psi)[a]**	**Bubble point (psi)**
untreated PES	194.63	24.55
treated PES	249.70	22.24
untreated PE	16.89	41.79
treated PE	21.68	38.10

[a]Experiments performed at 13 psi. gfsd = gal ft^{-2}

significantly more open than that of PE.

Comparison of SEM images for treated and untreated PES and PE membranes allows for determination of plasma-induced structural damage to the membranes. SEM images of the open sides of treated PES and PE membranes are shown in Figs. 4.5c and 4.6c, respectively. Surface 1 of each membrane was imaged as it was the side closest to the plasma glow, and, therefore, most susceptible to physical damage. Comparison to the images for untreated PES (Fig. 4.5a) and PE (Fig. 4.6a) membranes confirmed that our treated membranes are not significantly damaged by plasma treatment. Specifically, no visible pitting of the membrane surface is observable in the images of the treated membranes, similar to results for H_2O plasma treatment of PSf membranes under identical plasma conditions, Chapter 3. We did, however, detect structural damage to PSf membranes with longer treatment times (~10 minutes) and higher applied rf powers (100 W), Fig. 3.2. In contrast to PSf membranes, the structural integrity of PE membranes was not adversely affected by prolonged exposure to the plasma, Fig. 4.6d. Longer treatment times did not, however, afford any advantages in terms of the wettability of PE membranes. It should also be noted that the downstream placement of the membrane holder in the plasma reactor minimizes exposure of all of our membranes to ionizing radiation.[9] We have explicitly shown this using dosimeter foils, as discussed in Chapter 5.

One difference between the SEM images of the untreated and treated PE membranes not observed with our PSf or PES membranes is the disappearance of some of the fiber-like structures spanning the entrance of the pore cavities on the upstream side, Fig. 4.6c. Although this structural change is clearly the result of plasma treatment, no

visible pitting of the membrane surface was observed, even at high magnification (10,000X). Furthermore, a ~23% increase in the water flux is observed for PES and PE membranes after plasma-treatment, Table 4.3. This increase in water flux is consistent with our SEM results, indicating a more open structure for the plasma-treated membranes.[19] Bubble points measured for plasma-treated PES and PE also indicate a slight increase in pore size for the treated materials, Table 4.3. These data are consistent with porometry data for treated PSf membranes, indicating ~35% increase in the average pore diameter as a result of plasma modification, Table 3.2.

4.2.4 PENETRATION OF HYDROPHILIC MODIFICATION. To determine the depth of penetration of the membrane structure by the plasma, two PES membranes were placed in the membrane holder and simultaneously treated with a 25 W H_2O plasma for 2 minutes, Fig. 4.7a. Figure 4.7b shows CA data as a function of drop age for all four membrane surfaces in the PES stacked assembly. The surfaces of the membrane closest to the plasma (Surfaces 1 and 2) wet in <1 second of applying the drop to the membrane surface. Likewise, the open side of the second membrane (Surface 3) wet in ~ 2 seconds. Hence, the interior surfaces not directly exposed to the plasma (Surfaces 2 and 3) were treated by the plasma, confirming complete penetration of the membrane closest to the inductor coil by the plasma. In contrast, it took considerably longer, ~35 seconds, for the drop to wet the surface of the membrane farthest downstream (Surface 4). Similar results were observed for PSf membranes where Surfaces 1, 2, and 3 were wettable after plasma treatment and a small CA was measured on Surface 4; however, increasing the treatment time to 3 minutes resulted in complete wettability of all four surfaces of PSf stacked

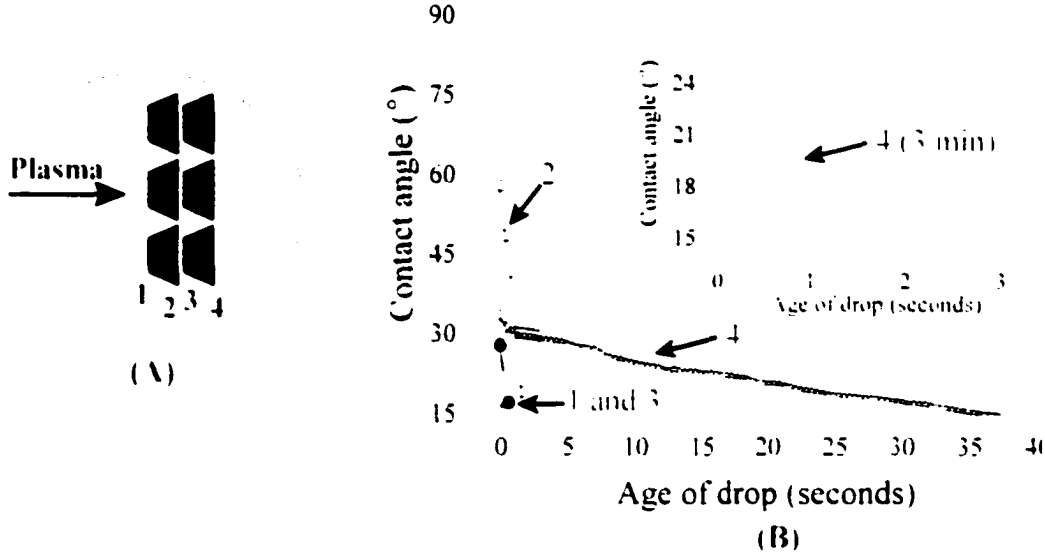

Figure 4.7 A) Schematic illustrating a stacked assembly of PES membranes with the open sides of the membranes (surfaces 1 and 3) oriented toward the plasma and the tight sides oriented (surfaces 2 and 4) downstream. B) Contact angle as a function of drop age for stacked assemblies of PES membranes treated with a 25 W H_2O plasma for 2 minutes. Measurements were made immediately after plasma treatment for Surface 1 (closed circles); Surface 2 (open circles); Surface 3 (closed triangles); and Surface 4 (open triangles). The inset shows contact angle as a function of drop age for Surface 4 (open triangles) of a PES stacked assembly treated with a 25 W H_2O plasma for 3 minutes.

assemblies. Table 3.4. Similarly, increasing the treatment time of multiple PES membranes also made all four surfaces wettable within 2 seconds. Fig. 4.7. Hence, for PSf and PES membranes, the depth of penetration of the plasma was estimated to be ~150-300 μm or the thickness of 1-2 membranes.

Figure 4.8a shows CA data as a function of drop age for two PE membranes treated simultaneously with a H_2O plasma. In contrast to PSf and PES stacked assemblies, only Surface 1 was wettable after plasma treatment. Those surfaces on the interior of the stacked assembly (Surfaces 2 and 3) were untreated by the plasma, as evidenced by contact angles of ~120°. These data suggest very little penetration of the first membrane by the plasma. Note that a decrease in the CA of ~20° was, however, observed on Surface 4. Figure 4.8b shows CA data as a function of drop age for PE stacked assemblies treated for 3 and 9 minutes. Note that, in contrast to PSf and PES stacked assemblies, increasing the treatment time to 3 minutes did not afford complete wetting of Surfaces 1-4. Indeed, the surfaces on the interior of the stacked assembly (Surfaces 2 and 3) treated for 3 and 9 minutes were still unchanged by the treatment, with contact angles of ~120°. Increasing the treatment time of PE stacked assemblies did, however, affect the wettability of Surfaces 1 and 4. With a 3 minute treatment time, Surface 1 is essentially the same as for a 2 minute treatment, but a CA decrease of ~60° was measured for Surface 4. The 9 minute treatment time afforded further improvement in wettability for both surfaces, with Surface 1 wetting in <10 seconds, and the average CA on Surface 4 decreasing to ~30°. Fig. 4.8b.

One possible explanation for the CA decrease for Surface 4 of the PE stacked

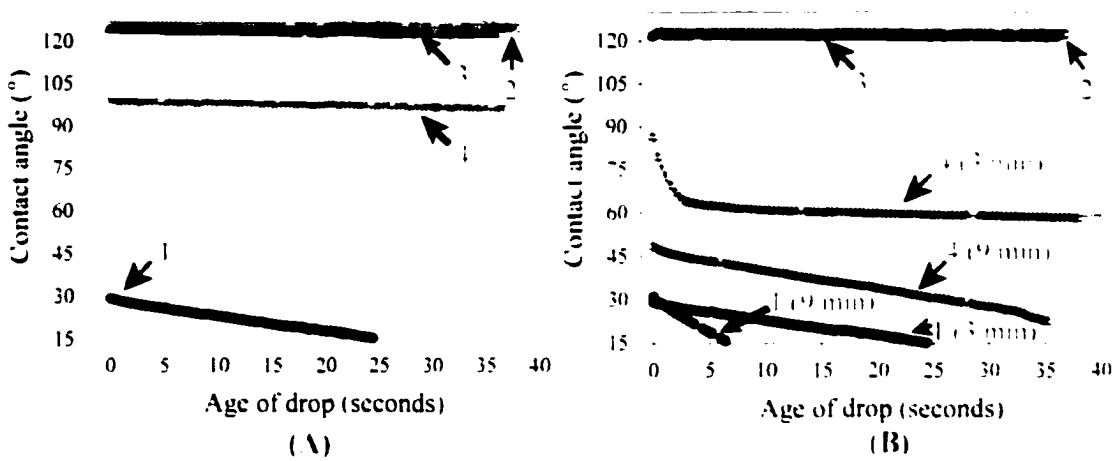

Figure 4.8 Contact angle as a function of drop age for stacked assemblies of PE membranes treated under different conditions. A) CA data for membranes treated with a 25 W H_2O plasma for 2 minutes immediately after treatment for Surface 1 (closed circles); Surface 2 (open circles); Surface 3 (closed triangles); and Surface 4 (open triangles). B) Data for membranes treated with a 25 W H_2O plasma for 3 minutes and 9 minutes. Surface 1 is represented by closed circles and Surface 4 by open triangles. Data shown for surfaces 2 and 3 is for a 3 minute treatment. The data for PE stacked assemblies treated for 9 minutes, not shown for clarity, are identical to that for the 3 minute treatment.

assembly at all treatment times is the non-hermetic seal between the membrane and the membrane holder. Indeed, Chapter 3 discussed similar results for a non-porous PSf resin treated in the membrane holder with a 25 W H_2O plasma for 2 minutes. Specifically, both sides of the resin showed improved wettability, including the downstream side not directly exposed to the plasma, Table 3.3. For comparison, a stacked assembly of PSf resin (2 pieces) was placed in the membrane holder and treated with a 25 W H_2O plasma for 9 minutes. Similar to PE membrane stacked assemblies, Surfaces 1 and 4 showed a significant improvement in wettability, with constant contact angles of ~25°, a decrease of ~50° from the untreated material. No change in the CA was observed on the interior surfaces, indicating that they were not treated by the plasma. As the non-porous PSf resin has a near-zero permeability, plasma treatment of the side farthest downstream is likely the result of penetration of the plasma around the non-hermetic seal between the membranes and the holder. This percolation of the plasma around the membrane does not, however, affect the CA on the interior surfaces of PSf resin and PE membrane stacked assemblies. In contrast, all surfaces of our PSf and PES membrane stacked assemblies were completely wettable after plasma treatment. Although permeation of the plasma around the membrane may contribute to the wettability of Surface 4, Surfaces 2 and 3 of PSf and PES stacked assemblies must be treated by penetration of the plasma *through* the membranes.

Our multiple membrane experiments confirm that all four surfaces of PSf and PES stacked assemblies are treated by the plasma. Demonstrating that the interior of the porous structure is also modified, however, is challenging as the interior of a porous

material is difficult to probe. ESEM images of the membrane cross sections wetting *in-situ* explicitly show whether hydrophilic surfaces were created throughout the porous structure. Figure 4.9 shows an ESEM image of the cross section of a treated PES membrane exposed to a saturated H_2O vapor environment. This image shows complete, instantaneous wetting of the entire membrane structure when exposed to water vapor. Specifically, the wetted areas appear dark and smooth, indicative of uniform wetting with no water droplet formation.[4] Hence, Fig. 4.9 demonstrates we have achieved hydrophilic modification of the entire PES membrane cross section.

A chronological series of ESEM images of a plasma-treated PE membrane are shown in Fig. 4.10. As shown in the first image (Fig. 4.10a), PE initially wets ~20 μm into the cross section from Side 1 (bottom of image), followed by wetting from Side 2 (top of image) also ~20 μm into the structure (Fig. 4.10b). This wetting pattern is consistent with our CA data, which indicate a difference in wettability between the upstream and downstream sides of the membrane. After extended exposure to H_2O vapor, portions of the cross section achieved complete wetting from top to bottom (Fig. 4.10c). However, bands of non-wetting structure remain sandwiched in the interstitial area as indicated by the presence of H_2O droplets on these hydrophobic areas. Hence, our ESEM data is indicative of non-uniform modification of the surfaces and interstitial pore area of PE membranes.[4] Furthermore, a substantial amount of the PE porous structure is not modified by plasma treatment, potentially contributing to the observed loss in hydrophilicity by migration of untreated polymer chains to the surface.

These results are consistent with our mass spectral experiments detecting plasma

Figure 4.9 ESEM image of the cross section of a PES membrane wetting *in situ* and instantaneously. Dark areas of the image indicate complete wetting of the membrane. The tight side of the membrane is oriented at the top of the image.

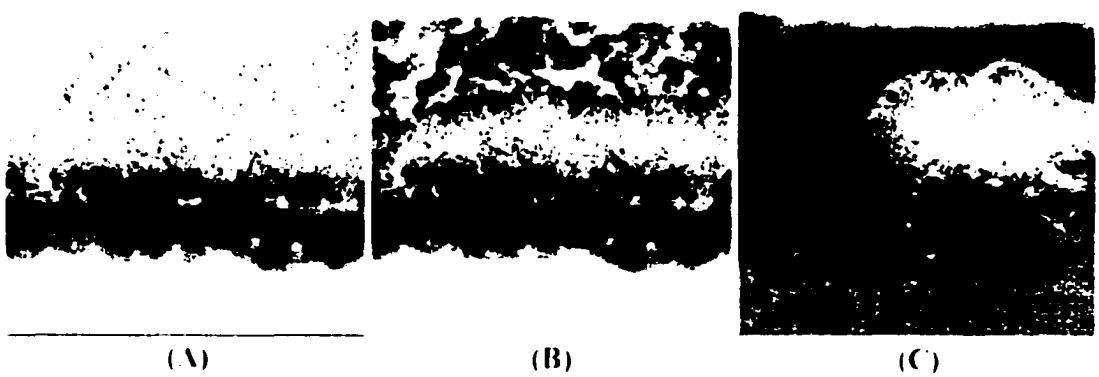

Figure 4.10 A chronological series of ESEM images (a-c) of the cross section of a PE membrane wetting *in situ*. The tight side of the membrane is oriented at the top of the image. Note that incomplete areas of wetting are lighter than areas of complete wetting.

species permeating the membrane cross section as well as gas-phase species generated directly in the plasma. Although Chapter 5 discusses our MS results in detail, Table 4.4 provides an abbreviated list of species present in a 25 W H_2O plasma molecular beam as well as those species detected downstream from PES and PE membranes. Although these data show that some of the same species present in the plasma were detected downstream from PES and PE membranes, it is clear that only a few plasma species penetrate PE membranes. Hence, the extent of hydrophilic modification through PES and PE membrane cross sections can be correlated to the degree of penetration of plasma species. Furthermore, the ability of plasma species to penetrate PES and PE membranes is related to membrane structure, with more plasma species detected downstream from the more open asymmetric PES membranes.

4.3 CONCLUSIONS

H_2O plasma treatment is a versatile method for treating a variety of porous materials as PSf, PES, and PE membranes all demonstrate improved wettability after plasma treatment. XPS analysis confirms that H_2O plasma treatment chemically modifies all three membrane materials similarly by incorporating oxygen-containing functional groups. Significant differences in the degree and permanency of hydrophilic modification were, however, observed for PE membranes. Although Surfaces 1 and 2 for treated PSf and PES were indistinguishable, differences in both wettability and oxygen incorporation were observed for the upstream and downstream sides of treated PE membranes. Furthermore, our ESEM images show non-uniform wetting of the PE membrane cross

Table 4.4 Mass spectral analysis of gas-phase species.

Conditions	m/z (amu)	Probable Assignments
H_2O plasma molecular beam[a]	1, 2, 17, 18, 28, 32	H, H_2, OH, H_2O, CO, O_2
Downstream from PES membrane[b]	1, 2, 28, 32	H, H_2, CO, O_2
Downstream from PE membrane[c]	2, 32	H_2, O_2

[a]Source conditions were: 100% H_2O, 25 W applied rf power.

[b]Species permeating through the thickness of a PES membrane.

[c]Species permeating through the thickness of a PE membrane.

[d]Experimental details are provided in Chapter 2.

[e]Detailed results are provided in Chapter 5.

section, with large areas of the porous structure unmodified by plasma treatment. Our membrane stacked assemblies and MS experiments demonstrate that incomplete modification of the PE membrane cross section can be correlated to the degree of penetration of the plasma through the membrane. In contrast to the permanent hydrophilicity of treated PES and PSf membranes, aging treated PE membranes resulted in a considerable loss of hydrophilicity. We attribute these changes to structural rearrangement of the polymer chains to decrease surface energy. Overall, the degree and permanency of hydrophilic modification depends on both the chemical composition of the polymer and the membrane structure.

4.4 REFERENCES

1. M. Mulder. *Basic Principles of Membrane Technology*: 2nd Ed. (Kluwer Academic Press. New York. 1996).
2. A. Ravve. *Principles of Polymer Chemistry*: (Plenum Press. New York. 1995. p. 327).
3. T. D. Brock. *Membrane Filtration: A User's Guide and Reference Manual*: (Science Tech. Inc.. Madison. Wisconsin. 1983).
4. R. E. de la Parra. *Micros. Res. Tech.* **25,** 362 (1993).
5. M. L. Steen. L. Hymas. E. D. Havey. N. E. Capps. and F. R. Fisher. *J. Membr. Sci.* **188,** 97 (2001).
6. M. L. Steen. C. I. Butoi. and E. R. Fisher. *Langmuir* submitted for publication.
7. R. d'Agostino. F. Cramarossa. F. Fracassi. and F. Illuzzi. *Plasma Deposition. Treatment and Etching of Polymers*: (Academic Press. San Diego. 1990).
8. T. R. Gengenbach. R. C. Chatelier. and H. J. Griesser. *Surf. Interface Anal.* **24,** 611 (1996); T. R. Gengenbach and H. J. Griesser. *Surf. Interface Anal.* **26,** 498 (1998).
9. A. Chilkoti and B. D. Ratner. *Surf. Interface Anal.* **17,** 567 (1991).
10. R. H. Hansen. J. V. Pascale. T. de Benedictis. and P. M. Rentzepis. *J. Polym. Sci. A* **3,** 2205 (1965).
11. F. D. Egitto and L. J. Matienzo. *IBM J. Res. Develop.* **38,** 423 (1994).
12. W. R. Harshbarger. R. A. Porter. T. A. Miller. and P. Norton. *Appl. Spectrosc.* **31,** 201 (1977).
13. E. O. Degenkolb. C. J. Mogab. M. R. Goldrich. and J. E. Griffiths. *Appl.*

Spectrosc. **30,** 520 (1976).

14. N. Inagaki. *Plasma Surface Modification and Plasma Polymerization:* (Technomic Publishing. Lancaster. PA. 1996).

15. S. H. Wheale. C. P. Barker. and J. P. S. Badyal. *Langmuir* **14,** 6699 (1998).

16. K. Asfardjani. Y. Segui. Y. Aurelle. and N. Abidine. *J. Appl. Polym. Sci.* **43,** 271 (1991).

17. All bond energies are derived from thermochemical data found in: S. G. Lias. J. E. Bartmess. J. F. Liebman. J. L. Holmes. R. D. Levin. and W. G. Mallard. *J. Phys. Chem. Ref. Data* **17,** Suppl. 1 (1988).

18. A. Mas. H. Jaaba. and F. Schue. *Pure Appl. Chem.* **A34,** 67 (1997).

19. A. S. Hoffman. *Macromol. Symp.* **101,** 443 (1996).

CHAPTER 5

IDENTIFICATION OF GAS-PHASE REACTIVE SPECIES AND CHEMICAL MECHANISMS OCCURRING AT PLASMA-POLYMER SURFACE INTERACTIONS

This dissertation chapter contains results from a full paper submitted for publication to *Langmuir*. The manuscript was written by M. L. Steen and edited by Professor E. R. Fisher. The coauthor was C. I. Butoi. The work presented here encompasses a systematic study of the underlying chemistry of the H_2O plasma surface modification. This chapter describes characterization of the gas-phase as well as molecules generated at the membrane surface during plasma modification using three gas phase analytical tools. In addition, alternate plasma reactor configurations were explored to examine the formation of reactive species and the effects of ions on the surface modification.

5.1 INTRODUCTION

As discussed in Chapter 1, plasma modification of polymers occurs when gas-phase species react at a surface to form stable products with physical and or chemical properties that differ from those of the bulk polymer.[1-3] Reactive neutrals, ions, electrons, and photons generated in the plasma can all interact with the polymer to alter surface chemical composition and wettability.[4-6] As a result, the nature and energy distributions of the species impinging on the polymer surface ultimately determine the observed change in the surface properties.[7-9,10,11] Electron impact processes influence the density of these species; however, direct energy transfer arises from ions and metastables. Alternatively, plasma species can abstract atoms from the surface and break polymer chains. Radical species can combine at free radical sites created in the polymer and implant new functional groups, thereby altering the surface composition of the polymer.[7]

Chapters 3 and 4 reported plasma modification of polysulfone (PSf), polyethersulfone (PES) and polyethylene (PE) membranes for permanent wettability.[12,13] PSf, PES, and PE surfaces are completely wettable immediately after plasma treatment and this wettability remains more than a year after treatment. The permanence of the hydrophilic modification is a direct result of covalently-bound O-H, C-O and C-O_x (e.g. C=O, O-C=O) groups introduced by H_2O plasma treatment. Furthermore, complete penetration of the plasma through the membrane is achieved with our experimental design. Accordingly, environmental SEM (ESEM) confirms complete wetting of the entire porous structure *in situ*.

To further explore the molecular-level chemistry, we determined the gas-phase

composition of our H_2O plasma under the same conditions used to process polymeric membranes (25 W, 50 mTorr, 2 min.). Excited-state OH and H atoms as well as H_2 were identified in the optical emission spectrum.[12,13] At the low plasma powers used to treat our membranes, no emission from excited O atoms was observed. Clearly, all of the species generated in the plasma, including ions and UV photons, may contribute to plasma modification. Direct evidence of the nature of the plasma-surface interactions, however, is needed to ultimately define the contribution of specific plasma species to the observed changes in composition and wettability. Hence, our first step toward this end was to identify excited-state species generated only during plasma modification. For example, OES confirmed the presence of excited-state CO, not observed without a membrane in the reactor, Fig. 3.7. Thus, we were able to detect reactive plasma species as well as products of the surface modification of PSf, PES, and PE.

Polymer modification processes can further benefit from a thorough description of the actual chemical reactions occurring within the plasma-polymer interface.[14] One such study was performed by Badyal and co-workers, who identified and monitored the time-dependent concentrations of plasma-polymer interfacial reaction products and intermediates.[15] These experiments entailed mass spectral detection of gas-phase species permeating across the plasma-polymer interface during O_2 plasma surface modification of a low-density PE film. A rapid rise in the concentration of oxidized permeant species, H_2O, CO, and CO_2, along with consumption of reactant O_2 was observed, indicating that surface oxidation coincided with plasma ignition. Mechanistic information was gleaned solely from mass spectrometric sampling at the oxygen plasma-polymer interface and XPS

analysis of the plasma-treated surface.

In this chapter, mass spectral experiments similar to those performed by Badyal and co-workers were performed to examine plasma-surface interactions occurring during processing of polymeric membranes. In our experiments, gas-phase species permeating porous membranes, were detected by mass spectrometry. In addition, all gas-phase species generated in the plasma, including nascent ions, were characterized through mass spectral identification. The contribution of these ionic species to the overall plasma process was assessed by utilizing reactor designs that limit bombardment by charged species. Furthermore, the amount of ionizing radiation the membranes are exposed to during plasma processing was quantified with dosimeter foils.

Although mass spectrometry is useful for identifying plasma species, our Imaging of Radicals Interacting with Surfaces (IRIS) experiments are uniquely suited to provide relevant mechanistic information about plasma systems.[16] This highly selective, laser-induced fluorescence (LIF) technique allows identification and independent study of one specific radical in a molecular beam populated with many different species. Experimentally-determined surface loss coefficients (or sticking probabilities) are obtained *in situ* and provide direct information on the physical and chemical mechanisms occurring at the plasma-surface interface. Here, the IRIS method was used to study OH radicals in a 100% H_2O plasma molecular beam during plasma processing of polymeric membranes. We have previously employed IRIS to study OH radicals interacting with 300 K SiO_2 and Si_3N_4 substrates, finding an intermediate reactivity of ~0.5 with these materials.[16,17] We have also used IRIS to study other polymer modification systems. Specifically, CF_4 and

NH_2 radical species were studied in plasma systems used to modify polymers by plasma deposition (hexafluoropropylene oxide, HFPO), etching (C_2F_6) and functional group implantation (NH_3).[18] A range of surface interactions was observed, depending on the dominant plasma process in each system.

Collectively, the three experimental techniques used here (OES, LIF, MS) provide extensive data on the underlying chemistry in the H_2O plasma modification system, from the gas-phase, to the plasma surface interface, to the actual surface modification. OES was used to identify *excited-state* species present in the plasma under the same conditions used to process the membrane as well as during plasma modification. Our LIF-based radical-imaging experiments afford identification of *ground-state* radical species and elucidation of steady-state plasma-surface interactions. Mass spectral experiments provide data on both neutral and ionic species. Accordingly, the combination of all three techniques provides a nearly complete profile of plasma species. To support the gas-phase characterization of the plasma, X-ray photoelectron spectroscopy (XPS) data are also presented along with contact angle measurements. In addition, alternate plasma reactor configurations are used to examine the formation of plasma species and the effects of ions on the surface modification. For comparison to our H_2O plasma surface modification, gas-phase and surface analysis data are also included for membrane treatments using an H_2 plasma.

5.2 RESULTS

5.2.1 OES. Figure 5.1a contains an OES spectrum obtained for a 25 W H_2O

plasma under the same conditions used to process membranes. This spectrum shows emission from OH and H radicals as well as H_2 in the plasma. No emission from other species, including O atoms, is observed. Figures 5.1b and 5.1c show the OES spectra for plasmas at higher applied rf powers (P). Although these signals do not represent absolute intensities, emission from OH, H, and H_2 clearly increases in intensity with P, suggesting more of these species are produced at higher P. Additional emission lines, observed at 410.09 and 434.15 nm are attributed to the more energetic atomic hydrogen lines, H_δ and H_γ, respectively.[19] Also observed at the higher rf powers are emission lines at 436.8, 533.1, 543.6, 615.60, and 648.16 nm. These lines, assigned to emission from excited O atoms,[20] demonstrate that O atoms are formed at higher P, presumably by increased fragmentation of the parent gas.

Alternate reactor designs. The OES spectrum shown in Fig. 5.2a was obtained using the L-shaped reactor, Fig. 2.1b, and that in Fig. 5.2b was acquired with the T-shaped reactor design, Fig. 2.1c using 25 W H_2O plasmas. In the L-configuration, the majority of charged species (e.g. ions and electrons) are lost at position 2 by recombination with the reactor wall. In the T-configuration, the OES port is relatively remote from the plasma. In both configurations, however, the OES spectra show the presence of OH and H radicals as well as molecular H_2, similar to results in Fig. 5.1a for our typical reactor design. Again, no emission from O atoms is observed in a 25 W H_2O plasma, regardless of reactor design. Hence, the same neutral species are present in the plasma, regardless of reactor design.

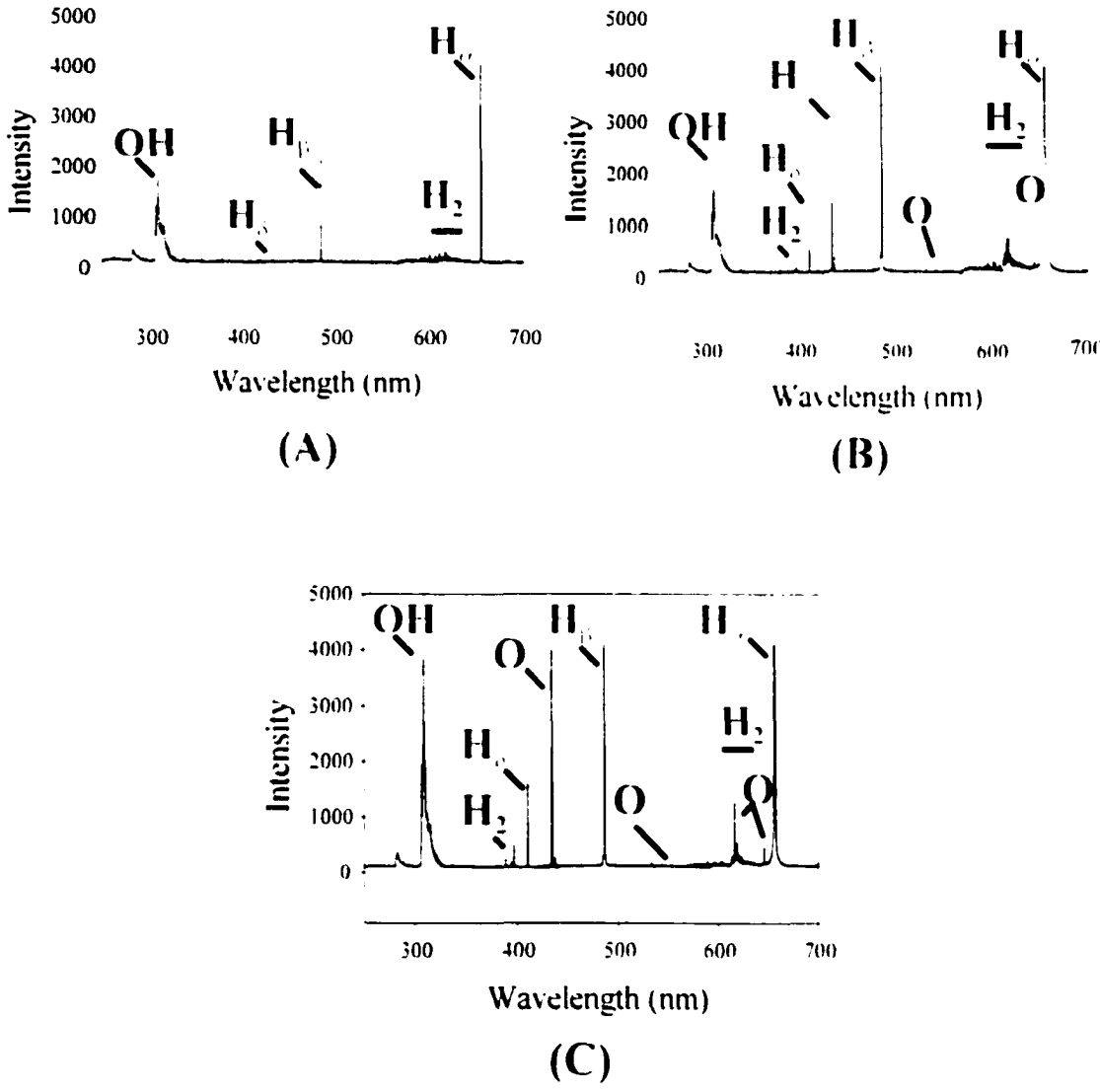

Figure 5.1 Optical emission spectra of a 25 W H_2O plasma (50 mTorr) acquired at (A) 25 W; (B) 75 W; and (C) 125 W in our standard plasma reactor.

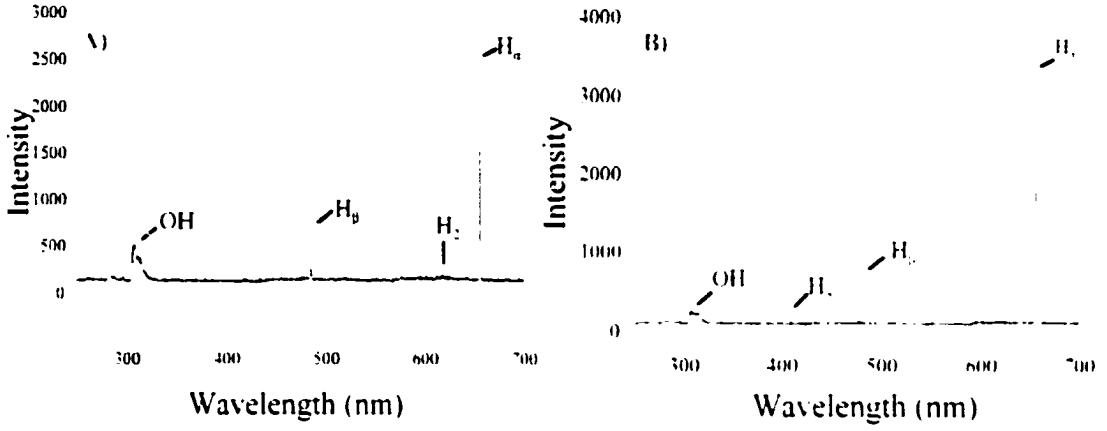

Figure 5.2 Optical emission spectra of a 25 W H_2O plasma (50 m Torr) acquired in (A) the L-shaped plasma reactor and (B) the T-shaped plasma reactor.

Plasma-surface interactions. OES was also used to detect excited-state species generated *during* membrane processing at 25 W. Figure 5.3 contains OES spectra obtained with two different polymeric membranes in the plasma reactor. Fig. 5.3a shows the OES spectrum obtained with a PE membrane, and clearly indicates emission lines attributable to CO at 282.73, 297.12, 312.61, 329.84, 450.65 482.90, 519.23, and 560.45 nm.[21] None of these emission lines were observed without a membrane in the reactor, Fig. 5.1. The observed generation of CO here is consistent with OES spectra obtained during plasma processing of PSf and PES membranes[12,13] and confirms that we are oxidizing these materials.[22] In contrast, however, emission from CO is not observed in the OES spectrum obtained for a 25 W H_2O plasma with a PTFE membrane in the reactor, Fig. 5.3b. The absence of CO indicates that this low power plasma does not effectively oxidize PTFE, a material known for its chemical inertness. Interestingly, emission from CO is observed in the PTFE system when the applied rf power is increased to 100 W, Fig. 5.3c. Note that HF* is not observed during plasma processing of PTFE membranes at any power.

Alternate plasma treatments. H_2 plasma was chosen as a comparative system to the H_2O plasma because these two systems have many of the same reactive species. As expected, Figure 5.4 shows emission from H radicals and H_2 in the OES spectrum obtained for a 25 W H_2 plasma. Emission from these species is also observed in the H_2O plasma under similar conditions, Fig. 5.1a. Additionally, CO was not observed in the OES spectrum of a H_2 plasma with a PES membrane in the reactor, Fig. 5.4b, which implies that the membrane is not efficiently oxidized by the H_2 plasma treatment. Likewise, no

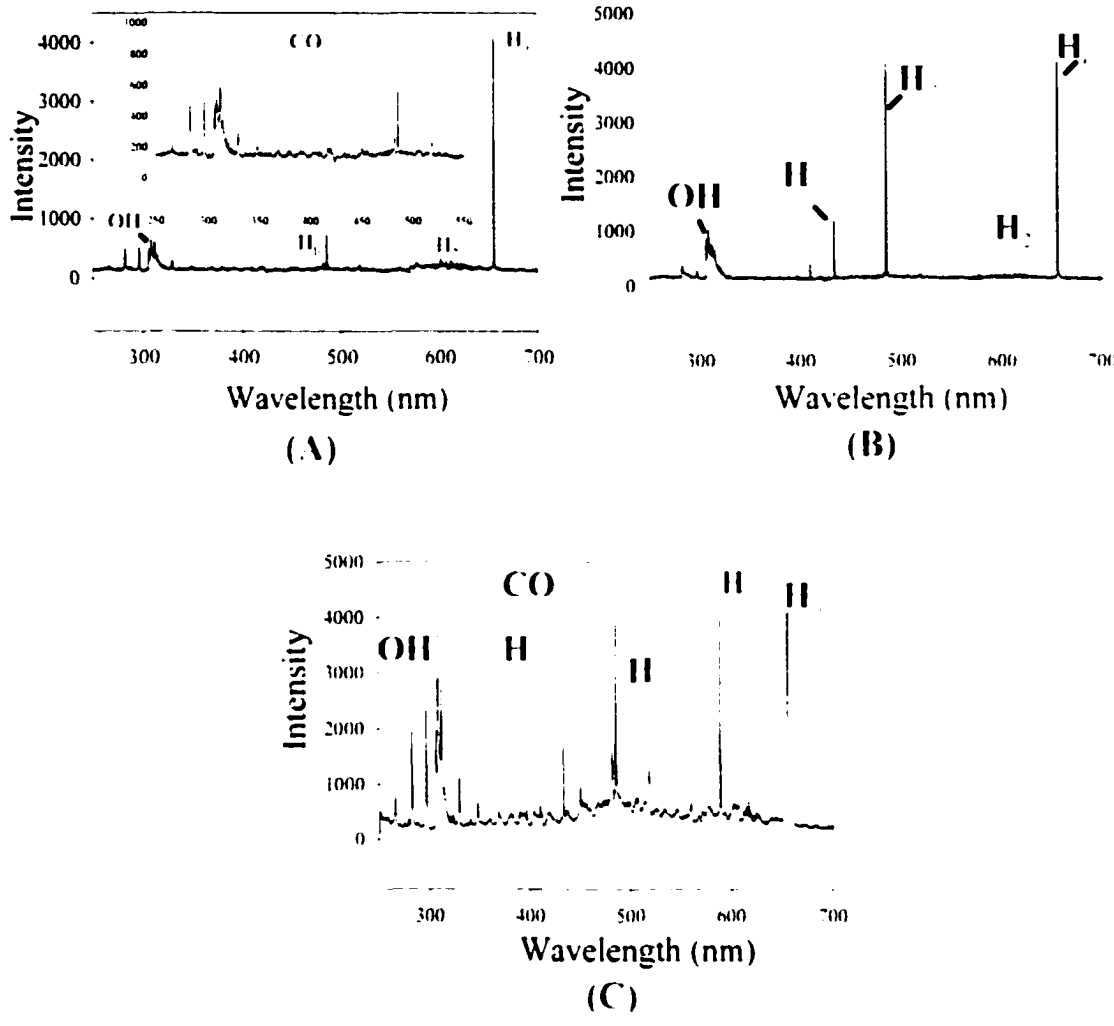

Figure 5.3 Optical emission spectra of a 25 W H_2O plasma (50 mTorr) acquired with (A) a PE membrane in the reactor and (B) a PTFE membrane in the plasma reactor. The spectrum in (C) was acquired with a PTFE membrane in the reactor at P = 100 W.

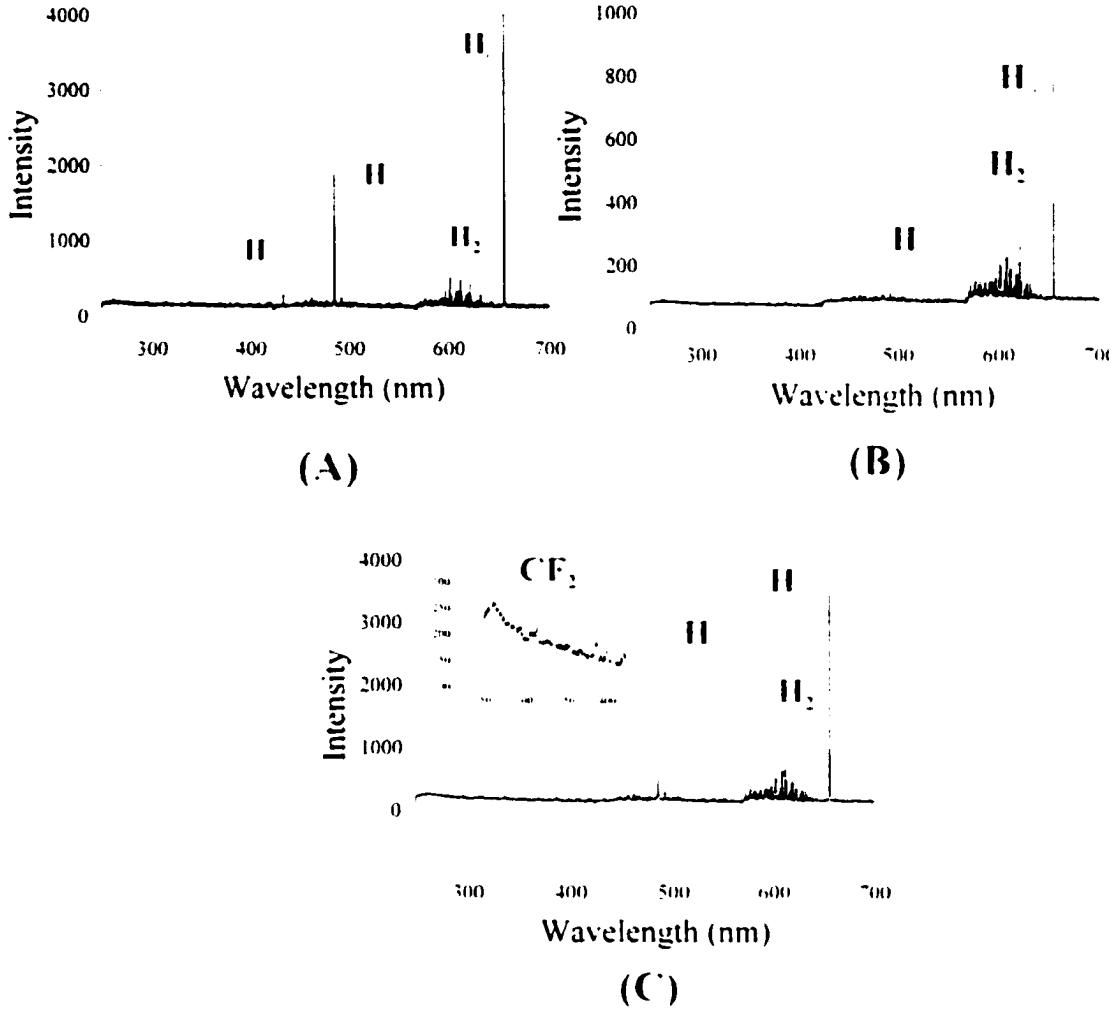

Figure 5.4 Optical emission spectra of a 25 W H_2 plasma. All three spectra were obtained with a flow rate of H_2 = 1 sccm (~100 mTorr). The spectrum in (A) was obtained without a membrane in the reactor. Spectra were also obtained with (B) PES: and (C) PTFE membranes in the reactor. The inset in (C) shows an expanded view of the 200-425 nm region.

CO emission was observed during 25 W H_2 plasma processing of PE and PTFE membranes. Notably, however, CF_2 emission (at 220-280 nm)[23] is observed in the OES spectrum of H_2 plasma with a PTFE membrane in the reactor, Fig. 5.4c.

We have also examined the results of H_2 plasma treatment on the surface properties of PES, PE, and PTFE membranes using contact angle measurements. For PES, an increase of ~15° was observed in the contact angles measured on both membrane surfaces after treatment, creating a more hydrophobic surface. With PE, no significant change in contact angle was measured on either membrane surface following H_2 plasma treatment. For PTFE, a decrease of ~10-15° in the contact angle is observed, creating a less hydrophobic surface. This is, however, only a slight improvement in the hydrophilicity as the contact angles on treated PTFE remain ~100°. In contrast, H_2O plasma treatment resulted in more hydrophilic surfaces for both PES and PE, and no discernible change in the wettability of PTFE.

5.2.2 LIF. We have previously reported the LIF excitation spectrum for OH radicals in a 100% H_2O plasma molecular beam.[16] Comparison to literature spectra verifies that the fluorescing species is indeed OH.[24] In the present work, we have characterized the composition of the H_2O plasma molecular beam by determining the relative amounts of ground-state OH in the molecular beam as a function of applied rf power, Fig. 5.5. OH LIF signal is detected at all P, with formation of OH increasing rapidly with P. Because we are saturating the probed transition, these intensities correspond to the relative densities for OH.

Plasma-surface interactions. PSf, PES, PE, PTFE membrane materials

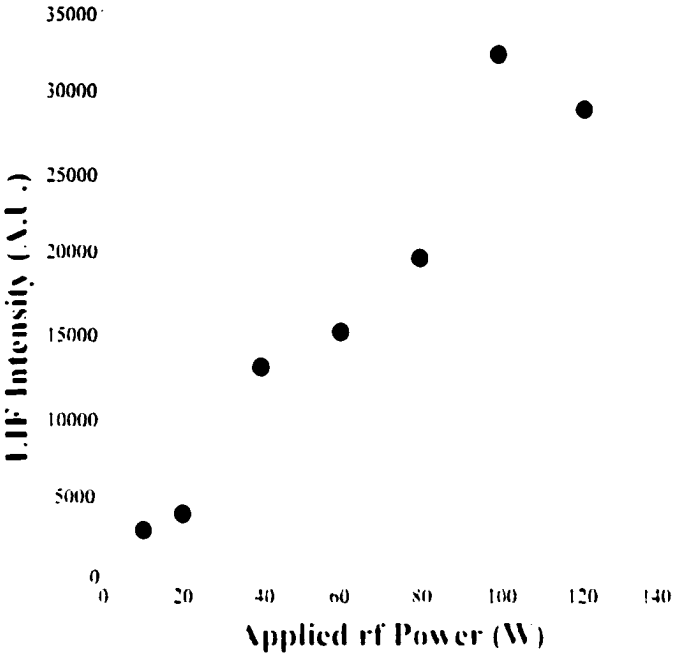

Figure 5.5 LIF signal intensity as a function of applied rf power (10-125 W) for ground-state OH radicals in a H_2O plasma molecular beam obtained using the IRIS apparatus.

were used in our IRIS studies to determine the steady-state reactivity of OH radicals at the membrane surface during H_2O plasma processing. Figure 5.6 shows three IRIS images depicting OH LIF signals using a 125 W H_2O plasma molecular beam and a PES membrane. In Fig. 5.6a, LIF signal from OH radicals just in the molecular beam is imaged, whereas Fig. 5.6b contains LIF signal from both incident OH radicals as well as OH radicals scattered from the membrane surface. The difference between the images shown in Fig. 5.6b and Fig. 5.6a provides a spatially-resolved image of the OH radicals scattered from the membrane surface, Fig. 5.6c. Clearly, there is a significant number of molecules leaving the plasma-treated substrate.

Figure 5.7a shows the data of Figs. 5.6a and 5.6c converted to cross sections along the laser axis. The broad spatial distribution and the shift of the scattered signal peak maximum away from the molecular beam maximum indicate the OH radicals scatter with a cosine angular distribution. Also shown in Fig. 5.7a are simulated curves for the incident beam and for scattered molecules, assuming an absorption-desorption mechanism, with $R = 0.47$. Averaging several data sets yields an overall value of $R = 0.44 \pm 0.03$. For comparison, Fig. 5.7b shows a representative set of experimental and simulated curves for OH radicals interacting with a PTFE membrane using a 75 W H_2O plasma. These data are also reproduced by the simulation assuming an absorption-desorption mechanism, with $R = 0.55$. Averaging several data sets leads to an overall value of $R = 0.47 \pm 0.06$ for these conditions. OH R values obtained for different microporous membranes as a function of applied rf power are listed in Table 5.1. These data confirm moderate OH reactivity ($R \sim 0.5$) for nearly all substrates and applied rf powers. The values measured

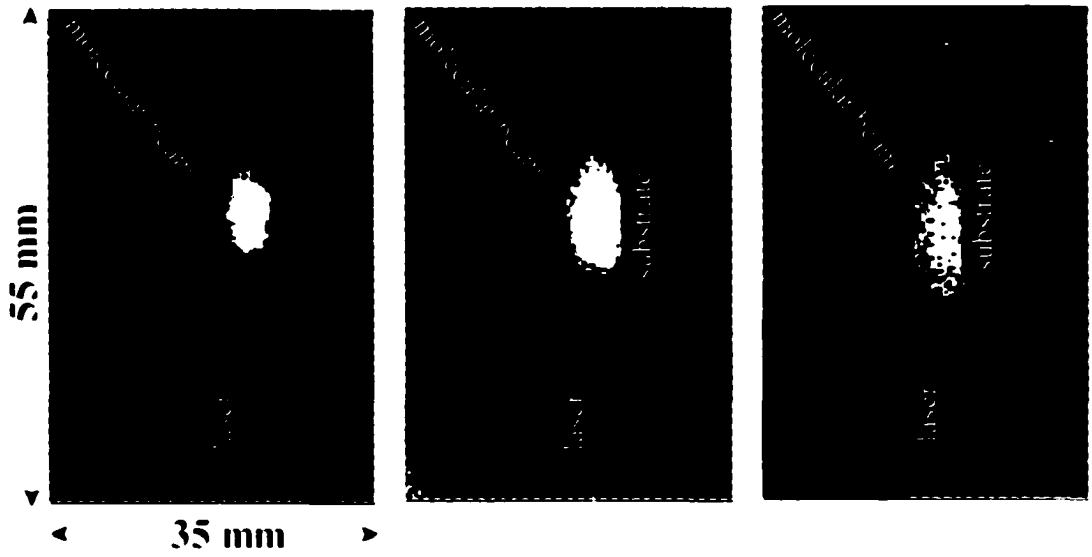

Figure 5.6 Spatially-resolved two dimensional ICCD images of LIF signals produced by OH radicals (A) in the 125 W H_2O plasma molecular beam; and (B) with a PES membrane rotated into the path of the molecular beam. The image shown in (C) is the difference between the images shown in (A) and (B), corresponding to OH radicals scattering from the membrane substrate.

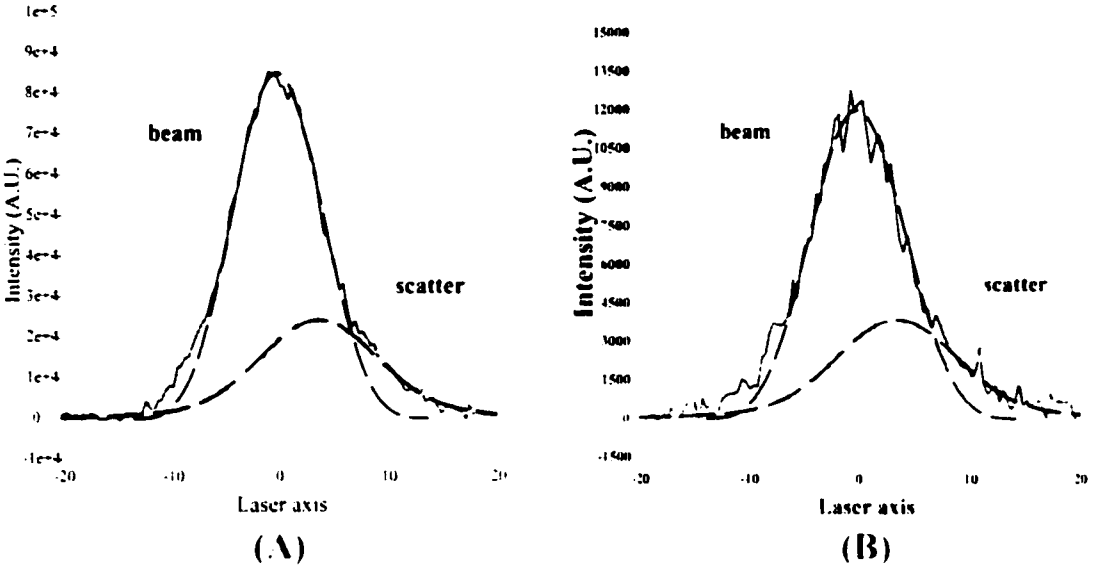

Figure 5.7 One-dimensional cross sections of the LIF signal for OH radicals interacting with (A) a PES membrane using a 125 W H_2O plasma molecular beam; and (B) a PTFE membrane using a 75 W H_2O plasma molecular beam. The dashed lines are the simulated fits to the experimental data, an adsorption-desorption model with $R = 0.47$ for (A) and $R = 0.55$ for (B). The laser-surface distance was 3 mm for both data sets.

Table 5.1 Surface reactivity (R) values determined for OH generated in a H_2O plasma.[a]

Substrate Material	Applied rf Power (W)		
	25	75	125
PES	0.45 ± 0.05	0.49 ± 0.1	0.44 ± 0.03
PTFE	0.31 ± 0.07	0.47 ± 0.06	0.51 ± 0.05
PE	0.50 ± 0.05	—	0.42 ± 0.03
PSf[b]	0.56 ± 0.07	0.48 ± 0.10	0.40 ± 0.07
UF-PSf[c]	—	0.47 ± 0.06	0.27 ± 0.03
PSf Resin	0.40 ± 0.03	0.44 ± 0.05	0.46 ± 0.04

[a]Dashes indicate reactivity values were not obtained for these conditions.

[b]These substrates were BTS-55 membranes from US Filter.

[c]These substrates were ultrafiltration membranes with an average pore diam. of ~0.01 μm.

here are very similar to OH R values measured previously for 300 K SiO_2 (0.55 ± 0.1)[16] and Si_3N_4 (0.57 ± 0.05)[17] substrates during H_2O plasma processing.

Notably, some of the R values in Table 5.1 significantly deviate from $R = 0.5$. First, applied rf power has an effect on OH reactivity on PSf and PTFE membranes. Microporous PSf and ultrafiltration (UF) PSf both show a decrease in R with increasing power. Of these, the effect was more pronounced for UF PSf membranes at $P = 125$ W. In contrast, R values measured at non-porous PSf substrates remain fairly consistent for the three applied powers studied here. This is also true for PES and PE substrates. A second trend in the reactivity values with power was observed for PTFE. Here, R increased from 0.31 ± 0.07 at $P = 25$ W to 0.51 ± 0.05 at $P = 125$ W. Possible explanations for these results are discussed in Section 5.3.

5.2.3 MS. Mass spectral data for a molecular beam generated from a 25 W H_2O plasma are shown in Fig. 5.8. The spectrum in Fig. 5.8a, corrected for the background H_2O molecular beam (i.e. no plasma), was obtained using the ionizer of the mass spectrometer. The observed peaks represent either neutral species ionized by the mass spectrometer or nascent ions present in the molecular beam. The most likely assignment for signals at 1, 2, 16, 17, 18, 28, and 32 amu are H, H_2, O, OH, H_2O, CO and O_2 and or S, respectively. The background-corrected spectrum obtained with the ionizer disabled is shown in Fig. 5.8b. The observed peaks in this spectrum represent nascent ionic species present in the plasma molecular beam. There are clearly fewer species present in this spectrum with only two major peaks at 2 and 18 amu, attributable to H_2^+ and H_2O^+, respectively.

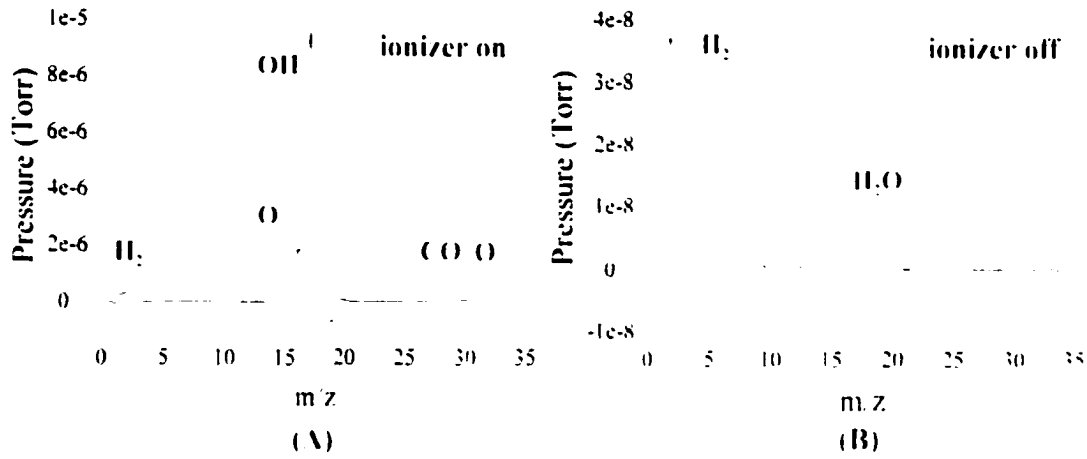

Figure 5.8 Mass spectra of a 25 W H_2O plasma molecular beam obtained (A) with and (B) without the ionizer of the mass spectrometer. All of the reported spectra were background subtracted, correcting for the spectrum obtained with just the H_2O molecular beam (i.e., no plasma).

Plasma-surface interactions. Our mass spectrometer was also employed to study plasma-membrane interactions by affixing the membrane to the beam collimating slits, Fig. 2.4. In this configuration, only molecular beam species permeating the membrane were detected. Figure 5.9 contains four mass spectra. The background corrected spectra in Figs. 5.9a and 5.9b were collected downstream from a PES membrane with and without the ionizer, respectively. Figure 5.9a contains signals from H, H_2, CO, and O_2 and/or S, whereas Fig. 5.9b clearly shows that no nascent ions are detected downstream from the membrane. The spectrum in Fig. 5.9a also contains an over-subtraction of the region between 16 and 19 amu because not all of the molecular beam species, Fig. 5.9a, penetrate the membrane. Figures 5.9c and 5.9d show similar results obtained for a PE membrane affixed to the beam collimating slits, indicating only a few species (H_2, O_2 and or S) penetrate the PE membrane. Furthermore, no nascent ions are detected downstream from the membrane, Fig. 5.9d.

5.2.4 DOSIMETER FOILS. The level of ionizing radiation our membranes experience from plasma ions and UV photons was assessed by dosimeter foils at various locations in the different reactor configurations. Dosimeter foils were placed in the coil region and at the membrane location during processing with the standard reactor configuration (Fig. 2.1a) and the T-shaped reactor (Fig. 2.1c). In both configurations, the membrane is exposed to ~10 kGy of radiation during 25 W H_2O plasma treatment. In contrast, the amount of radiation generated in the coil region of the plasma is ~20 kGy. This is consistent with the observation that membranes treated directly in the coil region display obvious damage and can be destroyed even under mild conditions.

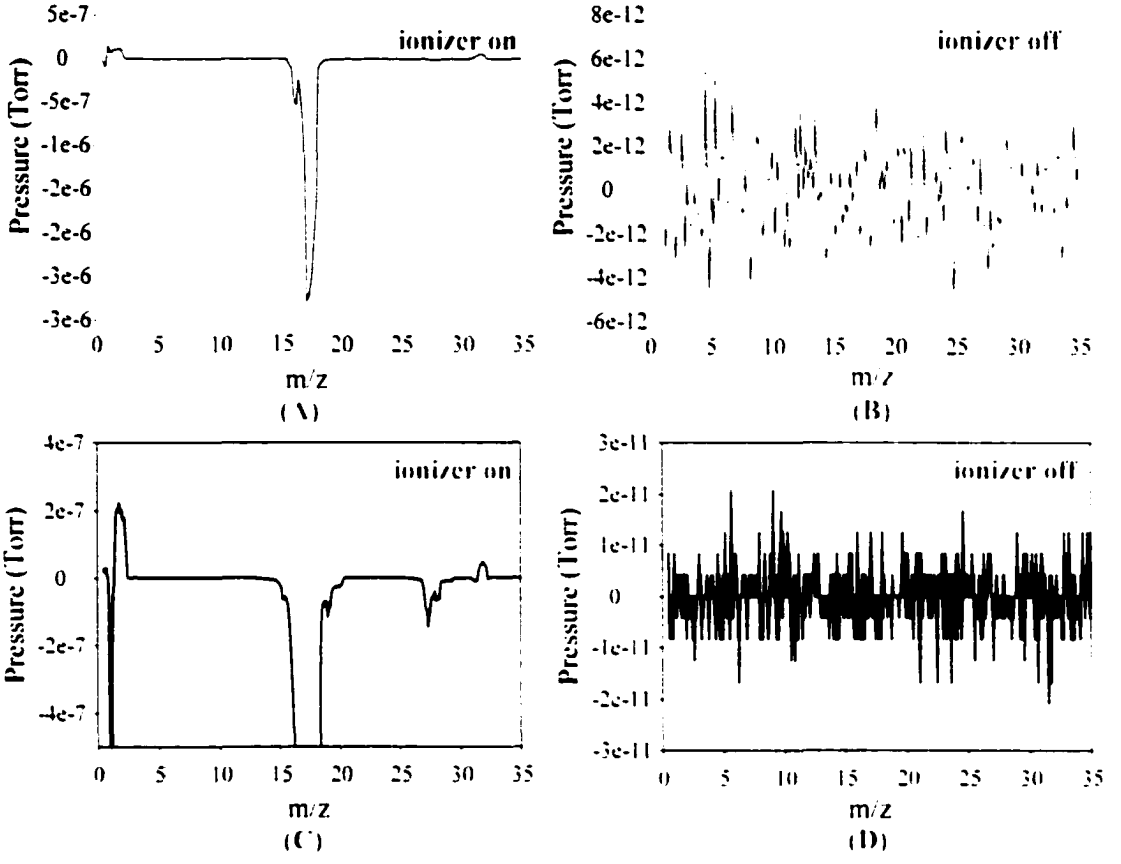

Figure 5.9 Mass spectra of a 25 W H_2O plasma molecular beam obtained with a membrane on the beam collimating slits. Spectra in (A) and (B) were obtained with a PES membrane placed on the beam collimating slits, with and without the ionizer, respectively. The spectra in (C) and (D) were obtained with a PE membrane on the beam collimating slits, with and without the ionizer, respectively. All of the reported spectra were background subtracted, correcting for the spectrum obtained with just the H_2O molecular beam (i.e. no plasma).

The downstream treatment, however, does not result in damage to the membrane surface under the same conditions.[12]

5.2.5 XPS. While the gas-phase is the focus of this Chapter, it is important to note the major chemical compositional changes that occur to the polymers during plasma modification. Figure 5.10 shows the C_{1s} spectra for a PE membrane treated in a 25 W H_2O plasma, demonstrating the incorporation of significant amounts of oxygen in the treated sample. Note that CH_x groups contribute 100% to the high resolution C_{1s} spectrum for untreated PE, Table 5.2. Details of the C_{1s} analyses for all of the membrane materials studied here are also listed in Table 5.2. In general, oxygen incorporation is the major result of the modification process for the nonfluorinated polymers. Although little oxygen incorporation is observed with PTFE, pronounced defluorination is observed with both the H_2O and H_2 treatments, Table 5.2. This has been observed previously with H_2 plasma treatment of fluoropolymers.[25]

5.3 DISCUSSION

As noted in the Introduction, the identification of reactive species and the plasma-surface interactions occurring during polymer processing constitutes an important step in determining the reactions involved in surface modification. Through our combined experimental approach, mechanistic implications for H_2O plasma processing are drawn from independent study of the surface, the gas-phase, and the plasma-surface interface. Of these, the plasma-surface interface is the most difficult to characterize. Our IRIS results, however, afford detailed chemical information about the interface not available through

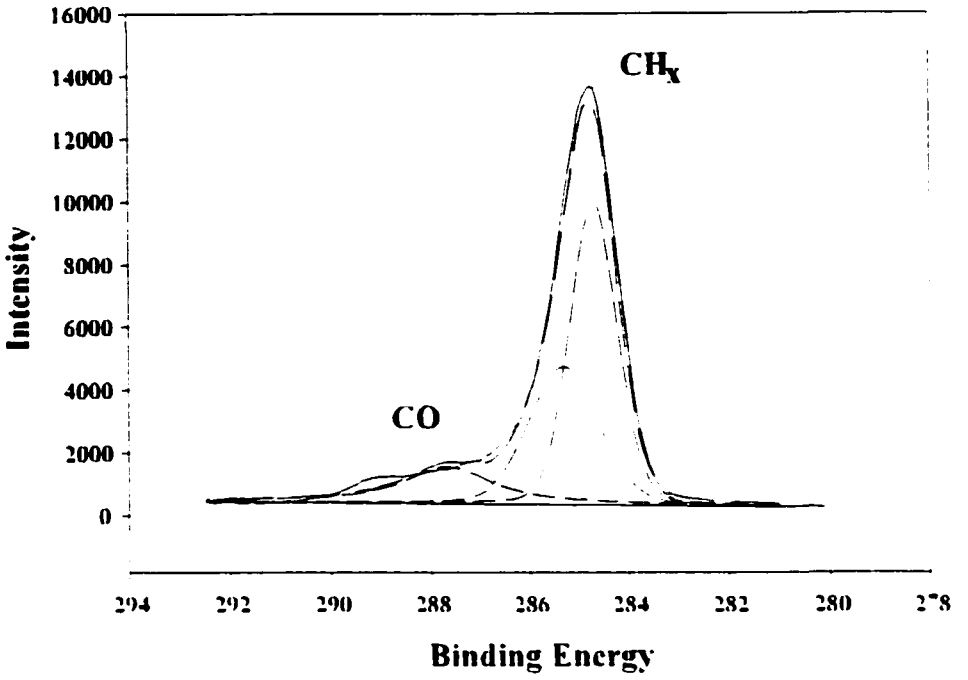

Figure 5.10 High resolution XPS C_{1s} spectrum for a PE membrane treated with a 25 W H_2O plasma using a photoelectron takeoff angle of 55°. Note that CH_x groups have a 100% contribution to the high resolution C_{1s} spectrum for untreated PE, Table 5.2.

Table 5.2. Abbreviated XPS results for plasma modification of membranes.[a]

		% contribution to C_{1s}				
Membrane Material	**O/C ratio**	**CH_x**	**CO**	**CO_x[b]**	**CF_2**	**OH (%)**
Untreated PSf	0.14	84	16	0	-	0
Treated PSf	0.30	74	19	9	-	1.7
Untreated PES	0.23	83	17	0	-	0
Treated PES	0.37	76	19	5	-	1.1
Untreated PE	0.00	100	0	0	-	0
Treated PE	0.38	74	18	8	-	1.7
Untreated PTFE	0.00	0	0	0	99	0
PTFE (25 & 100 W H_2O)[c]	0.03	-	-	-	88	-
PTFE (25 W H_2)[c]	0.06	-	-	-	63	-

[a]More detailed XPS results can be found in references 12 and 13. Data are listed for analysis of the upstream (facing the plasma) side of the membrane. Analysis of the high resolution C_{1s} spectrum provides percentages for the carbon centers (CO, CO_x, CF_2)

[b]CO_x is the total amount of C=O, O-C=O, etc.

[c]No values are listed for the CO and CO_x peaks as a unique peak fit of the C_{1s} spectra could not be obtained due to a low binding energy tail below the CF_2 peak. This tail contains contributions from added oxygenated species and defluorinated species from the PTFE membrane.

studies concentrating on isolated aspects of either the plasma or the surface modification. Moreover, the combination of IRIS with the gas-phase data presented here (both OES and MS) and the surface analysis data[12,13] provides a relatively complete chemical picture of the overall process.

Formulating reliable chemical mechanisms for plasma modification of polymers is particularly difficult as polymeric substrates often contain a variety of surface moeities, increasing the number and complexity of possible plasma-surface interactions. Understanding the fundamental aspects of polymer modification is further complicated by the observation that rearrangement, additional surface oxidation, and functional group migration can occur on a rapid time scale.[26] Moreover, different polymers may be modified by the same plasma via different mechanistic routes. All of these factors contribute to the difficulty in assigning exact mechanisms for plasma-mediated processes. Below we discuss our results as a function of the polymer being modified, with a focus on the specific mechanisms acting in each case.

5.3.1 PSf and PES. Of the polymer materials studied here, PSf contains the highest number of different moieties, including phenyl, ether, methyl and sulfone groups, Scheme 1.1. As discussed in Chapter 1, oxidation occurs at all three positions indicated in this scheme. The evidence for this comes largely from XPS data, which indicate that a substantial number of carbonyl groups, such as aldehyde, ketone, and carboxylic acid are introduced by plasma treatment, Table 5.2. In addition, production of gas-phase CO is observed during plasma processing of PSf membranes.[12] Most significantly, our direct, non-intrusive IRIS experiments confirm that OH reacts with a ~50% probability at the

surface of PSf membranes, Table 5.1. Combination of OH radicals with surface atoms resulting in the changes in surface composition noted above must occur through cleavage of C-S, C-C, C-O, or C-H bonds. As shown in Chapter 1, cleavage of the C-H bond on the methyl group by OH is the only path that would result in direct formation of an alcohol group in the membrane. However, this C-H bond requires the most energy to break (~4.5eV),[c] which may partially explain why only a small number of alcohol groups are incorporated in the treated material, Table 5.2.

Note that our IRIS results show a decrease in the OH reactivity with increasing rf power for the PSf substrates, Table 5.1. There is a slight decrease in R values with BTS55 between P = 25 and 125 W, and a more pronounced decrease with the less porous UF-PSf. The lower reactivity and thus higher OH scatter at the higher rf powers is likely the result of increased ablation of the polymer surface at higher powers. Indeed, we have observed considerable damage occurs when these membranes are treated at $P > 100$ W.

Similar to PSf, PES membranes also exhibited an increase (~5%) in the number of $C\text{-}O_x$ groups after plasma treatment, Table 5.2.[7] Overall, PES oxidation likely occurs through scission of the ether linkage (position 1, Scheme 5.1). A secondary oxidation pathway at the sulfone group results in sulfate functionalities as evidenced in the high binding region of the S_{2p} spectrum.[12,13] Hence, the C-O and C-S bonds are broken during functional group implantation. This mechanism is consistent with the formation of CO

---

[c]All bond energies are derived from thermochemical data found in: S. G. Lias, J. E. Bartmess, J. F. Liebman, J. L. Holmes, R. D. Levin, and W. G. Mallard, *J. Phys. Chem. Ref. Data* **17**, Suppl. 1 (1988).

during plasma modification of PES membranes as observed in our OES and mass spectral experiments.

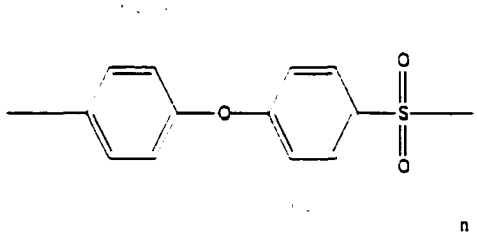

Scheme 5.1

In addition, IRIS data confirm the same moderate OH reactivity measured for PSf membranes, Table 5.1. In contrast to PSf, OH reactivity values for PES have no significant dependence on *P*. One possible explanation for this is the relative strengths of the C-O (~2.3 eV) and C-S (~1.1 eV) bonds. Hence, increasing the energy of the reactive species by increasing *P* has a less pronounced effect on the surface reactivity when the material being modified does not require high energy for bond cleavage.

5.3.2 PE. We have already established that PE, a simple hydrocarbon, is chemically modified by H_2O plasma treatment in a similar fashion to PSf and PES. PE also exhibited a significant incorporation of both C-O and C-O groups after plasma treatment, Table 5.2, with considerably more C-O groups than C-O groups. Notably, CO was also observed in the gas-phase during plasma treatment of PE. Given that PE does not contain any substituted carbons or oxygen groups, these results demonstrate that gas-phase CO and oxygenated carbon centers covalently bound to the polymer backbone are indeed the products of plasma-surface reactions. Mechanistically, these reactions proceed through abstraction of H from the surface and reaction of a plasma species, presumably OH, at this site. Hence, the C-H (~4.3 eV) and possibly the C-C (~3.8 eV) bonds are

broken during PE modification. Similar to PES, our IRIS values experimentally determined for PE membranes do not significantly deviate from $R = 0.5$. This suggests that increasing the energy of the reactive species also has a less pronounced effect on the surface reactivity when the surface bonds cleaved are of approximately equal strength.

5.3.3 PTFE. Of all the polymers studied here, PTFE is the most hydrophobic and therefore, the most challenging material for hydrophilic membrane modification. Although H_2O plasma treatment presents a possible hydrophilic modification strategy for PTFE via H atom abstraction of surface fluorine to form HF, PTFE membranes treated with H_2O plasmas remain highly hydrophobic with contact angles of ~110°. XPS results indicate no oxygen incorporation occurs with H_2O plasma treatment at either 25 or 100 W, Table 5.2. Furthermore, CO is not observed during plasma modification, suggesting poor oxidation of this highly inert material by a 25 W H_2O plasma. Mechanistically, modification of PTFE must proceed by breaking the C-F bond, a strong bond (~5.5 eV) relative to the C- S, C-C, C-O and C-H bonds in PES, PSf, and PE, all of which are ~ 5 eV.

The relatively high energy requirement for C-F bond scission helps explain our IRIS measurements for PTFE, which increase from $R = 0.31 \pm 0.07$ at 25 W to $R = 0.51 \pm 0.05$ at 125 W. This means that at low rf powers, ~30% of the incident OH are lost at the surface and ~70% desorb. At higher powers, the probability of loss and the probability of desorption are essentially the same, ~50%. Previous IRIS work described this behavior as a competition between desorption of physisorbed OH and its loss by reaction on the surface. With PTFE, this reaction is most likely at an active site created through defluorination of the polymer by H atoms. This defluorination is supported by our XPS

results for both H_2O and H_2 plasmas. Table 5.2. and has also been observed previously in the plasma treatment of a variety of fluorinated polymers.[7] Although the OES data in Fig. 5.1 demonstrate that at higher rf powers, there are more H atoms with higher energies, the XPS data suggest the same level of defluorination occurs for both 25 and 100 W H_2O plasmas. This behavior has also been observed previously by Clark and coworkers in the H_2 plasma treatment of PTFE and polyvinylidene fluoride (PVDF).[7] Although defluorination was treatment time dependent, at longer treatment times (>60 s), the final extent of reaction was independent of rf power, with a maximum of ~80% of the fluorine in the polymer surface being removed. Regardless of the level of defluorination, the creation of more reactive sites at high powers likely leads to increased surface reactivity for OH.

It is also instructive to compare IRIS results for OH on PTFE to those for NH_2, NH, and CF_2 on PTFE substrates. We have previously created three categories for radical-surface interactions: 1) systems in which radicals are consumed at the surface ($S \sim 1$, $R > 0$); 2) systems where radicals are generated at the surface ($S \sim 1$, $R < 0$); 3) systems where radicals are neither generated nor consumed at the surface, but adsorption-desorption takes place ($S \sim 1$, $R \sim 0$). For example, all OH-substrate interactions reported here appear to fall into the first of these categories, Table 5.1. Similar to H_2O plasma treatment, the ammonia plasma system interacts with polymer surfaces via functional group implantation.[18,27] In this system, NH_2 radicals fall primarily into Category 2 with a number of substrates including PTFE, in contrast to the present results for OH radicals. In addition, the highest increase in surface production for NH_2 radicals (50 W < P < 175 W)

was observed for PTFE substrates.[27] Results for NH interacting with polymer substrates (PTFE, polyimide) during NH_3 plasma processing belong in Category 1 at high powers ($P \geq 175$ W), and in Category 2 at low powers ($P < 175$ W).[28] Hence, for the same type of surface modification process (i.e. functional group implantation), different patterns in surface scattering arise from different radical species.

In the HFPO plasma system, which slowly deposits an ordered CF_2-rich fluorocarbon film, the surface reactivity of CF_2 radicals on PTFE appears to belong to the third category at all P.[27] Examining the effects of ion bombardment on the radical-surface interaction in this system showed a significant change in the surface reactivity. Under ion-free conditions, CF_2 radicals show an increase in the surface reactivity with increasing power ($R \sim 0.2$ at $P = 35$ W and $R \sim 0.4$ at $P = 135$ W), and display Category 1 behavior. Thus, PTFE is a substrate that displays all three types of radical-surface interaction behavior, depending on the plasma process occurring (deposition or implantation). Clearly, this demonstrates that the type of data available from IRIS data are important as not all radical species interact the same way with a particular substrate material.

5.3.4 GENERAL CONSIDERATIONS. Given the number of substrates, plasma systems, and techniques discussed here, it is constructive to draw some connections between these data. Overall, surface modification of PSf, PES, PE, and PTFE membranes is directly correlated to the energy requirements for bond cleavage, a primary step in functional group implantation. This mechanism is consistent with our XPS results, which indicate oxidation of these materials and functional group implantation. Furthermore, the energy requirements for bond cleavage increase in the following way: C-S < C-O < C-C <

C-H < C-F. Consequently, the ease of polymer modification follows a similar trend as nonfluorinated polymers are easier to modify (i.e. mild conditions produce desired surface properties) than PTFE. This mechanism is also consistent with IRIS data for polymeric membranes, which show that OH has the lowest reactivity on PTFE under the optimal membrane processing conditions for the nonfluorinated polymers (P = 25 W).

One interesting point about these data is that $R(OH) \sim 0.5$ under most processing conditions, regardless of substrate material. As noted above, this value is similar to what was measured for OH reacting with room temperature SiO_2 and Si_3N_4 substrates.[16,17] One explanation for this similarity is that, during IRIS experiments, the substrate is exposed to the full range of plasma species, including undissociated water, hydrogen atoms, and ionic species such as H_2^+ and H_2O^+. As individual species are not tracked in IRIS experiments, contributions of reactions such as dissociative adsorption of H_2O, process (5.1), and recombination of adsorbed OH and H atoms, process (5.2)

$$H_2O(g) + OH(ads) + H(ads) \rightarrow OH(g) + H(ads) \quad (5.1)$$

$$OH(ads) + H(ads) \rightarrow H_2O(g) \quad (5.2),$$

to the measured OH surface reactivity can not be fully assessed. In addition, during our steady-state measurements, the substrate surface may have other physisorbed molecules and potentially unpaired electrons, all of which are available to react with the incident OH radicals. Thus, it is plausible that although the underlying substrates are either polymers or Si-based materials, similar surface species may exist on all substrates. This is substantiated by the observation that H_2O plasma treatment of SiO_2 wafers results in a completely wettable surface,[29] similar to what we observe here with the porous polymer

membranes.

As a final note, the combination of OES and IRIS results show that plasma-generated OH radicals are contributing to the oxidation and creation of hydrophilic membrane surfaces. Although O atoms may also contribute to polymer oxidation, excited state O atoms are not observed under the same conditions as those used for membrane processing (i.e. P = 25 W), regardless of reactor design. Small amounts of oxygen atoms are, however, observed in the MS data even at low rf powers, such that this species can not be completely ruled out as an oxidant.

5.4 CONCLUSIONS

Three gas-phase analytical tools, OES, MS, and LIF, were used to examine the chemistry of the H_2O plasma surface modification system. These analyses provide a fairly extensive set of data from which information about the processes involved in surface modification can be gleaned. In addition, our radical-imaging experiments provide detailed chemical information about the plasma-surface interface. Specifically, we have determined moderate OH-surface reactivity (~0.5) for nearly all membrane substrates and plasma conditions employed. These data suggest OH radicals are involved in the hydrophilic surface modification of polymeric materials. Collectively, the data presented provide a comprehensive picture of the H_2O plasma system, from the gas-phase, to the surface modification, to the plasma-surface interface.

5.5 REFERENCES

1. J. R. Hollahan and A. T. Bell. *Techniques and Applications of Plasma Chemistry:* (Wiley: New York. 1974).
2. N. Inagaki. *Plasma Surface Modification and Plasma Polymerization:* (Technomic Publishing: Lancaster. PA. 1996).
3. R. d'Agostino. *Plasma Deposition. Treatment. and Etching of Polymers:* (Academic Press: San Diego. CA. 1990).
4. L. J. Gerenser. *J. Adhesion Sci. Technol.* **1,** 303 (1987).
5. F. D. Egitto and L. J. Matienzo. *IBM J. Res. Develop.* **38,** 423 (1994).
6. D. T. Clark and A. Dilks. *J. Polym. Sci. Polym. Chem. Ed.* **15,** 15 (1977).
7. R. J. Seebock. W. E. Kohler. and M. Romheld. *Contrib. Plasma Phys.* **32,** 613 (1992).
8. J. Janes and C. Huth. *J. Vac. Sci. Technol. A* **10,** 3522 (1992).
9. J. Hopwood. *Appl. Phys. Lett.* **62,** 940 (1993).
10. H. F. Winters. *Top. Curr. Chem.* **94,** 69 (1980).
11. V. A. Godyak and R. B. Piejak. *Phys. Rev. Lett.* **65,** 996 (1990).
12. M. L. Steen. L. Hymas. E. D. Havey. N. E. Capps. and E. R. Fisher. *J. Memb. Sci.* **188,** 97 (2001).
13. M. L. Steen. A. C. Jordan. and E. R. Fisher. *J. Memb. Sci.*. submitted for publication.
14. J. Hopkins and J. P. S. Badyal. *J. Phys. Chem.* **99,** 4261 (1995).
15. S. H. Wheale. C. P. Barker. and J. P. S. Badyal. *Langmuir.* **14,** 6699 (1998).
16. P. R. McCurdy. K. H. A. Bogart. N. F. Dalleska. and E. R. Fisher. *Rev. Sci.*

Instrum. **68,** 1684 (1997).

17. E. R. Fisher, P. Ho, W. G. Breiland, and R. J. Buss, *J. Phys. Chem.* **96,** 9855 (1992).

18. C. I. Butoi, N. M. Mackie, P. R. McCurdy, J. R. D. Peers, and E. R. Fisher, *Plasmas Polym.* **4,** 1 (1999).

19. K. J. Clay, S. P. Speakman, G. A. J. Amaratunga, and S. R. P. Silva, *J. Appl. Phys.* **79,** 7227 (1996).

20. M. Tuszewski, J. T. Scheuer, J. A. Tobin, *J. Vac. Sci. Technol. A* **13,** 839 (1995); F. Imai, K. Kunimori, H. Nozoye, *J. Vac. Sci. Technol. A* **13,** 2508 (1995).

21. W. R. Harshbarger, R. A. Porter, T. A. Miller, and P. Norton, *Appl. Spectrosc.* **31,** 201 (1977).

22. E. O. Degenkolb, C. J. Mogab, M. R. Goldrich, and J. E. Griffiths, *Appl. Spectrosc.* **30,** 520 (1976).

23. Q. S. Yu, E. Krentsel, and H. Yasuda, *J. Appl. Polym. Sci. A* **36,** 1829 (1998).

24. J. A. Coxon, *Can. J. Phys.* **58,** 933 (1980).

25. D. T. Clark and D. R. Hutton, *J. Polym. Sci. A. Polym. Chem.* **25,** 2643 (1987).

26. T. R. Gengenbach, R. C. Chatelier, and J. J. Griesser, *Surf. Interface Anal.* **24,** 611 (1996); T. R. Gengenbach and H. J. Griesser, *Surf. Interface Anal.* **26,** 498 (1998).

27. C. I. Butoi, M. L. Steen, J. R. D. Peers, and E. R. Fisher, *J. Phys. Chem.* **105,** 5957 (2001).

28. E. R. Fisher, *Plasma Sources Sci. Technol.*, submitted for publication; M. L. Steen, K. R. Kull, and E. R. Fisher, *J. Appl. Phys.*, submitted for publication.

29. M. L. Steen and E. R. Fisher. unpublished results.

CHAPTER 6

COMPARISON OF SURFACE INTERACTIONS FOR NH AND NH_2 RADICALS ON POLYMER AND METAL SUBSTRATES

This dissertation chapter contains results from a full paper submitted for publication to *Journal of Applied Physics*. The manuscript was written by M. L. Steen and edited by Professor E. R. Fisher. The coauthor was K. R. Kull. The aim of this study was to provide insight into the relationship between NH_x plasma radicals as well as their relationship with charged species, and with the surface during NH_3 plasma surface modification. Interactions of NH and NH_2 radicals with polymer and metal surfaces were investigated with the IRIS technique. The role of ions on the formation of NH_x radicals in the gas-phase and at the surface was investigated by removing ions from the plasma molecular beam prior to interaction with the substrate.

6.1 INTRODUCTION

Ammonia plasmas are used extensively for producing nitride materials and for modifying polymer surfaces.[1,2,3,4,5] Given the scientific and commercial use of NH_3 plasmas, little is known about the specific plasma-surface interactions, especially those responsible for surface modification and growth of new materials. Of particular interest is understanding the mechanisms through which surfaces are made hydrophilic during NH_3 plasma treatment.[6,7,8] We have used NH_3 plasmas to increase the hydrophilicity of metallic and polymeric substrates, including porous polymeric membranes.[9,10] These results are consistent with previous work of NH_3 plasma treatment of polymers resulting in higher wettability relative to untreated surfaces.[11,12,13] Modification occurs via amine functional group implantation primarily by NH_x radicals.[6,8] Indeed, d'Agostino and coworkers have achieved selective grafting of specific nitrogen groups by tuning the relative densities of these reactive plasma species, specifically NH radicals.[13] As these studies suggest, it is generally accepted that surface modification processes proceed through NH_x radical-surface interactions;[13] however, a complete understanding of the surface alteration processes has not been achieved. Mechanistic understanding of these plasma-surface interactions is critical to rational control of plasma-mediated processes as well as the development of predictive models.

As described in Chapters 2 and 5, the IRIS technique is a very versatile method for studying the interactions of plasma species with substrates. IRIS data for radicals produced in other plasmas,[14,15,16,17,18,19,20] as well as data for radical-surface interactions in ammonia plasmas have been recently published.[21,22] An early IRIS study of NH radicals in

NH_2 plasmas showed NH has very low reactivity with silicon nitride substrates (~ 0 - 10%).[23] These data were collected using a 45 W ammonia gas discharge and substrate temperatures ranging from 300 to 700 K. The effects of *P*, substrate material, and other plasma parameters were not investigated. We have also previously reported extensive IRIS studies of NH_2 radicals in NH_3 plasmas, including translational temperatures for both beam and scattered species as well as surface reactivities for a number of substrates.[21,22] Our IRIS reactivity data show that NH_2 radical production occurs at the surface of nearly all substrates during NH_3 plasma processing under most experimental conditions, suggesting that other species in the molecular beam are contributing to the surface generation of NH_2.

A fundamental question originated by these data revolves around the mechanism for observed surface production of NH_2. We explicitly assessed the influence of ion-assisted processes in the surface generation of NH_2 radicals during plasma processing of two materials, polyimide (PI) and platinum, using the grounded mesh (gm) experiments.[22] While less NH_2 desorbs from these surfaces when ions are removed from the plasma molecular beam, NH_2 was still generated at the surface without ion bombardment. This suggests that ion-induced processes are not the only mechanisms through which NH_2 surface generation occurs.

One hypothesis for alternate surface generation mechanisms, put forward in the original NH_2 study, was that gas-phase NH radicals contributed to surface production of NH_2. This can be envisioned as occurring via one or both of the two processes given in 6.1.

$$NH(g) + H(ads) \rightarrow NH_2(g) \quad (6.1a)$$

$$NH(g) + H(ads) \rightarrow NH(ads) + H(ads) \rightarrow NH_2(g) \quad (6.1b).$$

Process 6.1a represents an Eley-Rideal-type (ER) process, wherein a reaction occurs between a gas-phase species and an adsorbed species, before the gas-phase reactant has equilibrated with the surface. Process 6.1b is a Langmuir-Hinschelwood-type (LH) process wherein both reactants are equilibrated on the surface prior to reaction. While ER and LH interactions are primarily used to describe reactions that occur under ultrahigh vacuum (UHV) conditions,[24] they afford a reasonable means with which to discuss possible surface interactions that result in generation of NH_2. If either of these processes transpires at the plasma-surface interface, we would expect that NH radicals would be lost at the surface. In other words, in our IRIS experiments, $S(NH) \approx 1$ under conditions that result in surface production of NH_2 [$S(NH_2) < 1$]. To directly demonstrate that processes 6.1 occur, a thorough treatment of NH radical interactions is necessary. Specifically, IRIS measurements for NH radicals under ion-free conditions, as a function of applied rf power (P), and with the substrates used in the NH_2 study are critical to understanding the mechanisms at play in the NH_2 plasma surface modification system. This chapter presents IRIS data obtained for NH as a function of these parameters.

6.2 RESULTS

6.2.1 FORMATION OF NH_2 AND NH RADICALS IN NH_3 PLASMAS. Figure 6.1 shows the normalized NH_2 LIF signal intensities as a function of P. Because we are saturating the probed transitions, these intensities correspond to the relative species

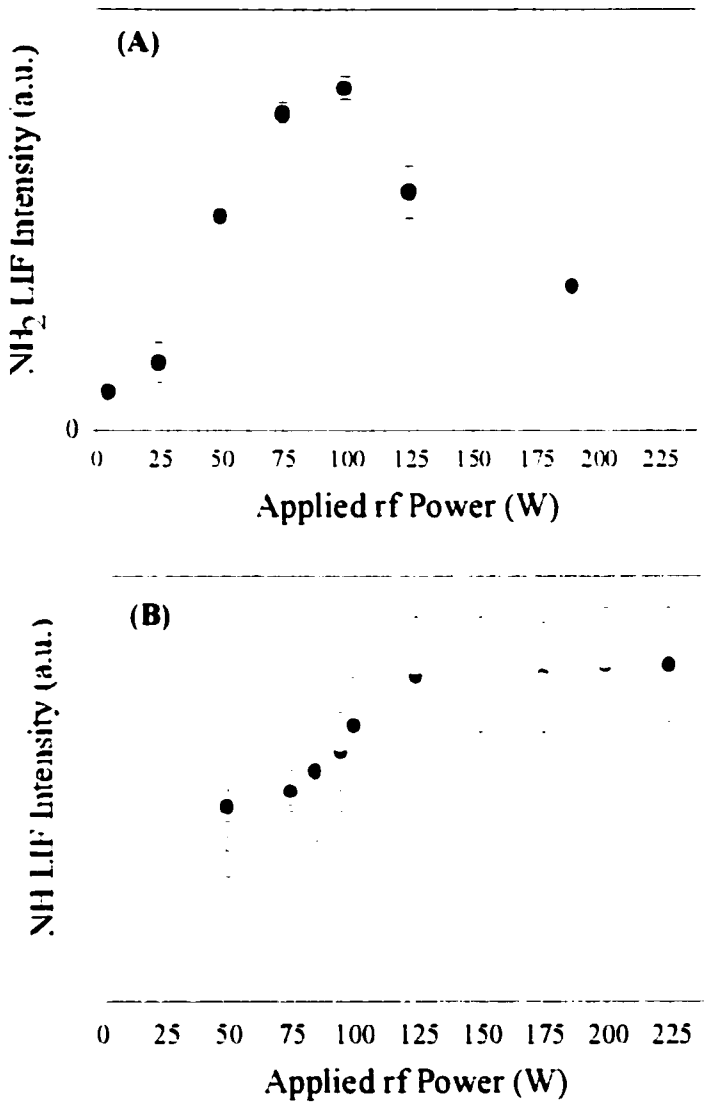

Figure 6.1 Relative intensities of (A) NH_2 and (B) NH radicals in a 100% NH_3 plasma molecular beam as a function of applied rf power. Data for NH_2 was taken from Reference 21. Also shown are results for NH radicals taken with the grounded mesh in the molecular beam (open circles).

densities. Formation of NH_2 increases rapidly with P, reaching a maximum at ~100 W, Fig. 6.1a.[21] The decrease at high P is likely the result of increased fragmentation of NH_2 (i.e. formation of NH and possibly N). This is substantiated by the power dependence of the NH radical density, which shows a relatively low density of NH at low P and a significant NH radical density at P > 120 W, Fig. 6.1b. Furthermore, no discernible decrease in the NH radical density is observed at high P. These data demonstrate that the relative densities of NH_x species in the plasma molecular beam are strongly affected by P, and are patently connected to each other.

6.2.2 RADICAL-SURFACE INTERACTIONS. Figure 6.2 shows three IRIS images depicting NH LIF signals using a 75 W NH_3 plasma molecular beam and a polyimide substrate. In Fig. 6.2a, LIF signal from NH radicals just in the molecular beam is imaged, whereas Fig. 6.2b contains LIF signal from both incident NH radicals as well as NH radicals scattered from the polyimide surface. The difference between the images shown in Fig. 6.2b and Fig. 6.2a provides a spatially-resolved image of NH radicals scattered from the polyimide surface, Fig. 6.2c. Clearly, there is a significant number of molecules leaving the plasma-treated substrate. Figure 6.3(a) shows the data of Figs. 6.2a and 6.2c converted to cross sections along the laser axis. The broad spatial distribution and the shift of the scattered signal peak away from the molecular beam maximum indicate the NH radicals scatter with a cosine angular distribution. Also shown in Fig. 6.3a are simulated curves for the incident beam and for scattered molecules, assuming an absorption-desorption mechanism, with S = 2.65. Averaging several data sets yields an overall value of $S = 2.59 \pm 0.12$. Note that an S value >1 indicates that NH radical

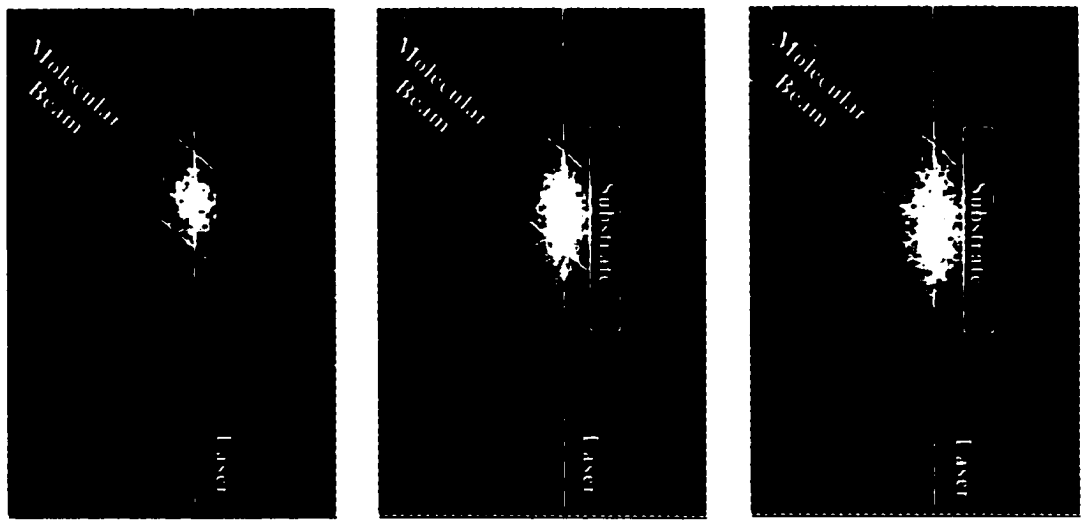

(A) (B) (C)

Figure 6.2 Spatially-resolved two-dimensional ICCD images of LIF signals produced by NH radicals A) in a 75 W NH_3 plasma molecular beam; and B) with a polyimide substrate rotated in the path of the molecular beam. The image shown in (C) is the difference between the images shown in (A) and (B), corresponding to NH radicals scattering from the substrate. The lines indicate the path of the molecular beam and the laser in the images.

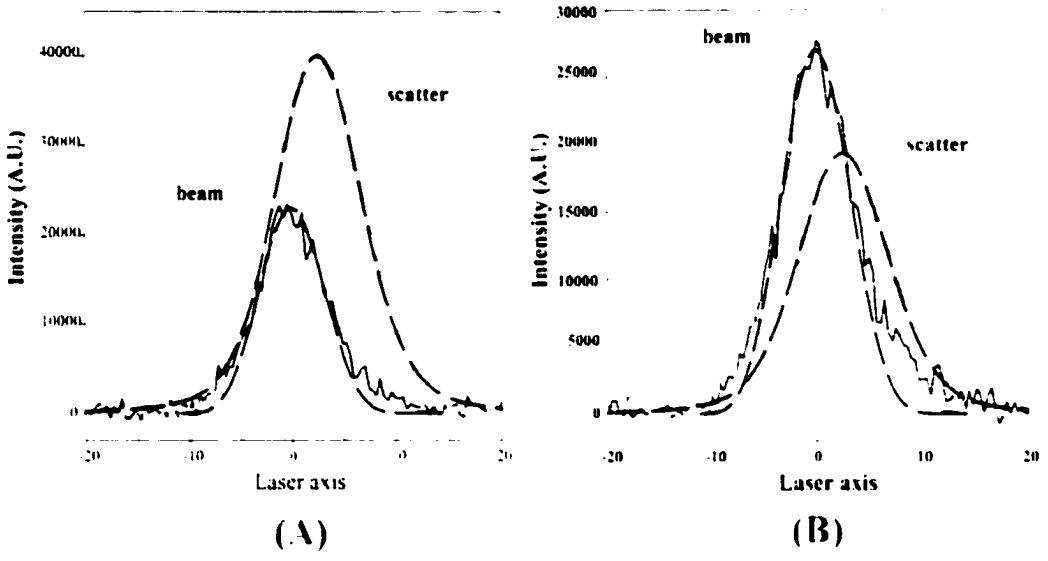

Figure 6.3 Cross sectional data for NH radicals generated in: (A) a 75 W NH_3 plasma molecular beam interacting with a polyimide substrate: and (B) a 175 W NH_3 plasma molecular beam interacting with a polyimide substrate. Dashed lines are simulated cross sections with $S = 2.65 \pm 0.10$ for (A): and $S = 1.08 \pm 0.10$ for (B). The laser-surface distance was 2.5 mm for both data sets.

production occurs at the polyimide substrate during plasma processing at 75 W.

Figure 6.3b shows a representative set of experimental data and simulated curves for NH radicals interacting with the same substrate at 175 W. These data are also reproduced well by the simulation assuming an absorption-desorption mechanism. Here, however, $S = 1.08$, significantly lower than that measured at 75 W. Furthermore, an S value of ~1 indicates that NH radicals are neither produced nor consumed at the polyimide surface. Thus, the data shown in Figs. 6.3a and 6.3b demonstrate very different scatter behavior for NH for the same substrate with P.

Table 6.1 lists S values for NH radicals interacting with PI, PTFE and Pt substrates for P = 75-225 W. Clearly, the substrate material affects the behavior of NH radicals. For platinum substrates, a relatively small increase in S is observed from 75 W to 125 W, followed by a leveling off at high powers. Interestingly, this trend is nearly identical to that observed for NH_2 radicals interacting with platinum and copper substrates.[22] For both polymer substrates, the S(NH) values decrease with increasing P. In contrast, $S(NH_2)$ values increased with increasing P, with the highest observed surface production of NH_2 occurring at PTFE surfaces at 175 W. $S(NH_2)$ and S(NH) for interactions with the PI and PTFE substrates as a function of P are also shown in Fig. 6.4.[22] These data point to very different scatter behavior with these two molecules. Note that the maximum surface scatter of NH_2 and surface loss for NH were observed under the same conditions (P = 175 W). These surface interaction results for NH_2 and NH suggest a connection between these two species.

6.2.3 MASS SPECTRAL DATA. Insight into the relationship between gas-phase

Table 6.1 NH scatter coefficients for CW NH_3 plasma processing.[a]

	Substrate				
Power	PI	PI (gm)[b]	PTFE	Pt	Pt (gm)[b]
75 W	2.59 ± 0.12	1.41 ± 0.08	1.95 ± 0.07	0.98 ± 0.07	1.47 ± 0.11
125 W	1.55 ± 0.14	1.50 ± 0.07	1.20 ± 0.10	1.19 ± 0.07	1.29 ± 0.08
175 W	1.02 ± 0.08	1.46 ± 0.08	0.50 ± 0.10	1.45 ± 0.06	1.45 ± 0.12
225 W	0.85 ± 0.10	1.50 ± 0.10	0.58 ± 0.10	1.30 ± 0.20	1.33 ± 0.11

[a]Scatter coefficients determined as described in the text. Errors given are one standard deviation of the mean of several data sets.

[b]Data taken with a grounded mesh screen in the path of the molecular beam (i.e. "ion-free" conditions).

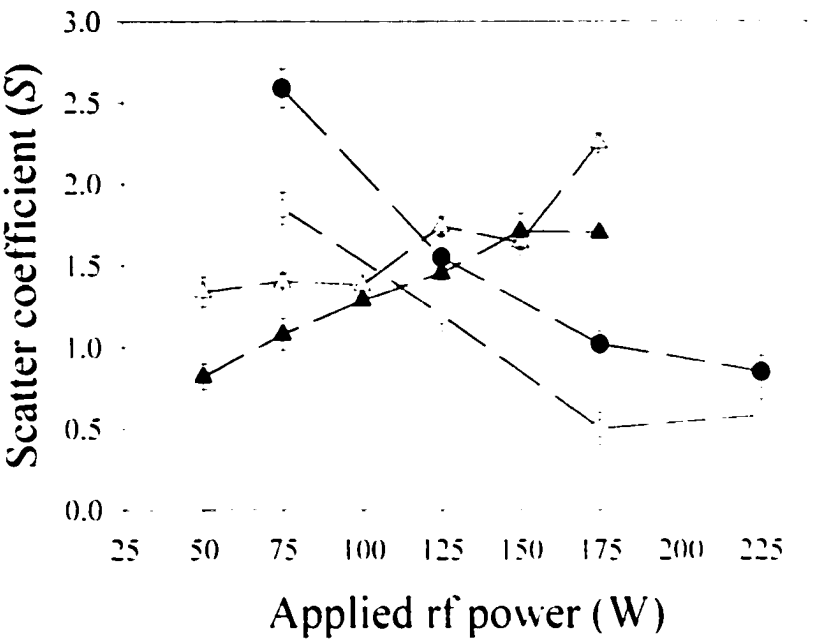

Figure 6.4 NH_2 (triangles) and NH (circles) scatter coefficients for interactions with polyimide (closed symbols); and PTFE substrates (open symbols) as a function of applied rf power.

NH_x radicals and ions can be gleaned from mass spectral data of the NH_3 plasma molecular beam. Data were obtained with the ionizer on to examine both ionic and neutral species, and with the ionizer off, to provide information on nascent ions in the plasma. With the ionizer on, the most prominent peaks in the spectrum occurred at m/z = 1, 2, 15, 16, 17, 18, and 28 amu, corresponding to H^+, H_2^+, NH^+, NH_2^+, NH_3^+, NH_4^+, and N_2^+, respectively. No significant peaks appear in the mass spectrum above 30 amu. Without the ionizer, the predominant species observed in the mass spectrum of the beam are NH_x (x = 1-4) and H_2. Figure 6.5 shows the power dependence of the ratios of the intensity of the NH_x species (x = 1-3) relative to NH_4 in the plasma molecular beam. Interestingly, as *P* increases, the amount of NH_x (x = 1-3) produced also increases, relative to the NH_4. This increase is most dramatic for the NH_2: NH_3 ration, which rises from ~0.3 at *P* = 25 W to ~0.9 at *P* = 150 W. This observation is consistent with more efficient ionization processes for the smaller NH_x species or with an increase in fragmentation at higher *P*.

MS data collected with and without the qm in the path of the molecular beam provide information on the extent to which ions were removed. For *P* = 125 W, the qm removes essentially all of the nascent ions from the molecular beam, Fig. 6.6a. Similar results were obtained for *P* = 50-150 W. For *P* = 175 W, however, a small amount (<2%) of charged species are transmitted through the qm, Fig. 6.6b. With 98-100% removal of the ions in the molecular beam at all *P*, the term "ion-free" is used below to describe data taken with this configuration. Note that NH LIF intensity data taken with the qm in the molecular beam shows no change in the relative density of NH radicals, Fig. 6.1a.

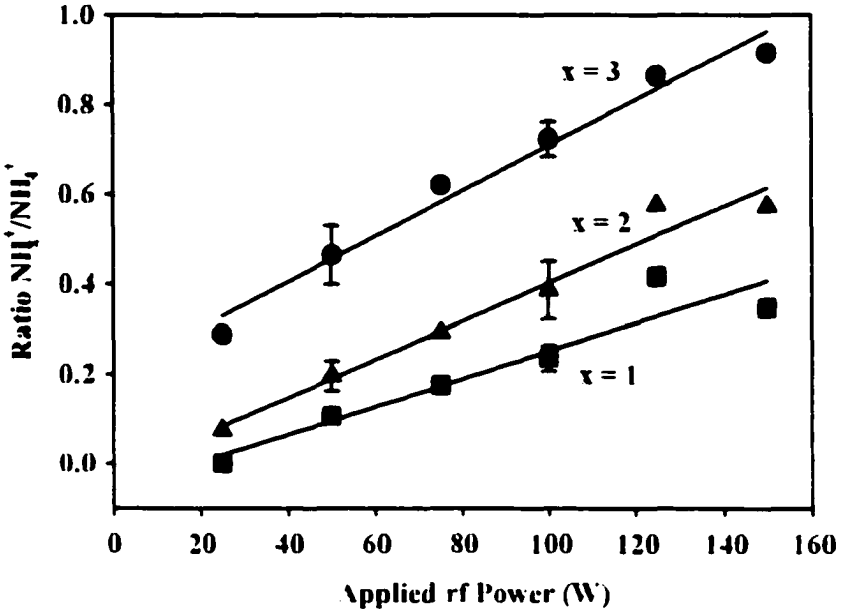

Figure 6.5 Ratio of mass spectral signal intensities for nascent ions (NH_x^+/NH_4^+, x = 1 - 3) in the NH_3 plasma molecular beam as a function of applied rf power. These data were taken without using the ionizer in the mass spectrometer. The solid lines are linear regression analysis fits to the individual NH_x data sets, with r^2 = 0.977 and m = 5.06 x 10^{-3} for x = 3, r^2 = 0.967 and m= 4.26 x 10^{-3} for x = 2; and r^2 = 0.900 and m = 3.11 x 10^{-3} for x = 1. Vertical lines represent one standard deviation error limits based on averages taken from multiple data sets where available.

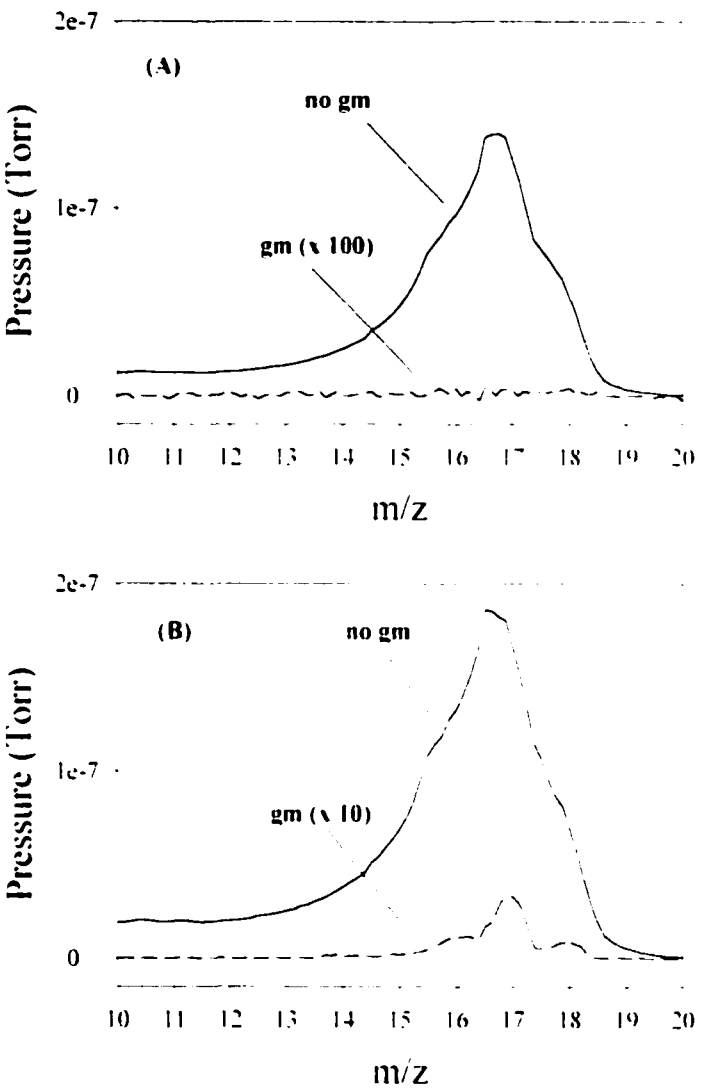

Figure 6.6 Mass spectra of nascent ions (i.e. the ionizer was off) in a NH_3 plasma molecular beam with (A) P = 125 W; and (B) P = 175 W. These data were obtained with no grounded mesh (solid line) and with the grounded mesh in the beam (dashed line). The spectra were corrected for background signals and the gm data has been scaled by: (A) a factor of 10; and (B) a factor of 100.

Although the use of the gm removes nearly all of the ions from the molecular beam, it does not significantly perturb the densities or the kinetic energies[21] of the neutral plasma species in the molecular beam.

6.2.4 EFFECTS OF ION BOMBARDMENT. To investigate the effects of ion bombardment in NH_x radical-surface interactions, $S(NH)$ values were measured with the gm for two different substrates, PI and platinum. Examination of these data, listed in Table 6.1, provides insight into the role that ions play in the surface scatter of NH. For example, the NH gm scatter coefficients are all very similar, with $S(NH) \sim 1.45$, regardless of substrate material or rf power. With the PI substrate at high P, comparing $S(NH)$ values with and without ions shows $S(NH)$ *increases* when ions are removed from the molecular beam. These data suggest that NH scattering is suppressed by the presence of ions at high P. Conversely, at low P with the PI substrate, removal of ions *decreases* the measured $S(NH)$ values, indicating ions enhance surface scatter for NH. Ion enhancement of surface scatter has been observed previously in IRIS experiments for SiF_x,[25] CF_x,[18] and NH_2[22] in fluorosilane, fluorocarbon, and ammonia plasmas, respectively. This type of behavior is consistent with recent work demonstrating that energetic ion bombardment yields radicals on surfaces by mechanisms of neutralization and dissociation and by sputtering of already deposited films.[26,27] The ion-induced suppression of radical scattering (i.e. NH at high P) has not, however, been previously observed in our laboratories or reported elsewhere.

It is useful to compare our IRIS results for NH to those obtained previously for NH_2 under identical conditions to those described here. $S(NH_2)$ and $S(NH)$ values for

interactions with PI are shown as a function of P in Fig. 6.7.[22] As described above, the $S(NH)$ values decrease dramatically with increasing P when ions are present in the molecular beam. Under ion-free conditions, $S(NH) \sim 1.45$ at all P. In contrast, $S(NH_2)$ values increase with increasing P with and without ions in the molecular beam. However, the values measured under ion-free conditions are significantly lower than those measured with ions. These two observations clearly suggest that 1) ions are contributing to the surface generation of NH_2; and 2) additional power-dependent mechanisms may also be contributing. The relationships between NH, NH_2, and ionic plasma species with each other and with the surface are explored in the following section.

6.3 DISCUSSION

Our approach to understanding NH_3 plasma surface modification on a mechanistic level considers the interactions of all NH_x plasma species (both neutral and ionic) to determine which species are active in substrate processing. All of the data presented here support the concept that the radicals, ions, and surfaces in this system affect the reactivity of each other. For example, the gas-phase data show that the NH and NH_2 radical densities in the plasma are connected, with the relative densities of both species being strongly affected by P. Specifically, the NH_2 density decreases above $P \sim 100$ W, whereas the NH density continues to increase with P, as a result of decomposition of NH_2. In addition, the mass spectral data show that the gas-phase NH_x ($x = 1$-3) ion density also increases with P. These data suggest increased fragmentation of larger NH_x and NH_x occurs at higher P.

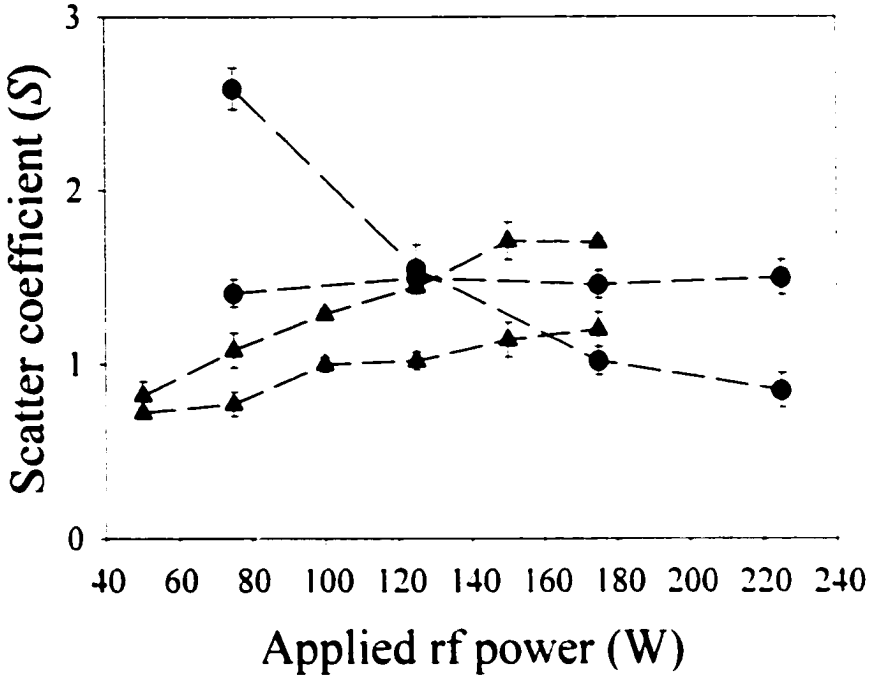

Figure 6.7 Ion effects on NH_2 (triangles) and NH (circles) scatter coefficients for interactions with a polyimide substrate. Closed symbols are for measurements made when ionic species were not removed from the plasma molecular beam. Open symbols are for measurements made when charged species were removed from the beam by placing a grounding mesh in the path of the molecular beam.

Although the relative densities of plasma species are affected by plasma parameters, at all *P* there are a variety of ionic and neutral species in the plasma molecular beam. In addition to NH_x and NH_x^+, hydrogen molecules, ions, and atoms are also present.[10,21] Each of these species has the potential to influence the surface interactions of other members of the ensemble. This leads to a complex combination of possible surface reactions, making it difficult to assign exact mechanisms for plasma-mediated surface modifications. The correlations we have observed for the two NH_x species, however, allow us to construct some mechanistic schemes for surface processes in the NH_3 plasma system.

To fully consider the data presented here for surface interactions of NH radicals, we must first discuss those for NH_2, which have been detailed previously.[11] As noted in Section 6.1, surface generation of NH_2 [i.e. $S(NH_2) > 1$] is observed under most experimental conditions. Surface scattering of NH_2 can occur through a simple adsorption-desorption mechanism, process 6.2.

$$NH_2(g) + * \rightarrow NH_2(ads) \rightarrow NH_2(g) \qquad (6.2),$$

where * represents an active site on the substrate surface and NH_2 is assumed to be thermally equilibrated on the surface prior to desorption. We believe this reaction accounts for a large fraction of the desorbed NH_2 observed in the NH_3 plasma system. It can not, however, account for production of NH_2. In addition to process 6.2, NH_2 can be formed through surface reactions involving other neutral beam species. For example, dissociative adsorption of NH_3 followed by desorption of NH_2, process 6.3,

$$NH_3(g) + * \rightarrow NH_2(ads) + H(ads) \rightarrow NH_2(g) \qquad (6.3),$$

is one possible pathway to surface generation of NH_2. Likewise, NH_2 can be produced at the surface through abstraction of a surface hydrogen by NH, processes 6.1.[22]

By investigating kinetic energy disposal at the surface, we can hypothesize as to which of the given processes are more likely to occur. For example, if only process 6.2 occurs, the kinetic energy, or translational temperature (Θ_t), of desorbed NH_2 should be characterized by the substrate temperature, T_s.[28] Likewise, processes 6.1b and 6.3 involve species that are fully accomodated at the surface, resulting in desorbed NH, with energies that are characterized by T_s. By measuring velocity distributions for NH, molecules in the molecular beam and scattered from the substrate, we determined that scattered NH_2 molecules possess kinetic energies that are greater than T_s under most experimental conditions. Thus, NH_2 radicals must be generated (at least in part) by pathways other than 6.1b, 6.2, and 6.3. Process 6.1a is, therefore, the most likely neutral-mediated reaction we have considered here that could cause the observed increase in the translational energy of desorbed NH_2.

In addition to energy arguments, our surface interaction results for NH and NH$_2$ also support processes 6.1 as contributors to surface generation of NH_2. Specifically, these processes lead to surface loss of NH radicals. If processes 6.1 are occurring, then S(NH) should be less than unity under conditions where $S(NH_2) > 1$. As these reaction pathways suggest, NH radicals are indeed consumed at polymer surfaces (PI and PTFE) at $P > 175$ W, Table 6.1. Moreover, the highest NH_2 scatter coefficients and the lowest NH scatter coefficients were measured under identical conditions (PI and PTFE, $P = 175$ W), Fig. 6.4. Hence, our IRIS results also suggest NH abstraction of H is a likely pathway to

surface generation of NH_2 in this system.

In addition to neutral-mediated processes, reactions involving ions can also contribute to surface production of radical species. Possible ion bombardment reactions in the NH_3 system include sputtering, surface neutralization, and neutralization-dissociation reactions, as exemplified by processes 6.4-6.6.

$$I^+(g) + NH_x(ads) \rightarrow NH_x(g) \quad (6.4)$$

$$NH_x(g) + * \rightarrow NH_x(ads) \rightarrow NH_x(g) \quad (6.5)$$

$$NH_x(g) + 2* \rightarrow NH_{x-1}(ads) + H(ads) \rightarrow NH_{x-1}(g) + H(ads) \quad (6.6),$$

where I^+ represents any ionic plasma species, x = 1-3 for process 6.4, and x = 1-4 for processes 6.5 and 6.6. The effects of ion bombardment reactions can be clearly seen with the scattering results for NH_2 shown in Fig. 6.7. When ions are removed from the plasma molecular beam, $S(NH_2)$ values decrease at all P, but remain above unity for $P > 100$ W. A similar decrease in $S(NH_2)$ when ions were removed was observed for Pt substrates.[22] These data suggest that although ion-induced processes (reactions 6.4-6.6) are clearly contributing to surface generation of NH_2, they are not the only mechanisms through which NH_2 is produced at the surface.

Interestingly, the translational temperature of scattered NH_2 (Θ_{tx}) is also affected by ion bombardment. Specifically, Θ_{tx} decreases substantially when ions are removed from the molecular beam for both Pt and PI. This shows that ion bombardment raises the kinetic energy of the NH_2 radicals desorbing from both substrates. With the Pt substrate, removal of ions results in $\Theta_{tx} = T_s$ at all P,[22] demonstrating that the elevated kinetic energies were due entirely to ion bombardment. Although removal of ions decreases Θ_{tx}

for the PI substrate, it remains above T_s at high P. Thus, ions do not fully account for the elevated Θ_{tot} values at high P for the PI substrate. These data again suggest that an Eley-Rideal-type mechanism, process 6.1a, is a contributor to surface production of NH_2 on the PI substrate.

One additional aspect of our NH IRIS data that remains to be addressed is the effects of ion bombardment on NH surface reactivity. NH can scatter from substrates via a simple adsorption-desorption process such as that given in 6.2 for NH_2. Alternatively, NH can also be produced by dissociative adsorption of NH_2, process 6.7.

$$NH_2(g) + 2^* \cdot NH(ads) + H(ads) \cdot NH(g) + H(ads) \qquad (6.7).$$

Furthermore, processes involving adsorbed NH_2 or NH_3 could also result in production of NH by further dissociation of these species on the surface, generally expressed by process 6.8.

$$NH_x(ads) + * \cdot NH(ads) + (x-1)H(ads) \cdot NH(g) + (x-1)H(ads) \qquad (6.8).$$

This process has been proposed by Selwyn *et al.* to explain their observations of NH and NH_2 reactions on catalytic metal surfaces.[29] Specifically, they found that 90% of NH was removed by 300 K Pt surfaces with only a small activation energy of 0.9 ± 0.3 kcal mol. Furthermore, the adsorbed NH_2 readily decomposed to NH and H. In contrast, no NH was removed by the Pt catalyst at room temperature and an activation energy for adsorption of 2.4 ± 0.2 kcal/mol was measured. At high T_s, desorption of NH from the Pt surface is observed, whereas no desorption of NH_2 is observed at any T_s. Selwyn and Lin have thus identified NH as a major decomposition product in catalytic removal of NH_3.[29b] Processes 6.8 could, therefore, account for our observation of $S(NH) > 1$ at low P.

Processes 6.8 can also help interpret our results for NH surface interactions with polyimide under ion-free conditions. To discuss these results, we use ΔS, which we define as $S - S_{gm}$ (i.e. the difference between scatter values measured with and without ions). With ions removed from the molecular beam, NH scatter coefficients decrease at $P \leq 125$ W, $\Delta S > 0$, and increase at $P \geq 175$, $\Delta S < 0$. One explanation for these data is the competition between ion sputtering, process 6.4, and dissociation of adsorbed NH_x, process 6.8. If NH_2 is produced by ion sputtering of the NH_x adlayer then a positive $\Delta S(NH_2)$ would be expected, which is indeed what is observed at all P, Fig. 6.7. Under ion-free conditions, sputtering of the NH_x adlayer is reduced, allowing for further dissociation of NH_x(ads) via process 6.8. This could explain the negative $\Delta S(NH)$ observed at high P. The positive $\Delta S(NH)$ at low P is consistent with what was observed with NH_2 at all P, and is likely the result of eliminating ion-assisted processes such as those shown in processes 6.4-6.6.

This is the first time we have observed different ΔS behavior at different P in IRIS studies. Indeed, with NH_2, CF_2, and SiF_2 radicals, ΔS was positive under all experimental conditions.[18,22,25] The change in sign for $\Delta S(NH)$ that occurs as a function of P suggests the densities of plasma species in the molecular beam are controlling the surface interactions of NH. Specifically, our gas-phase data demonstrates there are more NH_x, NH radicals, and H atoms at high P. An additional factor is that PI contains nitrogen, which could also be affecting the production of NH in this system. Additional experiments in our laboratory to explore ion effects with other polymeric substrates that do not contain nitrogen are currently underway.

The idea that substrate material can influence our results is substantiated by our results for Pt. This catalytic metal substrate yields ΔS values for both NH and NH_2 of nearly zero at all P. Table 6.1.[f] This suggests that the density of individual plasma species is not critical to the NH_x surface interactions. Rather, the substrate material appears to be more influential. It is generally believed that d orbital interactions are extremely important to promoting bond scission on metallic substrates.[30] This would suggest that metals such as Pt should exhibit higher reactivity (i.e. lower scatter) toward incident NH_x species relative to surfaces that do not readily accept electrons (i.e. polymers). Interestingly, Selwyn and coworkers observed significant differences between Pt and Fe as catalysts for decomposition of NH_3. Specifically, a thermal nonreversibility was observed with the Pt catalyst, resulting from N poisoning of the surface. In contrast, decomposition products did not appear to poison Fe catalysts. In addition, the ability of the catalyst to remove NH_x species was T_s dependent. Thus, IRIS studies of NH and NH_2 reactivity on metallic substrates as a function of T_s could further illuminate surface behavior in the NH_3 catalysis system. Notwithstanding, the results presented in this chapter for both gas-phase and gas-surface processes clearly indicate the interactions of NH, NH_2 and ions are synergistically related.

---

[f]The $\Delta S(NH_2)$ values ranges from 0.17 to 0.32 for P = 50-175 W, as detailed in reference 22.

6.4 SUMMARY

The IRIS data presented here for NH radicals in the NH_3 plasma system offer an opportunity to explore the effects of studying multiple species in a single plasma system. Comparison of previous results for NH_2 allow us to assert that the surface interactions of NH are directly associated with the observed surface generation of NH_2, primarily via an Eley-Rideal mechanism, process 6.1a. In addition, scatter coefficients measured for NH under ion-free conditions display scatter behavior not previously observed in IRIS experiments. Specifically, the value of ΔS relative to zero is influenced by plasma parameters, namely P. We hypothesize that this may be related to the ability of individual reaction pathways, processes 6.4-6.8, to contribute to surface interactions. This is clearly related to the density of gas-phase reactants in the incident molecular beam. Although IRIS experiments do not allow for selective elimination of a particular species from the plasma molecular beam, our gm data clearly show ions affect the surface interactions of both NH and NH_2. Another variable we have addressed is the effect of substrate material on surface reactivity of NH. For catalytic materials such as Pt, the substrate appears to be more influential than species densities on the measured S values. This is clearly an area that would be well served by additional IRIS studies.

6.5 REFERENCES

1. J. P. Badey, E. Espuche, and T. M. Duc. *Polymer* **37**, 1377 (1996).
2. M. Tatoulian, F. Arefi-Khonsari, and J. Amouroux. *Int. J. Adhes.* **15**, 177 (1995).
3. H.-C. Cheng, F-S Wang, and C.-Y. Huang. *IEEE Trans. Elec. Devices* **44**, 64 (1997).
4. M. E. Jones, J. R. Shealy, and J. R. Engstrom. *Appl. Phys. Lett.* **67**, 542 (1995).
5. X. Zhang, C. P. Grigoropoulos. *Rev. Sci. Instrum.* **66**, 1115 (1995); E. M. Liston, L. Martinu, and M. R. Wertheimer. *J. Adhesion Sci.* **6**, 2975 (1993).
6. D. L. Cho, and H. Yasuda. *J. Vac. Sci. Technol. A* **4**, 2307 (1986).
7. N. Inagaki, S. Tasaka, and H. Kawai. *J. Adhesion Sci. Technol.* **3**, 637 (1989).
8. C. Munkolm, D. R. Walt, F. P. Milanovich, and S. M. Klainer. *Anal. Chem.* **58**, 1427 (1986).
9. C. I. Butoi, Ph. D. thesis, Colorado State University, 2000.
10. K. R. Kull, M. L. Steen, and E. R. Fisher. *J. Memb. Sci.* manuscript in prep.
11. T. R. Gengenbach, X. Xie, R. C. Chatelier, and H. J. Griesser. *J. Adhesion. Technol.* **8**, 305 (1994).
12. P. Favia, M. V. Stendardo, and R. d'Agostino. *Plasmas Polym.* **1**, 91 (1996).
13. N. Inagaki. *Plasma Surface Modification and Plasma Polymerization:* (Technomic, Lancaster, PA, 1996).
14. P. R. McCurdy, K. H. A. Bogart, N. F. Dalleska, and E. R. Fisher. *Rev. Sci. Instrum.* **68**, 1684 (1997).
15. N. M. Mackie, V. A. Venturo, and E. R. Fisher. *J. Phys. Chem. B* **101**, 9425 (1997).

16. N. E. Capps, N. M. Mackie, and E. R. Fisher, *J. Appl. Phys.* **84,** 4736 (1998).

17. C. I. Butoi, N. M. Mackie, P. R. McCurdy, J. R. D. Peers, and E. R. Fisher, *Plasmas Polym.* **4,** 77 (1999).

18. C. I. Butoi, N. M. Mackie, K. L. Williams, N. E. Capps, and E. R. Fisher, *J. Vac. Sci. Technol. A* **18,** 2685 (2000).

19. K. H. A. Bogart, J. P. Cushing, and E. R. Fisher, *J. Phys. Chem. B* **101,** 10016 (1997).

20. M. L. Steen, C. I. Butoi, and E. R. Fisher, *Langmuir*, submitted for publication.

21. P. R. McCurdy, C. I. Butoi, K. L. Williams, and E. R. Fisher, *J. Phys. Chem. B* 6919 (1999).

22. C. I. Butoi, M. L. Steen, J. R. D. Peers, and E. R. Fisher, *J. Phys. Chem.* **105,** 5957 (2001).

23. E. R. Fisher, P. Ho, W. Breiland, and R. J. Buss, *J. Phys. Chem.* **96,** 9855 (1992).

24. C. T. Rettner, D. J. Auerbach, J. C. Tully, and A. W. Kleyn, *J. Phys. Chem.* **100,** 13021 (1996).

25. K. L. Williams, C. I. Butoi, E. R. Fisher, *J. Vac. Sci. Technol.*, submitted for publication; K. L. Williams, E. R. Fisher, manuscript in preparation.

26. H. Sugai, Y. Mitsouka, and H. Toyoda, *J. Vac. Sci. Technol. A* **16,** 290 (1998); Y. Mitsouka, H. Toyoda, and H. Sugai, *Jpn. J. Appl. Phys.* **34,** L1486 (1995).

27. C. F. Abrams and D. B. Graves, *J. Vac. Sci. Technol. A* 18, 411 (2000); C. F. Abrams and D. B. Graves, *Thin Solid Films* **374,** 150 (2000).

28. G. A. Somarjai, *Introduction to Surface Chemistry and Catalysis* (John Wiley, New York, 1994).

29. (a) G. S. Selwyn, G. T. Fujimoto, and M. C. Lin, *J. Phys. Chem.* **86,** 760 (1982); (b) G. S. Selwyn and M. C. Lin, *Chem. Phys.* **67,** 213 (1982).

30. R. I. Masel, *Principles of Adsorption and Reaction on Solid Surfaces;* (John Wiley, New York, 1996).

CHAPTER 7

PLASMA MODIFICATION OF POROUS STRUCTURES FOR FORMATION OF COMPOSITE MATERIALS

This dissertation chapter contains results from a communication published in *Chemistry of Materials*. The manuscript was written by M. L. Steen and edited by Professor E. R. Fisher. This chapter describes the synthesis of three different composite materials using plasma deposition as one of the synthetic steps. The preparation of concentric-tubular Au/polymer micro- and nanostructured composites by template synthesis is discussed. In addition, inorganic/polymer and organic polymer composite membranes were prepared with the surface coating distributed throughout the porous structure. These systems demonstrate the range of materials chemistry and surface properties possible for integrated composites prepared by plasma deposition.

7.1 INTRODUCTION

We have previously reported template synthesis of concentric composite micro- and nanostructured materials consisting of an outer tubule of one material surrounding inner tubes or fibers of different materials.[1] Composite nanostructures of metals, semiconductors, carbons, and polymers were prepared by several synthetic methodologies including electroless deposition, electropolymerization, carbonization, chemical vapor deposition (CVD), and sol-gel synthesis. Such materials are considered to have applications in microelectronics, chemical sensors, and electrochemical energy production.[2] Here, we report synthesis of three different composite materials utilizing Plasma deposition as one of the synthetic steps. First, template-synthesized micro- and nanostructured Au-polymer composites are presented, with the outer material produced via Plasma deposition. With this system, we show for the first time that a high degree of granularity exists in the morphology of Au nanotubules produced via electroless deposition.

We also demonstrate the use of Plasma deposition to produce two different types of microstructured materials, specifically integrated inorganic polymer composite membranes and fibers as well as integrated polymer/polymer composite membranes. Particularly attractive aspects of Plasma deposition for preparation of composites include production of conformal, pin-hole free materials with uniform thickness, availability of a wide range of chemistries and surface properties, and virtually unlimited monomer selection. Additional control of film chemistry is achievable via pulsed, downstream, and remote plasmas.[3] Here, we demonstrate the versatility of Plasma deposition by producing

integrated composite membranes where the surface coating is tailored for a specific chemistry. These novel materials have potential applications as replacements for spun-glass filters, air-vent filters and biomolecule separations.

7.2 RESULTS AND DISCUSSION

7.2.1 MICROSTRUCTURED AU/POLYMER COMPOSITES. Au tubes (200 nm-2 μm) were prepared from template track-etched PET membranes using electroless deposition as described in Chapter 2.[4,5] The membrane is removed with hexafluoro-2-propanol to reveal free-standing Au structures.[1] Figure 7.1a shows a field-emission scanning electron micrograph (FE-SEM) of Au tubes prepared from 200 nm template membranes. This image displays a level of porosity that has not previously been reported for Au tubes prepared by electroless deposition. This type of granularity has, however, been reported for metal nanotubes produced via electrochemical deposition.[7] In both processes, Au particles are deposited at metal complexation sites on the pore walls and membrane surfaces.[7] The nanoscopic holes (~50-100 nm diameter) in the structure of the Au tubes shown in Fig. 7.1a could be the result of a limited number of complexation sites on the pore walls. Alternatively, formation of grain boundaries, defects or vacancies in the metal could also explain the incomplete congealing of the growing material. Previously reported SEM images of similar Au structures taken with lower resolution instruments (only ~50 nm) did not contain enough detail to completely discern the morphology shown clearly in Fig. 7.1a.[7]

To form a Au/polymer composite, an outer tubule of the electronically conductive

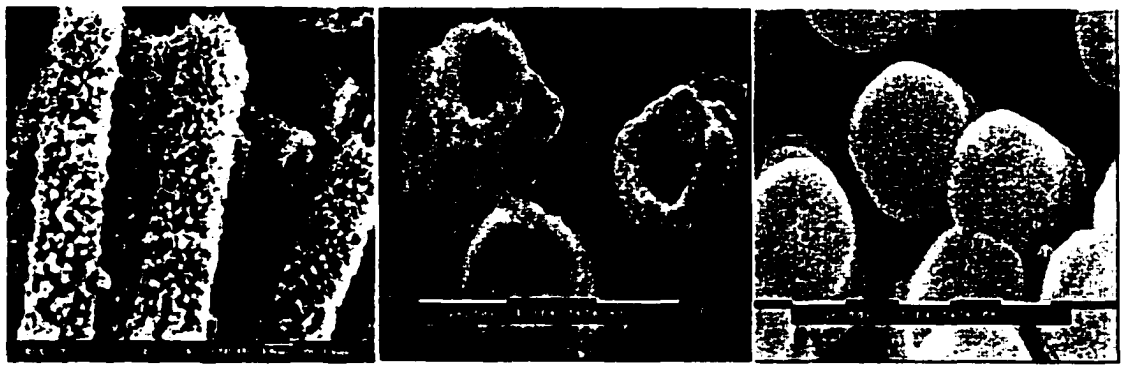

Figure 7.1 (A) A high resolution (10^5 X) FE-SEM of Au tubules grown in 200 nm membranes after dissolution of the template. Note the high porosity over the entire surface of the tubules. which is likely caused by the granularity of the metal. (B) SEM image of Au tubules grown in 1 μm membranes after dissolution of the template: and (C) SEM image fo the 1 μm Au tubules with a ~1 μm thick conformal coating of polypyrrole deposited using a pulsed pyrrole plasmas.

polymer polypyrrole was deposited on the Au tubules through a pulsed pyrrole plasma (5% duty cycle, 200 W peak applied rf power, pressure = 150 mTorr) using our inductively-coupled tubular glass plasma reactor described in Chapter 2.[8] Figure 7.1b shows a high magnification SEM of 1 μm Au tubules prior to plasma deposition and Fig. 7.1c shows the same tubules after deposition. It is clear from Fig. 7.1c that the polymer coating has clearly covered the entire length of the tubules, that the ends are capped with the coating, and that none of the underlying Au is exposed. Given the relatively high deposition rate (>1000 Å/min), it is unlikely that the polymer layer fills the interior of the tubule prior to capping.

FTIR spectra of the polymer layer indicate characteristic pyrrole absorbances such as N-H stretching at 3400 cm^{-1}, the =C-H in-plane deformation at 1037-1096 cm^{-1} from aromatic ring breathing of pyrrole, and the -C-H out-of-plane deformation at 740 cm^{-1}. Absorption peaks at 2219 cm^{-1} (C≡N stretching) and 2900 cm^{-1} (aliphatic C-H stretching), indicate partial ring-opening of pyrrole during Plasma deposition. Although thin film materials have been produced via CW plasma deposition of pyrrole,[9,10] our films retain more of the monomer structure because of the milder pulsed conditions. Indeed, we have shown that pulsed plasmas afford greater control over film chemistry in Plasma deposition, including retention of aromaticity.[11] Preliminary results from electrochemical characterization of the materials shown in Fig. 7.1c indicate our plasma-polymerized polypyrrole films are indeed conducting. The two most important results in this system are (1) that we can achieve smooth, pin-hole free, conformal and complete coating of the porous Au nanostructures (200 nm - 2 μm diam.) and (2) we can tailor the polymeric film

chemistry and thickness as desired. Indeed, we have also demonstrated this capability with both insulating and conductive polymer coatings, such as polystyrene-like materials from benzene plasmas.[12]

7.2.2 INORGANIC/POLYMER COMPOSITE MEMBRANES. Figure 7.2 shows SEM images of our second system with ~100 μm thick microporous symmetric polyethylene (PE) membranes, Fig. 7.2a, and non-woven PET fibers as host materials. Here, an inorganic coating is applied to the polymer substrates using a CW hexamethyldisiloxane (HMDSO)/O_2 (1:9) plasma (rf power = 25 W; pressure = 100 mTorr) which deposits SiO_x films.[13] To optimize modification of the entire cross section of these porous materials, the membrane holder described in Chapter 2 was used.[14] Fig. 7.2b demonstrates we have conformal coverage of the PE membrane, where the pore size is not significantly altered and there is no sign of pore filling. Furthermore, we have shown using ESEM that complete modification of the membrane cross section is achieved with our experimental configuration, Chapter 4.[15] Film growth on the PE membrane includes formation of thin, continuous fibers that span the entrance of the pore cavities. Although these fibers are not present in the SEM of the non-woven PET fibers, energy dispersive spectroscopy (EDS) did detect the presence of silicon on the plasma-treated PE and PET, which was not observed with the untreated materials.

Chemical analyses utilizing X-ray photoelectron spectroscopy (XPS), variable angle spectroscopic ellipsometry (VASE), and FTIR verified the deposited material is SiO_2. XPS analysis confirms the presence of silicon (~20%) on the treated PE and PET surfaces. The high resolution O_{1s} XPS spectrum confirmed that the deposited material

(A) (B) (C)

Figure 7.2 (A) SEM image of an untreated microporous polyethylene membrane; (B) the same microporous PE membrane with ~800 Å of SiO_2 deposited from a 25 W CW HMDSO:O_2 (1:9) plasma; (C) non-woven PET fibers coated with ~800 Å of SiO_2 using the same conditions as in (B).

consists primarily of SiO_x groups with stoichiometric O/Si atomic ratios of 2.6-3.0 for the plasma-treated polymers. VASE analysis using an SiO_2 model[16] also confirms that the plasma-deposited film is SiO_2. The model provides film thickness, 804 ± 33 Å, and refractive index (1.4422 to 1.4702 for λ = 200-700 nm), agreeing with literature values for SiO_2.[17]

Figure 7.3 shows a series of transmission FTIR spectra for SiO_x films deposited from HMDSO/O_2 (9:1) plasmas as a function of applied rf power. The prominent spectral features in these spectra are the absorption bands at ~1070 and ~820 cm^{-1}, corresponding to SiO stretching and bending modes, respectively.[18] In addition to these absorbance bands, films deposited at P ≤ 50 W have a broad absorbance centered about 3400 cm^{-1} (Si-OH stretch), indicating a substantial quantity of silanol is present in the film, Figs. 3a and 3b. No absorbance is detected for Si-OH species in films deposited at P ≥ 100 W, demonstrating that rf power serves to eliminate silanol contamination in these films. Figs. 7.3c and 7.3d also show a decrease in the shoulder on the Si-O absorbance band,[19] elimination of the two absorbance bands at ~924 and 798 cm^{-1} present in Figs. 7.3a and 7.3b,[20] and the presence of a new absorbance band at 804 cm^{-1}, assigned to the Si-O bend. All of these spectral features are characteristic of a more stoichiometric, higher quality SiO_2 film deposited at P ≥ 100W.

Although silanol incorporation is undesirable in many microelectronics applications, it is a criterion for filter applications needing hydrophilic surfaces. Thus, SiO_x films were deposited using HMDSO/O_2 (9:1) plasmas at P = 25 W for applications requiring hydrophilic surfaces. Our SiO_x/polymer composites wet immediately and

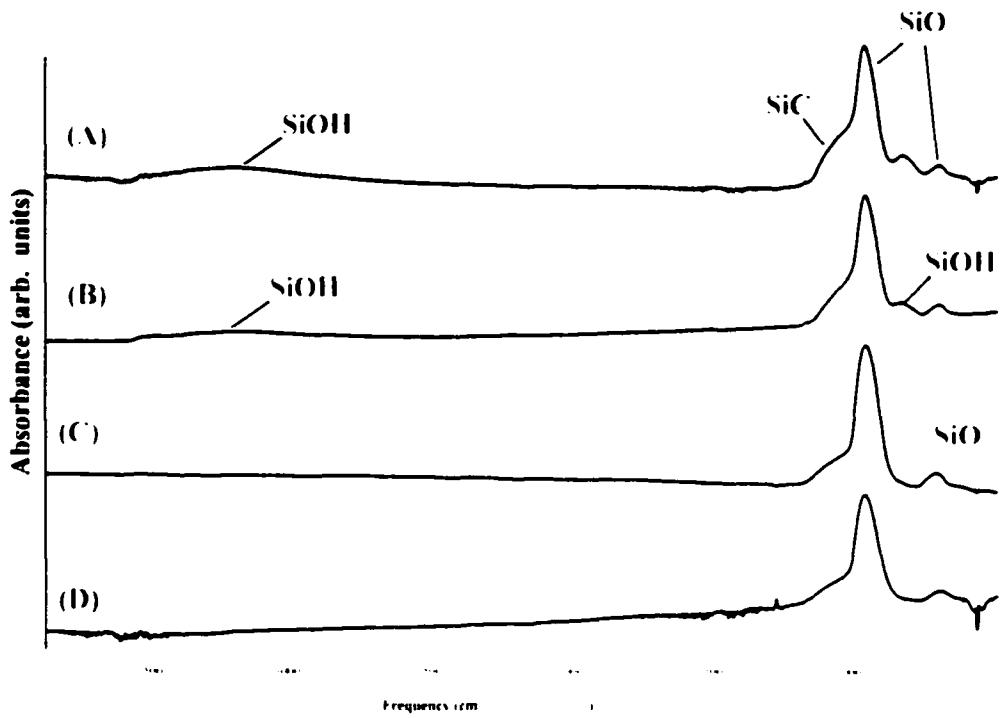

Figure 7.3 FTIR spectrum of films deposited from HMDSO O_2 (1:9) plasmas with (A) P = 25 W; (B) P = 50W; (C) P = 100 W; and (D) P = 125 W. The total chamber pressure was 100 mTorr and the treatment time was 10 minutes.

completely with water. In contrast, the untreated polymers are naturally hydrophobic with contact angles of 105.2 ± 6.5°(PE) and 132.9 ± 3.5° (PET). More importantly, both sides of the treated materials were wettable, further evidence that our process modifies the entire cross section,[21] and that the inorganic layer is integrated throughout the porous structure.[22,23] This maintains homogenous porosity throughout the modified materials, such that permeation characteristics are essentially unchanged.

Most composite membranes (a dense top layer with a microporous sublayer) have dissimilar permeation rates across the membrane.[24] Plasma processes have been employed to prepare such composite membranes by deposition of a second polymer onto a homogeneous membrane,[25] to deposit a skin layer onto an asymmetric membrane support,[26] or to chemically modify the existing skin layer to produce a composite membrane.[27] In each of these examples only one membrane surface was intentionally modified to produce a selective layer with a specific chemistry. In contrast, our synthetic strategy produces membranes with tailored surface properties, without significantly altering the porosity. To our knowledge, this is the first report of such integrated inorganic/polymer composite materials.

7.2.3 ORGANIC/POLYMER COMPOSITE MEMBRANES. The third system, microstructured polymer/polymer integrated membranes uses asymmetric polysulfone (PSf) membranes, Fig. 7.4, as the host material. As described in Chapter 3, these membranes have an average pore size of 1.2 μm on the open side, minimum pore diameters of ~0.133 μm on the tight side, and nominal bubble points of 57 ± 3 psi. Figure 7.4b shows a PSf membrane coated with ~80 Å of a fluorocarbon polymer using

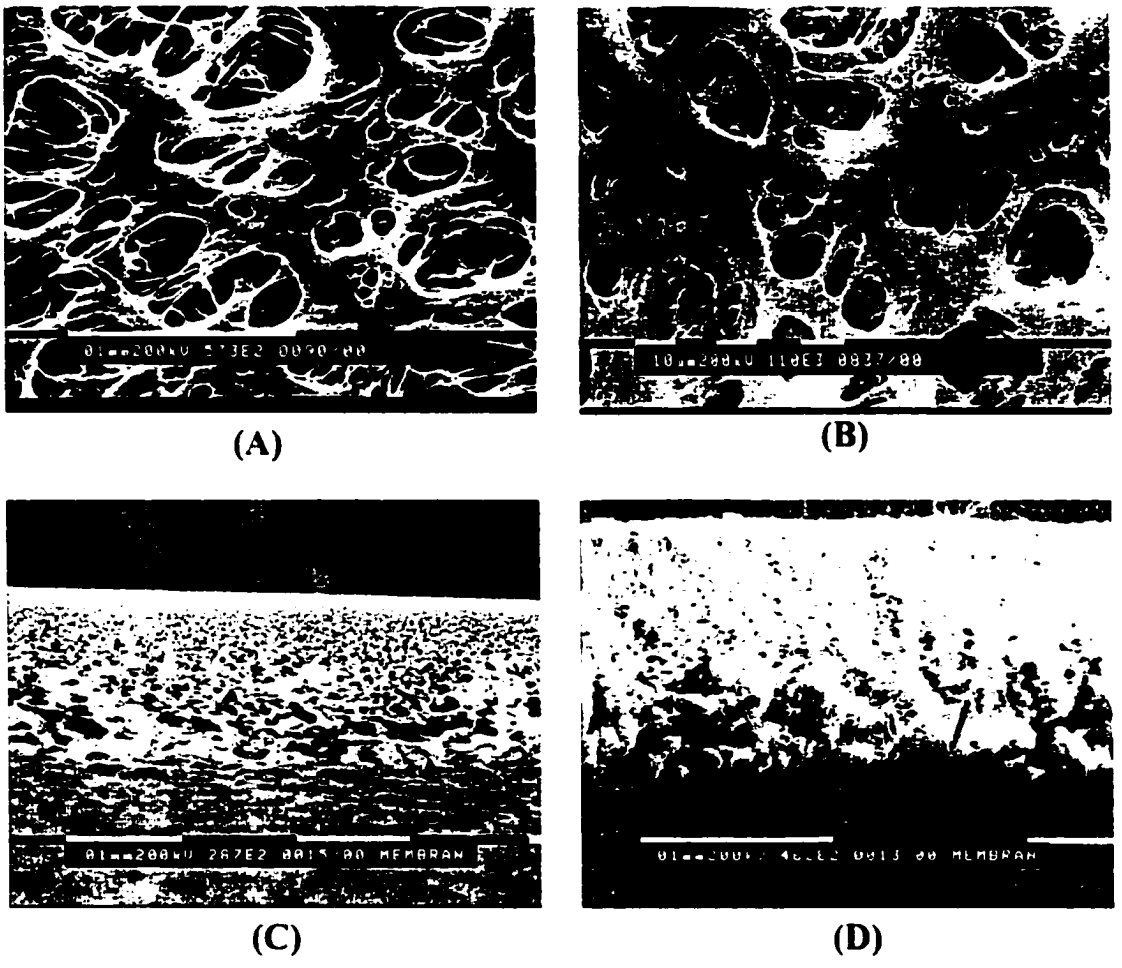

Figure 7.4 (A) SEM image of the surface of an untreated microporous polysulfone membrane; (B) the same PSf membrane ~80 Å of a conformal CF_2-rich fluorocarbon polymer deposited from a pulsed HFPO plasma; (C) cross sectional SEM image of an untreated PSf membrane; (D) cross-sectional SEM image of the same membrane treated with a CW CHF_3 plasma. Note that deposition in system (D) drastically alters the underlying membrane structure.

pulsed Plasma deposition of hexafluoropropylene oxide (HFPO) (16% duty cycle, 300 W peak applied rf power, pressure of 230 mTorr). Extensive surface analyses revealed these materials are highly ordered CF_2 chains, oriented perpendicular to the underlying substrate and terminated at the surface with CF_3.[28] Contact angle measurements made on both sides of this integrated composite membrane indicate an increase in the hydrophobicity of the material, from ~90° to ~110°, again indicating penetration of the plasma through the porous host. Highly hydrophobic membranes, such as those produced by the HFPO plasma surface modification system, have applications as moisture barriers and air-vent filters.[29]

Cross section SEM analysis of the treated membrane is nearly identical to that in Fig. 7.4c. Moreover, comparison to Fig. 7.4a shows film deposition has not adversely affected the porosity of the membrane. This is confirmed by bubble point measurements, which indicate no significant change in pore size. In contrast, hydrophobic modification with a CW CHF_3 plasma, forming an amorphous fluorocarbon polymer,[30] did not result in conformal coverage of the membrane structure. From the cross-sectional images in Figs. 7.4c and 7.4d, it is clear the deposited material has decreased pore diameter, thereby losing the membrane structure.[31] The primary reason for the differences observed between the HFPO and CHF_3 systems is the greater control over film chemistry and deposition rate realized by pulsed Plasma deposition. The HFPO system does, however, demonstrate the range of materials chemistry and surface properties possible for these integrated membrane systems. Thus, the synthetic strategies utilized here for these model systems point to numerous possibilities for other novel composite materials. We are currently exploring

some of these possibilities along with potential applications for all three composite materials presented here.

7.3 REFERENCES

1. V. M. Cepak, J. C. Hulteen, G. Che, K. B. Jirage, B. B. Lakshmi, E. R. Fisher, and C. R. Martin, *J. Mater. Res.* **13**, 3070 (1998); V. M. Cepak, J. C. Hulteen, G. Che, K. B. Jirage, B. B. Lakshmi, E. R. Fisher, and C. R. Martin, *Chem. Mater.* **9**, 1065 (1997).
2. G. Che, S. A. Miller, E. R. Fisher, and C. R. Martin, *Anal. Chem.* **71**, 3187 (1999).
3. We and others have demonstrated this previously with a variety of materials. See C. R. Savage and R. B. Timmons, *Chem. Mater.* **3**, 575 (1991); P. R. McCurdy, J. M. Truitt, and E. R. Fisher, *J. Electrochem. Soc.* **145**, 3271 (1998); C. I. Butoi, N. M. Mackie, J. E. Barnd, E. R. Fisher, L. J. Gamble, and D. G. Castner, *Chem. Mater.* **11**, 862 (1999).
4. M. Nishizawa, V. P. Menon, C. R. Martin, *Science* **168**, 700 (1995).
5. V. P. Menon and C. R. Martin, *Anal. Chem.* **67**, 1920 (1995).
6. C. Schonenberger, B. M. I. van der Zande, L. G. J. Fokkink, M. Henny, C. Schmid, M. Krueger, A. Bachtold, R. Huber, H. Birk, and U. Staufer, *J. Phys. Chem. B* **101**, 5497 (1997).
7. J. C. Hulteen and C. R. Martin, *J. Mater. Chem.* **7**, 1075 (1997).
8. K. H. A. Bogart, N. F. Dalleska, G. R. Bogart, and E. R. Fisher, *J. Vac. Sci. Technol. A* **13**, 476 (1995).
9. K. P. Lee, S. Y. Park, N. Kim, and S. K. Song, *Mol. Cryst. Liq. Cryst.* **224**, 53 (1993).
10. G. J. Cruz, J. Morales, and R. Olayo, *Thin Solid Films* **342**, 119 (1999).

11. (a) M. A. Leich, N. M. Mackie, K. L. Williams, and E. R. Fisher, *Macromolecules* **31,** 7618 (1998); (b) N. M. Mackie, D. G. Castner, and E. R. Fisher, *Langmuir* **14,** 1227 (1998).

12. Details of this polymerization, including extensive surface analysis (FTIR, XPS, SIMS) of the deposited materials and demonstration of their polystyrene-like nature can be found in Ref. 12b.

13. M. L. Steen and E. R. Fisher, *J. Electrochem. Soc.*, manuscript in preparation.

14. M. L. Steen, L. Hymas, E. D. Havey, N. E. Capps, and E. R. Fisher, *J. Memb. Sci.* **188,** 97 (2001).

15. See Chapters 3, 4, and 5.

16. J. A. Woolam, P. G. Snyder, and M. C. Rost, *Thin Solid Films* **166,** 317 (1988); S. Logothetidis and S. Boultadakis, *J. Appl. Phys.* **78,** 5362 (1995).

17. A. C. Adams, in *Plasma Deposited Thin Films*, Mort, J. and Jansen, F., Eds.; (Chemical Rubber: Boca Raton, FL, 1986).

18. R. T. Conley, *Infrared Spectroscopy*; (Allyn and Bacon, Boston, MA 1966.)

19. S. C. Deshmukh and E. S. Aydil, *J. Vac. Sci. Technol. B* **14,** 738 (1996); S. C. Deshmukh and E. S. Aydil, *J. Vac. Sci. Technol. A* **13,** 2355 (1995); S. C. Deshmukh and E. S. Aydil, *Appl. Phys. Lett.* **65,** 3185 (1994).

20. F. Fracassi, R. d'Agostino, and P. Favia, *J. Electrochem. Soc.* **139,** 2636 (1992).

21. See Chapters 3 and 4.

22. Penetration of non-woven fibers by polymer-forming plasmas was not observed by Yasuda and coworkers. T. Yasuda, T. Okuono, M. Miyama, and H. Yasuda, *J. Polym. Sci. A: Polym. Chem.* **32,** 1829 (1994).

23. See our multiple membranes experiments in Chapters 3 and 4 as well as our ESEM data. Chapter 4.

24. M. Mulder. *Basic Principles of Membrane Technology* (Kluwer Academic Press: Boston, 1996. p. 13).

25. X. Lin, J. Chen, and J. Xu. *J. Membr. Sci.* **90,** 81 (1994); N. Inagaki, S. Tasaka, T. Murata. *J. Appl. Polym. Sci.* **38,** 1869 (1992).

26. J. Hopkins and J. P. S. Badyal. *Langmuir* **12,** 4205 (1996).

27. J. Hopkins and J. P. S. Badyal. *Langmuir* **12,** 3666 (1996).

28. C. I. Butoi, N. M. Mackie, L. J. Gamble, D. G. Castner, A. E. Miller, J. E. Barnd, and E. R. Fisher. *Chem. Mater.* **12,** 2014 (2000).

29. Jerry Ditter, US Filter, Inc., personal communication.

30. N. E. Capps, N. M. Mackie, and E. R. Fisher. *J. Appl. Phys.* **84,** 4736 (1998).

31. This has been observed previously for high deposition rate systems. M. Onishi, K. Shimura, Y. Seita, S. Yamashita, A. Takahashi, T. Masuoka. *Radiat. Phys. Chem* **39,** 569 (1992).

CHAPTER 8

RESEARCH SUMMARY

This dissertation chapter recaps the major findings of this work, particularly with respect to the hypotheses proposed in Chapter 1. In addition, future directions for this work are briefly discussed.

The results presented in this dissertation establish the H_2O plasma treatment developed in our laboratory as a permanent surface modification for PSf and PES membranes.[1,2] To our knowledge, our work is the first report of permanent hydrophilic membrane modification by low-temperature plasmas. This treatment is also general to variety of membrane materials and porosities. Furthermore, H_2O plasma treatment modifies the entire cross section of highly asymmetric polymeric membranes. We attribute the extensive membrane modification to the high porosity of these materials and the unique design of our membrane holder, which allows maximal penetration of the plasma through the membrane. As the hydrophilic membrane modification developed in our laboratory satisfies several important criteria for an industrial membrane surface treatment, further testing of our plasma-treated membranes in industrial-scale separation processes is currently underway. In the broadest sense, this work has potential applications for membranes used in the biotechnology, pharmaceutical, and food and beverage industries as well as waste water treatment.[3]

The unifying hypothesis of this work was that plasma surface modification would best be understood, and ultimately controlled, through independent study of all aspects of the plasma system. The results of this dissertation demonstrate that our multi-faceted approach affords better process control by considering the molecular-level chemistry as well as achieving the desired membrane modification. For example, other researchers have recommended processing PSf membranes at high plasma powers ($P > 100$ W), which produce the highest concentration of excited-state OH radicals in H_2O plasmas.[4] Although our direct, gas-phase measurements confirm that the relative densities of both ground- and

excited-state OH radicals increase with plasma power, we have also experimentally determined that higher plasma powers (e.g., P = 125 W) do not afford an increase in the reactivity of OH radicals with PSf membranes.[5] Additionally, we have shown that PSf membranes are damaged under these conditions.[1] As a result, we recommend low applied rf powers and pressures, brief treatment times, and downstream plasma treatment to minimize exposure to energetic species. Hence, the optimal conditions for achieving the desired surface properties for PSf and PES membranes with minimal alteration to the bulk membrane properties were 25 W H_2O, 50 mTorr, for 2 minutes.

The results of this study also demonstrated that chemical nature of the plasma species is the important factor contributing to the observed differences in membrane treatments between the H_2O plasma system and the alternate plasmas chosen for this study. As proposed in Chapter 1, OH radicals in the H_2O plasma system were determined to be the primary reactive species involved in hydrophilic membrane modification. To supplement the largely empirical approach of other researchers, the role of OH radicals in the H_2O plasma surface modification system was *directly* determined with our non-intrusive radical-imaging experiments.[5] As expected, surface loss of OH radicals was observed under all experimental conditions. Our hypothesis was that OH radicals produced in H_2O plasmas modify these materials by producing covalently-bound C=O, C-O, O-H, O-C=O, and sulfate groups at the surface. Although it is infeasible to assign exact mechanisms without any kinetic information about these systems, we proposed possible oxidation pathways for PSf and PES, Chapter 1. Our XPS results confirm incorporation of a C-O, $C=O_x$, O-H, and sulfate groups and support the concurrent

oxidation pathways we predicted based on organic structural theory.

A moderate reactivity of ~50% measured for OH interacting with the polymeric membranes employed in this study suggests that H_2O plasma may be general to a variety of polymeric materials. Indeed, PSf, PES, and PE membranes show improved hydrophilicity as a result of H_2O plasma treatment. Despite the moderate reactivity of OH radicals measured for PTFE membrane surfaces, hydrophilic modification of hydrophobic PTFE remains an important goal. This suggests that OH is involved in alternate surface processes, as evidenced by our XPS data showing significant defluorination of PTFE by H_2O plasmas. Hence, independent analysis of the surface, the gas phase, and the plasma-surface interface was again contributory to understanding the overall polymer surface modification. Future work employing alternate plasma systems and our combined experimental approach to optimize hydrophilic modification of PTFE is currently underway in our laboratories.

The work involving the NH_3 plasma modification system was primarily motivated by the hypothesis that NH radicals are involved in the observed generation of NH_2 radicals at the surface. Indeed, surface loss of NH radicals was observed under the same conditions that produce NH_2 at the surface during NH_3 plasma processing, Chapter 6. This supports our hypothesis that NH radicals contribute to NH_2 surface production through hydrogen abstraction by an Eley-Rideal-type or Langmuir-Hinschelwood-type process, with the distinction between these two processes being whether NH thermally equilibrates at the surface prior to reaction.[7] Although independent data on the translational energies of incident and desorbed NH_2 radicals point to an Eley-Rideal

reaction as the dominant process.[7] data on the energies of incident and desorbed NH radicals are needed to differentiate between thermal (e.g., Langmuir-Hinschelwood) and non-thermal (e.g., Eley-Rideal) processes. Additionally, NH surface interaction results obtained under ion-free conditions display scatter behavior not previously observed in IRIS experiments.[8] Clearly, this is an area that would be well-served by additional IRIS studies

REFERENCES

1. M. L. Steen, L. Hymas, E. D. Havey, N. E. Capps, and E. R. Fisher, *J. Memb. Sci.* **188,** 97 (2001).

2. M. L. Steen, A. C. Jordan, and E. R. Fisher, *J. Memb. Sci.*, submitted for publication.

3. The results of this dissertation are included in part in our PCT application filed July 2001 entitled, "Surface Modified Membranes and Methods for Producing the Same".

4. K. Asfardjani, Y. Segui, Y. Aurelle, and N. Abidine, *J. Appl. Polym. Sci.* **43,** 271 (1991).

5. M. L. Steen, C. I. Butoi, and E. R. Fisher, *Langmuir*, submitted for publication.

6. B. C. Gates, *Catalytic Chemistry*, (John Wiley, New York, NY, 1992), p. 223.

7. C. I. Butoi, M. L. Steen, J. R. D. Peers, and E. R. Fisher, *J. Phys. Chem.* **105,** 5957 (2001).

8. E. R. Fisher, *Plasma Sources Technol.*, submitted for publication; M. L. Steen, K. R. Kull, and E. R. Fisher, *J. Appl. Phys.*, submitted for publication.